May 25, 1973

To the Graduate Council:

I am submitting herewith a thesis written by Edwin A. Merrick entitled "A Study of Wear Reactions on Mechanical Face Seals of Nickel and Nickel-20 Atomic Percent Molybdenum." I recommend that it be accepted for 18 quarter hours of credit in partial fulfillment of the requirements for the degree of Master of Science, with a major in Metallurgical Engineering.

C R Brooks

Major Professor

We have read this thesis
and recommend its acceptance:

C. F. Fisher, Jr.

Carl D. Lundin

Accepted for the Council:

Dean A. Smith

Vice Chancellor for
Graduate Studies and Research

A STUDY OF WEAR REACTIONS ON MECHANICAL FACE SEALS OF NICKEL AND NICKEL-20 ATOMIC PERCENT MOLYBDENUM

A Thesis

Presented to

the Graduate Council of

The University of Tennessee

In Partial Fulfillment

of the Requirements for the Degree

Master of Science

---

by

Edwin A. Merrick

August 1973

ACKNOWLEDGEMENTS

The author wishes to thank his advisor Dr. C. R. Brooks for his continued interest, guidance, and suggestions during this investigation, and his wife Meg for her patience and support.

Credit must be given, also, to Mr. Bob McGill. Without his expertise and dedication, the electron microscopic facility at The University of Tennessee would not exist in the fine operating condition that it does today.

1194106

ABSTRACT

The wear of commercially pure nickel and nickel-20 atomic percent molybdenum was investigated. Nickel-20 atomic percent molybdenum undergoes a disorder-order transformation on cooling from above 868°C. The disordered structure can be retained by rapid quenching from above that temperature. This fact was used to vary the mechanical properties, transforming the material used for tests from a soft ductile condition to a hard brittle condition. Yield strength (0.02 percent) can be varied from approximately 60 ksi to over 120 ksi, and microhardness can be increased from about 225 DPH to over 400 DPH. Material was machined from cast rings into a stator and a rotor approximately two and one-half inches in diameter for each test made. Tests were run under conditions simulating the wear of mechanical face seals, relative velocity of sliding was 975 centimeters per second. In order to minimize chemical reaction of the test rings with their environment, tests were performed in an argon atmosphere.

Scanning electron microscopy was used to observe and characterize surface topography. Soft ductile nickel undergoes gross surface distortion while the much harder ordered nickel-molybdenum alloy exhibits wear of a less severe nature. Evidence of material transfer was observed along with particle formation, wedge or prow formation, scuffing, galling, smearing, adhesion, and abrasion.

Thin film transmission electron microscopic observation of regions of the alloy cut parallel to the surface of the wear track indicated

that plastic deformation of the material is localized in a very thin region (less than 35 mils thick) near the surface of the wear track. The microstructural features observed were very complex in nature and in the case of the ordered material appeared similar in nature to observations of nickel-20 atomic percent molybdenum deformed slightly by rolling.

TABLE OF CONTENTS

CHAPTER	PAGE
INTRODUCTION	1
I. LITERATURE SURVEY	6
Friction	6
Wear	12
Adhesive wear	13
Abrasive wear	17
Corrosive wear	22
Surface fatigue	25
Lubrication	27
Boundary lubrication	28
Contact lubrication	31
Nickel-20 Atomic Percent Molybdenum (Ni_4Mo) and the Effect of the Disorder-Order Transformation on Friction and Wear	31
II. EXPERIMENTAL PROGRAM	37
The Test Apparatus and Instrumentation	37
Procedure	43
Specimen preparation	43
Scanning electron microscopy	46
Transmission electron microscopy	46
III. DISCUSSION OF RESULTS	50
Test Data	50

CHAPTER PAGE

Temperature data. 50

Face loading and torque data. 60

Characterization of Interfacial Wear Reactions. 62

Nickel wear surface 62

Disordered nickel-molybdenum wear surface 91

Ordered nickel-molybdenum wear surface. 107

Transmission of Electron Microscopic Examination of Substrate 122

IV. CONCLUSIONS AND RECOMMENDATIONS 128

LIST OF REFERENCES. 132

VITA. 136

LIST OF FIGURES

FIGURE		PAGE
1.	Typical Face Seal Configuration	3
2.	Surface Waviness with Smaller Irregularities or Asperities Imposed Upon It	7
3.	Relative Wear Coefficient (e) versus Hardness (H) for Several Hardening Mechanisms	21
4.	Nickel Rich Portion of the Nickel-Molybdenum Phase Diagram	33
5.	Isothermal Time-Temperature-Transformation Diagram for the Disorder-Order Transformation in Nickel-20 Atomic Percent Molybdenum	34
6.	Microhardness and Yield Strength versus Ageing Time at 775°C	34
7.	Hot Hardness, Young's Modulus of Elasticity, and Coefficient of Friction versus Test Temperature for Ordered Cu_3Au Sliding Against 440-C Stainless Steel	36
8.	Schematic Diagram of the Test Apparatus	38
9.	Photograph of Torque Tube	40
10.	Wheatstone Bridge Circuits Used to Measure Face Loading and Torque	41
11.	Scanning Electron Micrograph of the Ground Surface of a Test Ring	45
12.	Scanning Electron Micrograph of the Lapped Surface of a Test Ring	45
13.	Schematic Diagram Showing Origin of Specimens for Microstructural Observations of the Test Rings	49

FIGURE PAGE

14. Temperature versus Test Time for Test 1 54
15. Temperature versus Test Time for Test 3 54
16. Temperature versus Test Time for Test 4 55
17. Temperature versus Test Time for Test 8 55
18. Temperature versus Test Time for Test 10. 56
19. Temperature versus Test Time for Test 11. 56
20. Thermal Gradient for Test 1 58
21. Thermal Gradient for Test 4 58
22. Cyclic Nature of Face Loading and Torque Data, from Test 11 . . 61
23. Scanning Electron Micrograph Showing Two Differently Worn Areas (A and B) on a Nickel Test Ring 63
24. Scanning Electron Micrograph Showing Area C from Figure 23. . . 65
25. Scanning Electron Micrograph Showing a Large Particle (A) Welded to the Side of a Groove (B). 67
26. Scanning Electron Micrograph of a Small Groove (A) and Micro-asperities (B). 67
27. Optical Micrograph of Two Deep Abrasive Grooves (Small Arrows). 68
28. Optical Micrograph of an Island (A) of Welded Material Showing an Up-Raised Lip of Material at Top of Micrograph (see Small Arrow). 68
29. Scanning Electron Micrograph Showing Lip Noted in Figure 28 . . 70
30. Higher Magnification View of Center of Lip in Figure 28 70
31. Optical Micrograph Showing Island of Ordered Nickel-Molybdenum Alloy Welded to the Surface of Pure Nickel Test Ring. 71
32. Scanning Micrograph of Feature Shown in Figure 31 72

FIGURE PAGE

33. Scanning Micrograph of Feature Shown in Figure 31 73

34. Higher Magnification of Area Shown in Figure 33 73

35. Portion of the "Island," Shown in Previous Figures, in Which Non-Dispersive X-Ray Analysis for Nickel and Molybdenum was Performed 75

36. Area Map of Island in Figure 35 Showing Distribution of Molybdenum as Evidenced by Excitation of MoL_{α} X-Rays by the Electron Beam 75

37. Area Map of Island in Figure 55 Showing Distribution of Nickel as Evidenced by Excitation of NiK_{α} X-Rays by the Electron Beam. 76

38. Scanning Electron Micrograph of Polished and Etched Cross-Section from Nickel Test Ring 78

39. Optical Micrograph of Layered Material (B) on Test Ring 8 . . . 78

40. Scanning Micrograph of Feature Shown in Figure 39 79

41. Higher Magnification of Edge of "Island" (A) Shown in Figure 39. 79

42. Area B of Figure 41 at Higher Magnification 81

43. Smeared and Layered Appearance of Nickel Test Ring. 82

44. Hole Created by Smeared Material in Area Shown as Figure 43 . . 82

45. Deformation on the Surface of the Nickel Stator of Test 1 . . . 84

46. Initial Stages of Wedge Formation 84

47. Another View of Wedge Formation on the Surface Shown in Figure 46. 86

FIGURE PAGE

48. Trailing Edge of Another Wedge and Hole Being Formed as Material is Removed 86
49. Spall Cavity or Hole Formed on Wedge Removal. 87
50. Spall Cavity Left as a Result of Perhaps Several Related Instances of Wedge Formation. 88
51. Magnified View of Area A Shown in Figure 50 89
52. Magnified View of Area D Shown in Figure 50 89
53. Magnified View of Area C Shown in Figure 50 90
54. Higher Magnification of Center of Figure 53 92
55. Area A of Figure 53 92
56. Optical Micrograph Showing the Surface of a Disordered Test Ring. 93
57. Scanning Micrograph of the Surface of a Disordered Test Ring. . 93
58. Higher Magnification Showing the Edge of the Raised Area Shown in Figure 57. 94
59. Characteristic Surface Flow of Disordered Material. 94
60. Scuffed Region (A), Surrounded by the Layering and Surface Flow of a Disordered Test Ring 95
61. Another Test Ring (8) Showing a Large Particle with an Abrasive Groove (Marked A and B) It Has Created. 95
62. Magnified View of the Surface of Test Ring 8. 96
63. Bottom of Groove Shown as Area A in Figure 61 98
64. Side of Particle Shown in Figure 61 98
65. Another Area on the Side of the Particle Shown in Figure 61 . . 100
66. Magnified View of Center of Figure 65 100

FIGURE PAGE

67. Optical Micrograph Showing a Particle on Disordered Test Ring 4. 101
68. Scanning Electron Micrograph Showing Particle Noted in Figure 67. 101
69. Surface of Particle in Figure 67. 102
70. A Different Area on the Surface of the Particle in Figure 67. . 102
71. Optical Micrograph Showing Large Groove 103
72. Optical Micrograph Showing a Magnified View of One of the Changes of Direction in Figure 71 103
73. The Wedge, or Portion of the Asperity that Created the Groove Shown in Figures 71 and 72. 104
74. One of Many Particles Welded to the Surface of Test Ring 9. . . 106
75. Scanning Electron Micrograph Showing Wear Typical of the Ordered Test Rings. 108
76. High Magnification View from the Center of Figure 75. 108
77. Area A from Figure 76 109
78. Area C from Figure 76 109
79. Area D from Figure 76 110
80. Mild Wear of Ordered Test Ring 3. 112
81. Abrasion and Scuffing on Ordered Test Ring 3. 112
82. Initial Stages of Debris Formation on Ordered Test Ring 3 . . . 113
83. Abrasion and Scuffing 113
84. A Particle Welded to the Side of Ordered Test Ring 3. 114
85. Magnified View of the Particle in Figure 84 114

FIGURE PAGE

86. Close Up of Dendritic-Like Structure Seen in Figure 85. 115

87. Optical Micrograph of "Islands" of Welded Material (A) and Surface Cracks (Small Arrows) on Ordered Test Ring 11 115

88. Welded "Islands" of Material Similar in Appearance to Those Observed in Figure 87 117

89. Scanning Electron Micrograph Showing Surface Crack, Probably Formed During the Disorder-Order Heat-Treatment 118

90. Optical Micrograph of Another Welded Island on Test Ring 11 . . 118

91. Scanning Electron Micrograph of "Island" Shown in Figure 90 . . 119

92. Magnification of the "Lip" (Area B in Figure 91) of the "Island". 119

93. High Magnification of One of the Surface Cracks on the "Island" in Figure 91. 120

94. Transmission Electron Micrograph Illustrating the Microstructure of Undeformed Disordered Ni_4Mo 123

95. Transmission Electron Micrograph of Disordered Ni_4Mo Observed Near the Wear Track 123

96. Transmission Electron Micrograph of Disordered Ni_4Mo (Deformed); Bands are of Unexplained Origin 123

97. Deformed Material Near the Wear Track of a Disordered Test Ring. 123

98. Microstructure of Undeformed Ordered Ni_4Mo. 125

99. Deformed Material Near the Wear Track of an Ordered Test Ring . 125

100. Microstructure of Deformed Material Near the Wear Track of Test Ring 3. 126

FIGURE PAGE

101. Another Area Showing Bands Similar in Appearance to Those Observed in Figures 99 and 100. 126

102. Superdislocations Observed Near the Wear Track on Ordered Test Ring 3 127

103. Subsurface Slice Showing Recrystallization in the Ordered Material. 127

INTRODUCTION

One of the major problem areas in the design of mechanical elements is wear. Each year wear leads to the premature failure of many thousands of parts resulting in many hours of downtime and much expense to industry. Due to the complexity of the wear phenomena and new unfamiliar applications, design solutions based on past experience alone are often inadequate. Thus it is necessary that underlying wear mechanisms be fully understood in order to provide the engineer with proper design criteria. It is with this philosophy, i.e., of obtaining information on basic wear mechanisms, that the present work is undertaken.

It is the purpose of this paper to describe continuing research on interfacial wear reactions in mechanical face seals. The program was initiated with the design and construction of a wear test machine by David K. Matthes (1) in 1968 as a part of the Dynamic Sealing program at The University of Tennessee.

In preparation for the study of relatively complex commercial alloys, mechanistic information is needed concerning the reactions that occur in some of the less complex binary alloy systems. Emphasis has been placed on detailed metallurgical evaluation of materials with the long-range goal of routine study of commercial face seal materials under a variety of lubricating conditions.

By definition, the term "face seal" designates a device which forms a running seal between flat precision-finished surfaces. Face

seals are used for rotating shafts in which case the sealing surfaces are located in a plane normal to the axis of the shaft. Usually some means such as a spring is used to force the two faces of the seal together. A typical face seal configuration is shown in Figure 1. Some advantages of using this type of seal rather than some other type are to (1) reduce friction and power loss, (2) eliminate wear on the shaft or shaft sleeve, (3) control or eliminate leakage over a long period of running, (4) reduce sensitivity to shaft deflection or end play, and (5) provide relative freedom from maintenance.

During normal face seal operation hydrodynamic lubrication tends to prevent excessive friction and failure by wear. It is during periods of start up and shut down that wear increases. During this period hydrodynamic lubrication breaks down and boundary lubrication takes over as the dominant mode of operation. The close proximity of the mating surfaces increases surface interaction and wear becomes a major problem. For this work, the test apparatus built by Matthes is used to simulate this damaging period in the life of a mechanical face seal.

The literature abounds in studies devoted to low speed, simple configuration friction, and wear research. Little fundamental work has been performed on wear under conditions simulating mechanical face seal operation, a probable reason being that tests of this type involve a very large number of variables that must be controlled in order to obtain useful information.

Some of the variables involved are: (1) mating force; (2) relative speed of rotation; (3) temperature; (4) test duration; (5)

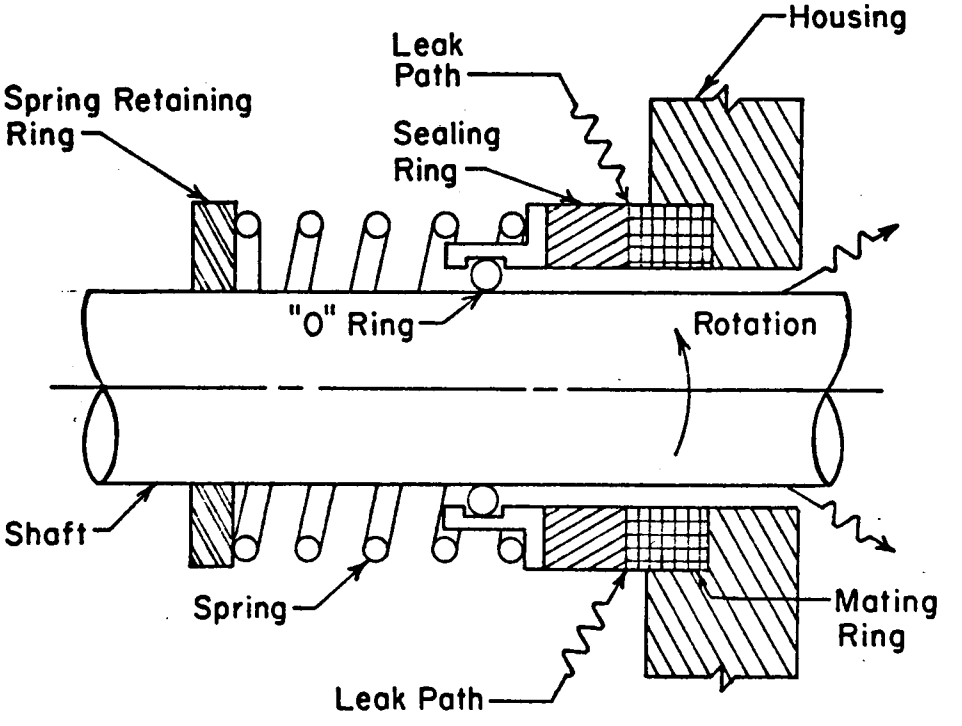

Figure 1. Typical Face Seal Configuration.

Source: After Matthes (1).

leakage or pressure drop across the seal interface; (6) face seal material properties; and (7) surface finish characteristics.

Previous research at The University of Tennessee was limited to qualitative metallography upon the test specimens. Primary emphasis was placed on the use of transmission electron microscopy of thin films and surface replicas supplemented with optical metallography. Optical metallography was found to be useful in ascertaining the particular type of wear occurring. Use of transmission electron microscopy allowed observation of the deformed substructure itself, lending information on the applied state of stress. The high resolution, magnification, and great depth of field obtained in electron microscopy was found to be an indispensable tool for evaluating the wear mechanism.

The wear machine has been modified to provide more information than was previously possible. A load cell was designed to allow measurement of face load and torque, and thermocouple instrumentation was added to yield information on bulk specimen temperatures developed.

At this point in the program the choice of material to be studied and variables to be controlled is a difficult decision. As will be seen, the number of material and mechanical variables possible can be enormous. For the goal of attaining information on the wear mechanisms, rather than simply documenting the relative wear resistance of a number of commercial alloys, a material offering wide variability in metallurgical properties is desirable. Previous work has been performed on a range of nickel and nickel-chromium alloys. These materials are not wear resistant metals but their properties are well documented, are easily varied, and they are well suited for electron microscopy.

Nickel-molybdenum alloys will be concentrated on in this study. In particular, those properties affected by the order-disorder transformation in nickel 29.1 weight percent molybdenum alloys (Ni_4Mo) are studied. Emphasis is placed on the use of the scanning electron microscope as a tool for studying surface topography and relating that information to known operating conditions.

CHAPTER I

LITERATURE SURVEY

The following is the result of a literature survey on friction, lubrication, and wear. An attempt has been made to concentrate on areas pertinent to a discussion of wear in mechanical face seals. For any detailed discussion of wear it is necessary that one discuss the interrelated and interdependent topics of friction and lubrication. The discussion will therefore be subdivided into four parts concentrating in succession on friction, wear, lubrication, and metallurgical properties of the nickel-molybdenum alloys to be studied.

I. FRICTION

One of the most important concepts to be grasped when studying friction, wear, and lubrication is that of real area of contact between two surfaces versus apparent area of contact. The real area of contact is usually much smaller than the apparent area. The surfaces of solids are not smooth but are, in fact, very rough and irregular. Kragelskii (2) stated that the smoothest surfaces one encounters have irregularities 0.05 - 0.1 micron high (1 micron = 10^{-4}cm), while the roughest for general application may have irregularities as high as 100-200 microns. Generally, a surface will have a waviness associated with it, with these smaller irregularities or asperities imposed upon that waviness (see Figure 2). It is obvious, then, that when two surfaces come into contact under light loads they will touch only at the tops of the highest

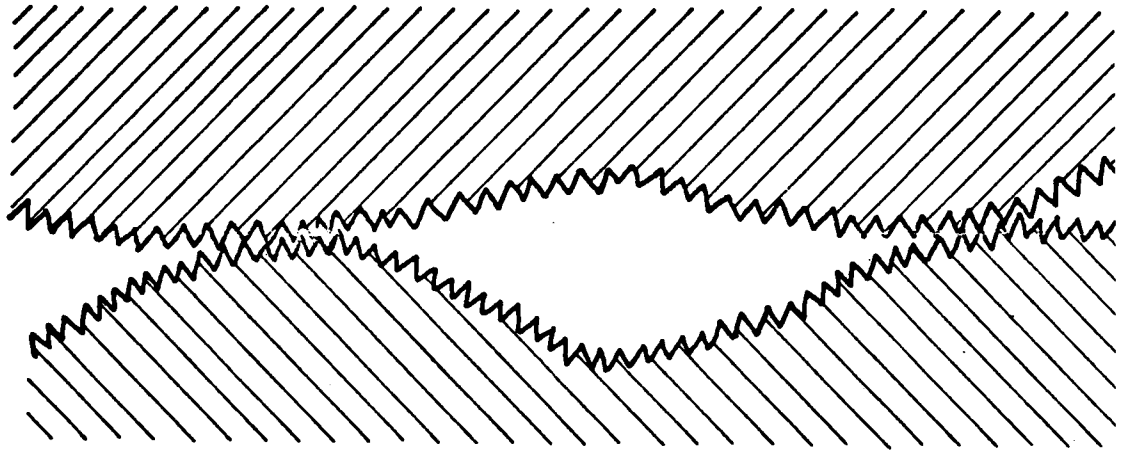

Figure 2. Surface Waviness with Smaller Irregularities or Asperities Imposed Upon It.

asperities. As the load is increased, the highest asperities will deform, allowing more of the load to be carried by more and more asperities; thus as load is increased the real area of contact will increase.

There have been many theories proposed to explain friction and the effects associated with it. One of the oldest was proposed around 1699 by Amontons (3), in which asperities were considered rigid and nondeformable. Friction was the amount of force necessary to raise asperities over one another. Amonton's model compared this effect with the simple raising of a load up an inclined plane. Coulomb (3) generalized a bit on this theory by allowing elastic deformation of the asperities. Kragelskii (2) stated that there are four empirical laws arising from these early theories: the frictional force is directly proportional to load, is independent of apparent area of contact for a constant load, is independent of sliding velocity, and depends on the properties of the materials in contact.

Most workers now agree that friction is due to a type of molecular force. There are several theories proposed based on molecular interaction between surfaces. Perhaps the most viable and widely accepted of these is the so-called welding or adhesion theory of friction set forth by Bowden and Tabor (3). As stated earlier, when a normal load is applied forcing two surfaces together, plastic deformation of the asperities occurs, breaking up whatever surface film may be present until the real area of contact is high enough to support the applied normal load. At the points of intimate contact, i.e., the tips of the asperities, localized welding or adhesion occurs between the two metals. As the surfaces are slid against one another, these localized welds are

being continually formed and broken. Wear or metal transfer occurs when the junctions are broken not at the point of initial contact, but in one or the other of the surfaces (just where the break occurs depends upon the mechanical properties of the material, and will be discussed later). Consequently, friction for clean metals, rather than being constant as was commonly hypothesized, is observed in some cases to be of almost a discontinuous nature, corresponding to a stick-slip or intermittent motion caused by the formation and shearing of the local junctions.

In addition to the molecular interaction between asperities, there is also a bulk material deformation frictional factor that must be accounted for when making friction calculations. This added factor was called by Bowden and Tabor (3) the ploughing force. Consider the action of hard asperities of one surface on the surface of a softer mating part. The asperities will tend to dig into the softer material. Thus, in order for the harder sliding material to move relative to the softer, material must either be pushed ahead of hard asperities, moved to the side of the groove caused by them, or the harder asperities must in some other manner bypass the mounds of material that have been built up.

According to Bowden and Tabor (3) the total frictional force can be written:

$$F = S + P = As + A'p' \qquad (1)$$

where S = the force required to shear the metallic junctions formed at the points of intimate contact between the two metals,

P = the force required to displace the softer metal from the front of the tips of the asperities,

A = real area of contact,

s = force per unit area which, acting in a direction tangential to the interface, is required to shear the junctions,

A'= cross sectional area of the grooved track,

and p'= mean pressure required to displace the metal in the surface.

In general it can be shown that $A = \frac{W}{H}$ where W is the applied load and H is the yield pressure or hardness of the softer material (H = cY, where c is a constant approximately equal to 3 and Y is the elastic limit of the softer material), and, unless there is a very marked difference between the hardness of the two mating surfaces the ploughing term can be neglected. This is due to the fact that the ploughing mechanism is dependent upon the ability of asperities on one surface to literally penetrate into the surface of its mate. Thus, the coefficient of friction can be written as an expression involving the bulk properties of the materials.

$$f = \frac{sA}{W} = \frac{sA}{HA} = \frac{s}{H} \qquad (2)$$

$$f = \frac{\text{shear strength of softer material}}{\text{hardness of softer material}}$$

The above theory has been objected to for several reasons. Most objections are able to be rationalized by the theory, but the inability of experimental and theoretical data to correlate well for an unlubricated ideal plastic material necessitated a modification of it to include the

effect of a contaminating film. Under a high enough load and with a thoroughly clean and ductile metal the coefficient of friction will grow to infinity since the real area of contact approaches the apparent area of contact and seizure occurs. A small amount of contaminant decreases the ability of the interface to sustain an applied shear stress, thus decreasing the coefficient of friction. Therefore, $f = \frac{S_i}{H}$, where S_i is the critical shear stress of a contaminant layer.

The above analysis only applies to a situation in which plastic deformation of the softer asperities occurs. If both surfaces deform elastically, the area of contact, according to Hertzian analysis, will be proportional to $W^{2/3}$. Therefore, the coefficient of friction would be expected to fall with increasing load. The Hertzian analysis, however, is based on a single contact point. Archard (4) has shown that as the number of contact points increases the area of contact will again be proportional to W.

The concepts regarding friction up to now have been limited to relatively low sliding velocities. The question more pertinent to the present research is to determine the effect of high sliding velocities on the coefficient of friction. Of primary importance here is the effect of an increase in interfacial temperature on the friction coefficient. In general, it has been noted that as sliding speed increases there is a value at which the coefficient of friction becomes a minimum corresponding to high temperatures, localized hot spots at asperity tips, and ease of shearing interfacial junctions. The interface thus corresponds to a thin film of low shear strength material on a hard substrate.

As the speed is increased, widespread melting occurs at the interface. A molten film may be created over the entire area of contact. The friction now depends on viscosity, thickness of film, sliding speed, and area of contact. At this point friction will no longer decrease, but will increase with increasing speeds and times.

II. WEAR

Clearly it is absurd to classify the formation and breaking of metallic junctions, the essence of frictional force, as being a form of wear. Kragelskii (2) offers interesting definitions for friction and wear that will serve to clarify this point: "Friction is the resistance to motion associated with overcoming the frictional bonds when the material flows around the penetrating asperities and when the adhesive bonds are localized in the thin surface films." On the other hand, wear is defined as the "destruction of material produced as a result of repeated disturbance of the frictional bonds." It appears, then, that it is the ability of a material to resist such repeated disturbance that determines its relative resistance to wear. Thus, wear is the loss of material from a surface by some type of mechanical action.

Wear is affected by many different variables; viz., type and mode of loading, quantity and type of lubricant, speed, temperature, hardness, surface finish, presence of foreign particles, and the chemical nature of the environment. Most researchers agree that there are four basic wear mechanisms: (1) adhesive wear, classified according to severity of action as galling, scuffing, scoring, or seizing; (2)

abrasive wear, known also as gouging or scratching; (3) corrosive wear; and (4) surface fatigue. In any instance no one mechanism is responsible for the wear that occurs. A special combination of adhesive, abrasive, and corrosive wear leads to what is termed "fretting." Wear can also be classified according to the type of debris that results. Severe wear results in mostly metallic wear particles and mild wear results in the production of oxidized debris.

At this point it will be particularly useful to discuss known information on the mechanism of each type of wear. Fretting is a very special case and will not be discussed in detail since it involves very small relative motions between two mating parts, and is therefore not pertinent to the sliding of mechanical face seals.

Adhesive Wear

As may be inferred from its name, adhesive wear is the wear that results as a consequence of the interfacial welding of junctions and subsequent breaking that must occur if motion is to continue. Whenever two metal surfaces make intimate contact under load, the possibility exists that cold welding of the junctions will occur. Certain conditions existing at the welded interface govern the formation of wear particles. According to Bowden and Tabor (5), there are four different situations that may occur:

1. The interface is slightly weaker than either of the two sliding metals. Shearing will then occur in the interface itself and the wear will be extremely small. The presence of surface or lubricant films will be important in minimizing wear.

2. The interface is stronger than one of the sliding metals and shearing occurs in the softer metal. Fragments of the soft metal adhere to the harder metal.

3. The interface is stronger than one metal and occasionally stronger than the other. There is marked transfer of the soft metal to the harder, but fragments of the harder are also removed.

4. The interface is always stronger than both metals. In the sliding of similar metals the interface becomes work hardened and severe damage occurs to both surfaces.

In the process of welded junction formation and subsequent shear, the transference of metal from one surface to another is the first of a series of stages in the formation of wear particles. In severe wear repeated sliding over the same area may cause metal transfer from one surface to another until such time as a steady state situation is reached. Further sliding may cause the transferred metal to be released as wear particles and the process of metallic transfer can occur again.

While all of the interfacial junctions formed by cold welding contribute to friction, by no means do all of them contribute to wear. Archard (4) introduced a factor k which is used to represent the fraction of friction junctions that produce wear. Burwell (6) has been quoted several times in the literature as giving an equation dealing with volume of wear materials:

$$V = kAL \tag{3}$$

where V = volume of wear materials,

k = wear coefficient as discussed above,

A = real area of contact,

and L = distance traveled.

Now, $A = \frac{W}{H}$ where W is the load and H is the yield pressure or the hardness of the material, so we can write:

$$V = \frac{kWL}{H} = k'WL \tag{4}$$

Bowden and Tabor (3) stated that for perfectly clean materials, k ranges from 0.1 - 0.01, and for contaminated surfaces, k may be less than 10^{-6}. If we divide both sides of equation (4) by the apparent area of contact, we find that $h = \frac{kPL}{H} = k'PL$, where h is the average wear depth and P is the average "design" contact pressure. We now see that k', the adhesive wear coefficient, is a function of h, P, and L, which are determinable quantities for given wear conditions. When k' is used to determine volume of material removed, calculations are found to compare well with observed amounts of wear debris. However, when the average pressure reaches approximately one-third of the indentation hardness, k' begins to increase sharply with increased pressure until large scale welding and seizure occurs.

One might expect that a quantitative relationship between the wear coefficient and the coefficient of friction might exist. Rabinowicz (7) has postulated such a relationship as $k = cf^n$, where c is some constant, and n has been found to have a value of approximately 3. He has also proposed a model, supported fairly well by experimental evidence, to estimate the average diameter of wear particles on the basis

of stored elastic energy in a wear particle and adhesional energy acting at the interface. According to this model, a transferred particle will be separated from the interface only if the elastic energy is greater than the adhesional energy. His equation is $d = 60{,}000 \frac{W_{ab}}{H}$, where d is the diameter of the wear particles in microns, H is the hardness of the softer material in kg/mm^2, and W_{ab} is the interfacial energy between materials a and b in $kg\text{-}cm/cm^2$. Since W_{ab} depends on the materials and their interaction, we may assume it equal to γ_a, the surface energy of the softer material for surfaces of average compatibility. Compatibility will depend on the degree of mutual solubility. For highly compatible surfaces, W_{ab} is approximately $2\gamma_a$ and for highly incompatible surfaces it is approximately $\frac{\gamma_a}{2}$. An immediate application of this equation for design purposes is in the estimation of clearance between parts to allow the particles to escape from the system and by so doing prevent in some small measure the initiation of abrasive wear.

At this point it would be well to compare the wear debris resulting from adhesion of brittle material to that resulting from adhesion of ductile material. A helpful analogy can be drawn here when one realizes that a ductile failure is characterized by large amounts of plastic deformation while brittle failure is not. Thus, shearing of the junctions in a brittle material will normally occur cleanly in the junction with little flow and wear. In a ductile material, however, it is possible for the junction to elongate and be rolled over itself in sliding to form a ball, thus forming a

larger wear particle than in the brittle case.

Abrasive Wear

Abrasive wear is one of the most common forms of wear observed in industry. It is accomplished not by the plucking or galling action of adhesive wear as previously described, but by a gouging or ploughing action. There are basically two conditions that lead to abrasive wear. The first is due to the presence of small particulate matter in nearly every piece of machinery. This matter may be present either as wear debris (metallic particles or oxides) or as a result of improper cleaning procedures. It is important in this type of wear to allow for removal of particles by allowing sufficient clearances between machine elements. The second condition of abrasive wear is one in which hard asperities on one surface tend to abrade a softer mating surface. Of the two conditions, the first is perhaps more prevalent in industry in causing abrasive wear.

A large amount of research on the abrasion of a metal surface by abrasive paper has been published. Results generally indicate a relationship between abrasive wear, hardness, and Young's modulus for a material. Oberle (8) reasoned that a good indication of a material's ability to resist abrasive wear is its ability to recover elastically after deformation by an abrasive particle. For this reason, he felt that a good yardstick of the abrasion resistance of a metal is its elastic limit.

Perhaps one of the most important factors in abrasive wear is the shape of the abrading particles. It has been shown that hard,

rounded particles are less abrasive than softer particles having more angular shapes. In the preceding discussion on adhesive wear, an equation dealing with the amount of wear debris produced was presented. Finikin (9) presented a similar equation for volume of material worn away in abrasive wear:

$$V = \frac{kWL}{H} \tag{5}$$

where V = volume of wear materials,

k = wear coefficient,

W = applied load,

L = distance traveled,

and H = hardness of the material.

As in the adhesive wear case, the constant k can be determined experimentally for a given material. Intuitively, it would seem that a differentiation between wear caused by large particles and wear by small ones would constitute a more correct model. Finikin (9) cited two equations developed by Nathan and Jones considering these cases. They are:

$$V = K'Ll(V+b)D \text{ (for small abrasive particle size)} \tag{6}$$

and, $$V = K'Ll(v+b)(D+a) \text{ (for large abrasive particles)} \tag{7}$$

where D = mean abrasive particle diameter,

l = length of abrasive path,

v = surface velocity,

V = wear volume,

L = applied load,

and K', a, b are constants characteristic of the metal under investigation.

It has been shown (7) that the effect of particle size is very great with small particles and decreases rapidly as the particles increase in size.

Another important consideration is the effect of an inhomogeneous material on abrasive wear. Finikin (9), after Kruschov and Babichev (10), considered a two-phase system for which $\alpha + \beta + \gamma = 1$, where α is the volume fraction of component 1, β is the volume fraction of component 2, and γ is the volume fraction of voids. He stated that the basic assumption in development of this theory is that the interface under abrading conditions will wear evenly, i.e., that there is no preferential wear of one component or another. As one would suspect, this assumption is not valid for a number of instances, for example in the case of a hard precipitate surrounded by a softer matrix material. Kragelskii (2) expressed wear of rubbing components either as linear wear or as mass wear:

$$\text{linear wear} \equiv \frac{h}{L} \tag{8}$$

$$\text{mass wear} \equiv \frac{q}{AL} \tag{9}$$

where h = depth of worn layer,

L = distance of sliding,

q = mass of worn material,

A = apparent area of contact,

and mass wear = linear wear times density of the material.

The linear wear of a specimen made of the material in which one is interested divided by the linear wear of a specimen made of a standard

material yields what Finikin (9) termed the relative wear coefficient "e." Both tests are performed under the same conditions; consequently, effects of experimental variation should be nullified. Relative wear resistance of a two-phase, inhomogeneous material can be expressed as $e = \alpha e_1 + \beta e_2$, where e_1 and e_2 are the linear wear coefficients of phases 1 and 2, respectively. This expression can be generalized to apply to a material with any number of phases. Kruschov and Babichev (10) have validated this result with experimental work on copper and iron sintered powders differing widely in porosity.

Earlier it was stated that abrasive wear was a function of hardness. Results have indicated that relative wear rate is linearly proportional to hardness for pure metals--as hardness increases, wear resistance increases. This indicates that abrasive wear resistance could be increased by one of several hardening mechanisms. In Figure 3 is shown e versus H for various hardening mechanisms. It is seen that the method of producing increased hardness is a controlling factor. Note that for a given alloy strain hardening has almost no effect, while quenching and tempering have more. One explanation as to why strain hardening has no effect is evident when one considers that during abrasion the surface of a given alloy will be work hardened and thus the relative wear resistance is inherently dependent on work hardening and to reconsider this effect is superfluous.

Miller (11), studying the abrasion of hard solids at high sliding speeds, observed that appreciable abrasive wear of hard solids was possible even when rubbing against a much softer material. This effect, seemingly contradictory to what might be expected, can

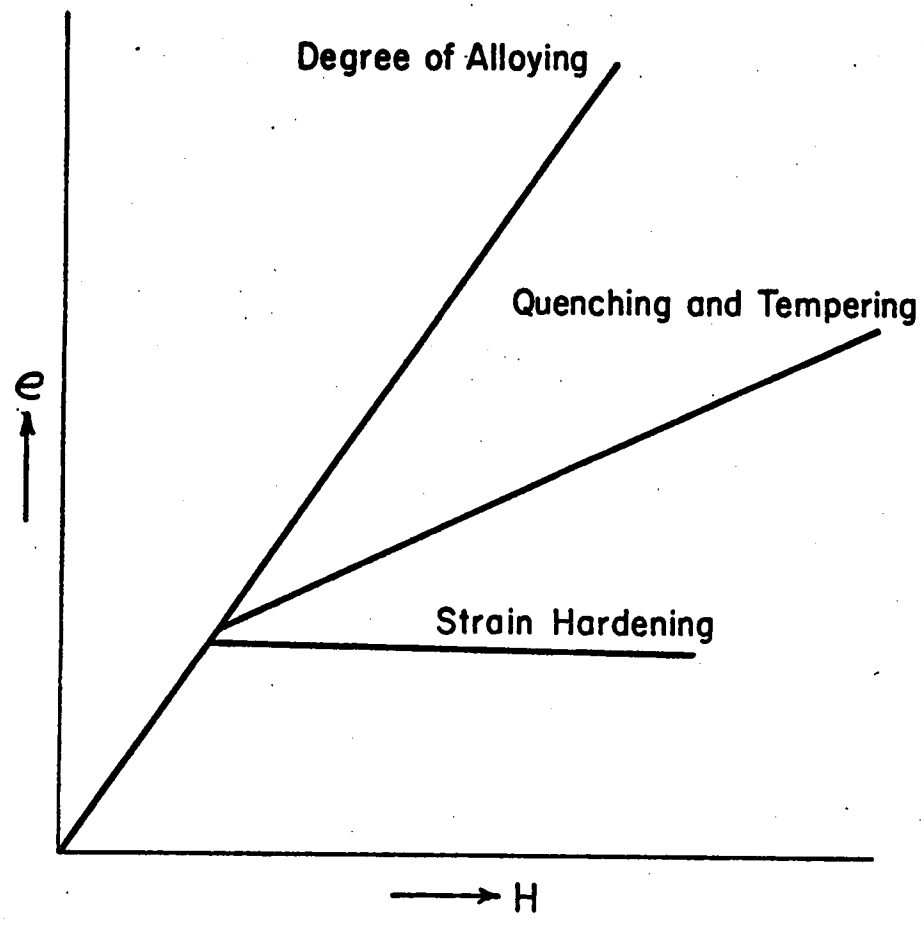

Figure 3. Relative Wear Coefficient (e) versus Hardness (H) for Several Hardening Mechanisms.

Source: After Finkin (9).

be explained when it is realized that even a small number of fragments of the hard surface under high speed can cause appreciable surface damage. The sites from which particles may be removed can include inclusions, surface defects, stress raisers produced during manufacture, or possibly asperities that, having been subjected to thermal shock or fatigue, are worked loose. The effect of thermal shock should not be dismissed lightly. Crack initiation due to thermal shock may be the rule rather than the exception in materials of low thermal shock resistance. As noted earlier, very high temperatures are developed at points of intimate contact between rubbing surfaces.

Corrosive Wear

Corrosion of materials receives widespread attention in industry. When corrosion is coupled with some type of mechanical action to remove material, it constitutes a form of wear. Corrosion debris may be loosened by rubbing action to become wear debris and either be used as a third body in the abrasive wear mechanism, adhere to one or the other of the rubbing surfaces, or be flushed out of the system by the lubricant. When compared to wear by other mechanisms, corrosive wear except at high temperatures normally assumes only a small role. All corrosion is basically electrochemical or galvanic in nature and is strongly dependent upon environmental conditions.

Lipson (12) stated that, for galvanic corrosion to occur, regions of different potential must exist in a metal or between metals and an electric circuit must be completed in the presence of an electrolyte or ion-carrying medium. The region of higher potential is called the anode and that having a lower potential is the cathode. During galvanic

corrosion the anode will corrode while the cathode will be protected. Anodic and cathodic regions may be very difficult to determine. For instance, on the surface of a specimen a potential difference may exist between grain boundaries and the grains themselves. Corrosion thus may result due to potential differences on a microscopic scale. Under suitable environmental conditions this situation will result macroscopically in uniform corrosion of the surface. The coexistence of anodic and cathodic regions coupled with a suitable electrolyte constitutes a "cell." There are two basic classifications of corrosion which are determined by the type of cell that is formed: (1) material differential cells, and (2) environmental differential cells.

In sliding, both types of cells may be set up. When two different metals contact each other, a galvanic cell may be set up, due simply to the electrochemical differences of the materials. Any lubricating fluid, depending on its inherent properties, may act as an electrolyte between the two surfaces. For corrosive wear a more important type of cell is set up between regions of highly deformed and undeformed surface material. Material that is highly deformed, as it is in wear, is always more anodic than surrounding undeformed material.

For many materials, surface oxidation, a particular form of corrosion, can be especially beneficial. The presence of the oxide film may serve to reduce the coefficient of friction as well as reduce wear by providing for less metal-to-metal adhesion and a harder surface for sliding that is more resistant to deformation than the substrate (13). It also serves as a barrier to further corrosion. On the other

hand, if the oxide film is unstable or incoherent with the underlying metal, it may easily be removed under wear deformation, forming abrasive particles and paving the way for further oxidation and wear.

The presence of a surface oxide or solid lubricant film will reduce the real area of metal to metal contact. Consequently, all friction and wear data must be considered with this fact in mind. Unless great pains are taken to provide clean running surfaces and experiments are performed in vacuum, there is always the complicating metal-surface film interactions that must be considered. With true metal to metal contact, large scale seizing and surface damage occurs even under moderate loading. Campbell (14) stated that for a number of metals the coefficient of friction in air ranges from 0.2 to 0.6, while in a vacuum it will range from 0.8 to 4.0.

In the design of mechanical face seals corrosive wear may be a large factor, depending on the nature of the lubricant and on other variables such as speed, time, temperature, and loading. At low loads the oxide or surface film may resist penetration. As loading is increased, film damage is likely. Repeated running over the same area is likely to create a similar effect. Temperature plays an important part in determining the reaction rate of the surface with its environment. Thus, in temperature ranges where the rate of break up of an oxide film is greater than the formation of more oxide, the coefficient of friction will increase. Likewise, when the oxide forms faster than it can be broken up and removed, there is a tendency for dissociation, evaporation, or spalling caused by stresses induced by differences in volume or by differences in the coefficients of expansion of the oxide

and of the metal.

What, then, can all this mean to the wear characteristics of a system? The presence of an oxide film can change the dominant wear mechanism. An oxide film in a wear track, although decreasing the coefficient of friction, may increase the amount of wear considerably. For example, when one considers the mild wear of steel, it is found to be greater in air than in an inert atmosphere or a vacuum, and wear debris may be all oxide. Wear will increase significantly, particularly if the oxide does not form a stable junction with its metal. As oxide is removed in operation, more will be formed. If the rate of removal is slightly less than the rate of oxidation, the coefficient of friction will be low but wear will occur at a rate close to the initial oxidation rate. This type of wear is sometimes termed fretting corrosion or fretting oxidation. Oxide particles may also participate in abrasive corrosion.

Oxide particles may be beneficial by forming under some conditions (high temperature sliding) a low melting eutectic by oxide-oxide reaction. The product thus formed may act as a kind of plastic lubricant. It may also be beneficial if compacted into a surface, for then it may cause a type of dispersion hardening.

Surface Fatigue

Pitting and spalling are the result of the fatigue of a material's surface due to cyclic loading that exceeds the endurance limit of the material. Up to now the review has concentrated on mechanisms common to sliding members. Surface fatigue occurs when two members are in rolling contact or combined rolling and sliding contact. Pitting may

be of two types--incipient and destructive. Incipient pitting is that pitting which occurs at the beginning of motion when the surface asperities are not sufficient to maintain the applied load. It is characterized by the formation of very small micro-cracks whose propagation is impeded by induced compressive stresses on the surface or slightly below the surface of a material. Incipient pitting is not destructive and serves only to remove asperities until the real area of contact can maintain the applied load.

Lipson (12) stated that pitting involves a number of factors, including high contact stresses, sliding action accompanying rolling action, possible formation of an elastic wave ahead of the instantaneous area of contact, surface flow, and the distribution of inclusions. Fatigue failure of the part may be hastened by the ability of pits to act as stress raisers. Spalling occurs when larger pits are formed by the joining of smaller adjacent pits due to the failure of the weakened material separating them. It may also occur as flaking of the surface due to crack propagation parallel to it.

Work (12) has shown that pitting will not occur in the absence of a lubricant. One proposed mechanism is that, upon formation of a small surface crack, lubricant is forced into it. As sliding or rolling proceeds, the lubricant is trapped in the crack. It then acts as a wedge under high pressure to force propagation of the crack and hence cause pitting with associated spalling. Whether or not pitting occurs will also depend on the viscosity of the lubricant. It seems that there is a critical viscosity above which pitting will not occur for a given material, surface finish, load, and operating temperature.

Corrosion will also play a significant part in surface fatigue. As one might expect, crack propagation is hastened with a subsequent increase in pitting when the material is chemically reactive with its environment.

III. LUBRICATION

In a mechanical face seal, lubricants are present between the two contacting faces to reduce the coefficient of friction between them. In so doing, wear of the parts can be minimized and power loss due to friction is made negligible. A discussion of lubrication is therefore a necessary part of this wear study. There are basically two different forms of lubrication--hydrodynamic and boundary lubrication. Hydrodynamic lubrication is present when two parts are separated by a relatively thick film of inactive lubricant. It is obvious, then, that the only wear occurring in hydrodynamic lubrication will be caused by metal-fluid interaction. Wear of this type is negligible when compared to the amount of wear that occurs under the boundary lubrication regime. Boundary lubrication is present when the distance between the surfaces is smaller. It is defined as being a condition in which two sliding surfaces are separated by a layer of lubricant of molecular dimensions. Thus contact between the surfaces is possible due to asperities piercing through the thin layer of lubricant to touch the mating surface. The properties of the lubricant are of negligible importance when compared to metallic properties due to intimate surface contact. The lubricant can, however, be important, as has been seen in determining the mode of wear present and consequently should not be overlooked as a contributing factor.

Braithwaite (15) stated that there should be a third type of lubrication process--contact lubrication. In this mode of lubrication, the lubricant is not a liquid simply attached or adsorbed to the metallic surface, but is a solid lubricant and is actually a part of the metal itself. This is the manner in which graphite and molybdenum disulfide may serve as effective lubricants.

Contact and boundary lubrication occur during periods of start-up and slow-down in a mechanical face seal. During these periods of operation, speeds are slow when compared to running speeds, thus causing boundary lubrication to predominate. When a shaft is stopped, the lubricant used in the usual hydrodynamic regime must remain sealed. The parts of the face seal are forced together by some mechanical means (possibly a spring) to accomplish this. Upon start-up, Braithwaite's "contact lubrication" will initially act between the surfaces during a short period of dry sliding; as the speed increases, boundary lubrication takes over, giving way finally at the higher operating speeds to hydrodynamic lubrication.

Boundary Lubrication

Thus, it is seen that high loads, a particularly rough surface, or moderate to slow speeds are sufficient to cause a breakdown of hydrodynamic lubrication. The boundary lubrication that takes over is a very complex phenomenon. In general, it has been found that the properties governing the action of hydrodynamic lubricants, such as viscosity, are unimportant in determining the effectiveness of a boundary lubricant, that effectiveness being determined by the

chemical constitution of the lubricant and the underlying metal. Empirically, it is known that the addition of EP (extreme pressure) materials such as certain sulfur, phosphorus, and chlorine compounds to a lubricant will greatly enhance the load carrying and wear prevention properties of lubricants. It is thought that this effect is the result of the formation of a low shear strength corrosion product at the contacting surfaces. Much work has been done on the mechanism of boundary lubrication friction and wear, and there are as many schools of thought of the process as there are on friction itself. Akhmatov (16) noted this fact but stated that there are no irreconcilable differences between the various theories, all being basically correct for stated conditions. The problem is that if some universal principle governing friction and effects of boundary lubrication does indeed exist, our present knowledge of the subject is so limited as to make determination of that, or those, principles involved impossible.

During boundary lubrication the surfaces are separated by at most one or two molecular layers of lubricant at points of closest proximity. For boundary lubrication to efficiently reduce friction and wear, it is necessary that: (1) the lubricant form a thin film to eliminate if possible metallic contact completely, and (2) reduce stresses on asperities. There are two properties of these films--adherence and coherence--that accomplish the first objective above. Adherence refers to the ability of the lubricant to reach and maintain an attached position position at asperity tips where real metallic contact occurs. Coherence is the ability of the lubricant to maintain an unbroken film. The reduction

of stresses on asperities is believed accomplished via three mechanisms:

1. Provision of a low shear strength solid film between the surfaces will allow shear in the film rather than in metallic junctions formed at tips of asperities.

2. The thermal conductivity is important. Since heating of the lubricant will tend to reduce its shear strength, it is desirable to use a lubricant of low thermal conductivity in order to maximize frictional heating in the boundary film.

3. By providing a sufficiently thick solid-like boundary film, having a lower elastic modulus than its substrate, one creates a cushioning effect that serves to minimize asperity normal stresses.

Long chain molecules are well suited for boundary lubrication. The use of long chain paraffins and alcohols provides effective lubrication up to their melting points, but above this temperature increased metallic contact with increased friction and wear occurs due to an inability to support compressive stresses. Fatty acids on the other hand are able to provide effective lubrication to well above their melting points due to an ability to form a "metallic soap" on chemical reaction with the metallic surface. The soap has a higher melting point and lubrication can continue up to that point.

Some points of interest made by Bowden and Tabor (5) concerning lubricated friction and wear characteristics are:

1. Metallic transfer is particulate, indicating that contact and adhesion have occurred at isolated points through the lubricant film.

2. The amount of metal transfer may be reduced by a factor of

10^5 or more, while friction is reduced by a factor of approximately 20.

3. The major part of the transfer is concentrated in a relatively small number of fragments. Although the number of fragments may be reduced by only a factor of three or four, the amount of transfer may be reduced by, as above, a factor of 10^5 for lubricated versus clean surfaces. The point is that the effect of the lubricant is to reduce the severity of wear by reducing the ability of the two surfaces to form large, strong, welded junctions.

Contact Lubrication

The effect of contact lubrication, said Braithwaite (15), is to increase the yield strength of the surface by interfering with dislocation motion. This is due to the presence of a thin coherent film of solid. Some typical contact lubricants are graphite, molybdenum disulfide, talc, and vapor deposited films of metals. The study of these solid contact lubricants represents still another dimension for friction and wear research that will receive increased emphasis in the future search for better wear resistant materials. The interested reader is referred to Braithwaite's book on contact lubrication (15) for further information.

IV. NICKEL-20 ATOMIC PERCENT MOLYBDENUM (Ni_4Mo) AND THE EFFECT OF THE DISORDER-ORDER TRANSFORMATION ON FRICTION AND WEAR

There are many reasons for choosing this particular alloy for study. It has wide variability in mechanical properties due to the disorder-order transformation that occurs; its properties are well

documented as is the transformation itself; the material is well suited to electron microscopy; and it is fairly close in composition to a commercial alloy (Hastelloy B--nominal composition 28 weight percent Mo, less than 6 weight percent Fe, 0.4-2.0 percent V, and the balance Ni). A phase diagram (17) for the nickel-molybdenum alloy system is shown in Figure 4.

Ni_4Mo above 868°C exists as a face-centered cubic disordered structure (α phase) that is normally retained by quenching from approximately 1200°C in air or in water. The equilibrium structure at room temperature is the ordered phase β, described by Harker (18) as a body-centered tetragonal unit cell containing eight nickel and two molybdenum atoms.

Material quenched from above 868°C, that having the disordered structure, is very ductile and soft. The presence of the β phase increases the hardness and decreases the ductility. In Figure 5 is shown the isothermal time temperature transformation curve for this system (19). It can be seen that the transformation occurs most rapidly at about 775°C. Snyder (20) aged alloys at this temperature for times up to 100 hours and obtained the microhardness and yield strength data (at 25°C) shown in Figure 6. It can be seen that both curves exhibit a maximum after approximately one-tenth hour of aging at 775°c. Yield strength (0.02 percent) increases from approximately 60 ksi to over 120 ksi, and microhardness increases from about 225 DPH to over 400 DPH. Thus, by a simple heat treatment, both microhardness and yield strength can almost double. One would expect that since the disorder-order transformation has such a profound effect on properties such as

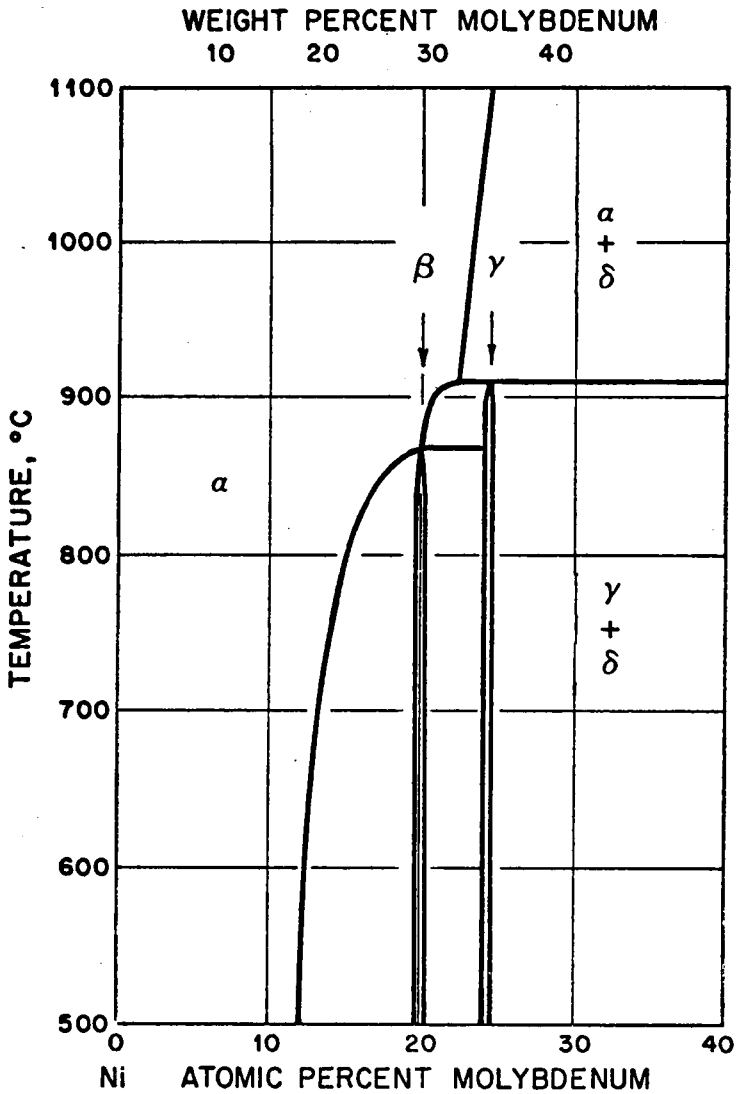

Figure 4. Nickel Rich Portion of the Nickel-Molybdenum Phase Diagram.

Source: After Snyder and Brooks (20).

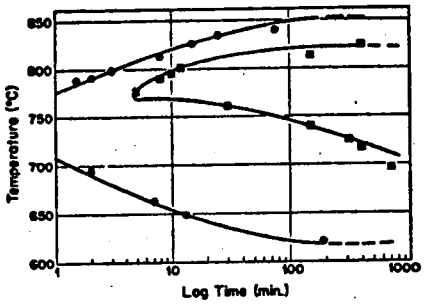

Figure 5. Isothermal Time-Temperature-Transformation Diagram for the Disorder-Order Transformation in Nickel-20 Atomic Percent Molybdenum.

Source: After Lampe (33).

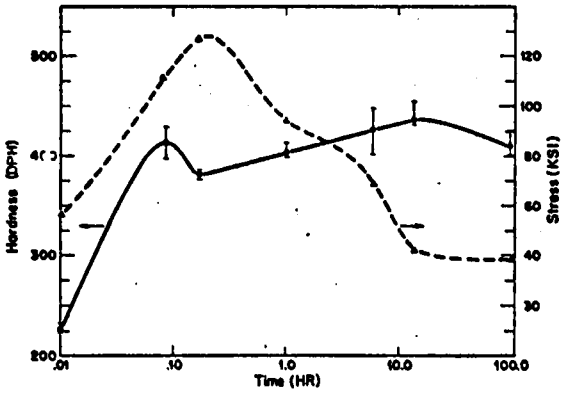

Figure 6. Microhardness and Yield Strength versus Ageing Time at 775°C.

Source: After Snyder and Brooks (20).

hardness, shear strength, elastic modulus, and electrical resistivity, it should also have an effect on friction and wear characteristics of a metal. Work by Buckley (21) with the copper-gold alloy Cu_3Au supports this possibility.

Buckley examined Cu_3Au in the ordered state by sliding it against 440-C stainless steel and obtaining friction data at various temperatures. His results are presented in Figure 7. Temperatures measured by him are bulk sample temperatures rather than interfacial temperatures due to the complexity of obtaining accurate interfacial data. Up to a temperature of about 260°C, the coefficient of friction is roughly constant. The transformation temperature for Cu_3Au is 390°C, somewhat higher than the observed 260°C transition temperature. Interfacial temperatures were undoubtedly much greater than 260°C; therefore, it is believed that the increase in friction is a result of the disorder-order transformation at 390°C. Thus, Buckley has offered evidence that the disorder-order transformation does indeed influence the frictional characteristics of a metal alloy. It will also undoubtedly exhibit some influence on the wear characteristics of a system.

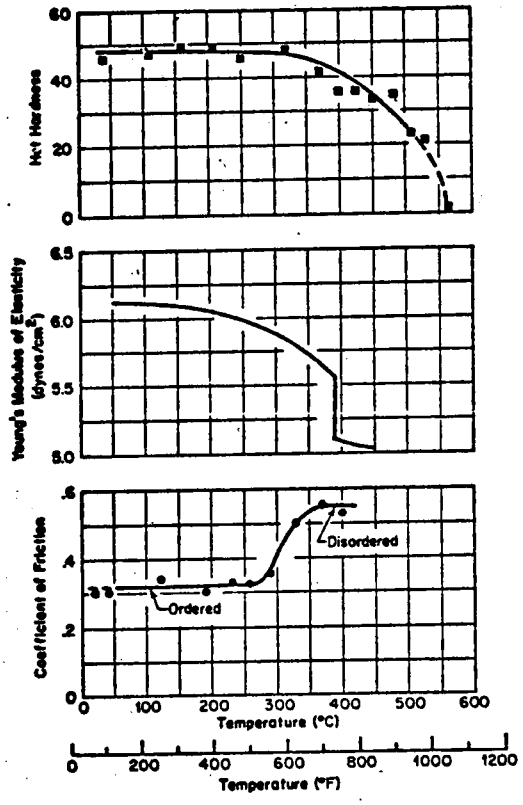

Figure 7. Hot Hardness, Young's Modulus of Elasticity, and Coefficient of Friction versus Test Temperature for Ordered Cu_3Au Sliding Against 440-C Stainless Steel.

Source: After Buckley (21).

CHAPTER II

EXPERIMENTAL PROGRAM

Six types of test runs were performed using the following combinations of materials: (1) nickel against nickel; (2) nickel against Ni_4Mo (disordered); (3) nickel against Ni_4Mo (ordered); (4) Ni_4Mo (ordered) against Ni_4Mo (disordered); (5) Ni_4Mo (ordered) against Ni_4Mo (ordered); and (6) Ni_4Mo (disordered) against Ni_4Mo (disordered). From the tests were obtained data on bulk specimen temperature, normal loading, and frictional torque.

The rings were then analyzed metallographically to characterize the worn surfaces and to obtain information on dominant operational wear mechanisms. Primary emphasis was placed on scanning electron microscopy supplemented by optical microscopy for surface characterization. Transmission electron microscopy was performed on selected samples to detect changes in degree of ordering and information on states of stress.

I. THE TEST APPARATUS AND INSTRUMENTATION

Basic operation of the apparatus has remained the same as in previous research (1) despite modifications made on it to provide better instrumentation and more flexibility. A schematic cross section of the modified test rig is shown in Figure 8. There are two wear specimens, a stator and a rotor. As implied from their names, the stator remains stationary, while the rotor is rotated in relation to it. Power for rotation is supplied from an alternating current motor delivering five

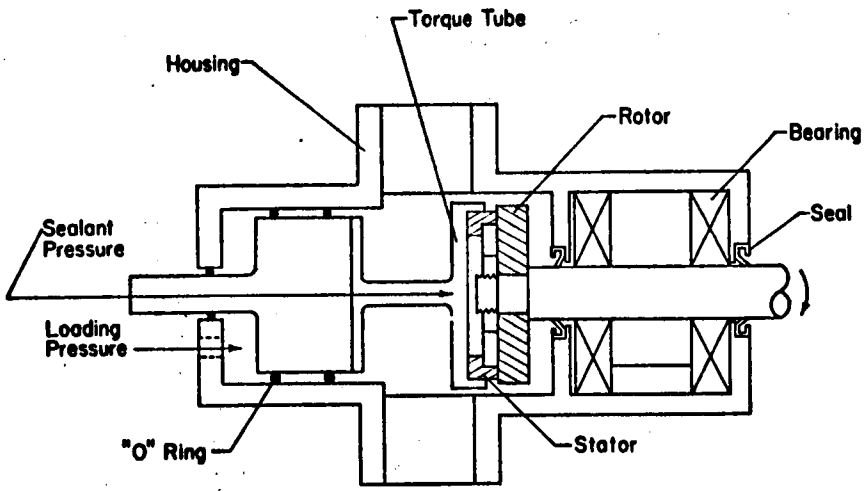

Figure 8. Schematic Diagram of the Test Apparatus.

brake horsepower at a constant armature speed of 1800 rpm. Rotational speeds may be continuously varied from 1450 to 4300 rpm. The seal rings are forced together by pressurizing the chamber behind a piston holding the stator with some gas or fluid. In order to provide for the boundary lubricated wear regime, the same fluid used in face loading is admitted via the sealant fluid canal. A pressure balance is achieved between this chamber and the loading chamber so as to allow controlled leakage across the interface between the two seal rings and boundary lubrication is achieved. In order to minimize reaction of the seal rings with the lubricant and prevent possible formation of Mo_2N due to the high interfacial temperatures expected, argon was used in this research as a sealant instead of nitrogen.

Initial tests by Matthes (1) provided no information concerning actual test conditions other than test duration, rotational speed, and initial face loading. To provide continuous data on test conditions, thermocouple instrumentation was provided and a torque tube to allow measurement of frictional torque and normal face load was designed.

A photograph of the torque tube is presented in Figure 9. Measurement of face load and frictional torque was made utilizing two wheatstone bridge circuits as shown in Figure 10. Design of the tube was similar to that of a device used by Headrick (22). Voltage was supplied to the bridges using a Honeywell Accudata 105 Gage Control Unit. Besides supplying input voltage, the gage control unit was used to balance the two circuits and to provide a ready calibration check by the introduction of a parallel resistance into one leg of the circuit, creating an electrical imbalance in the circuit similar to a

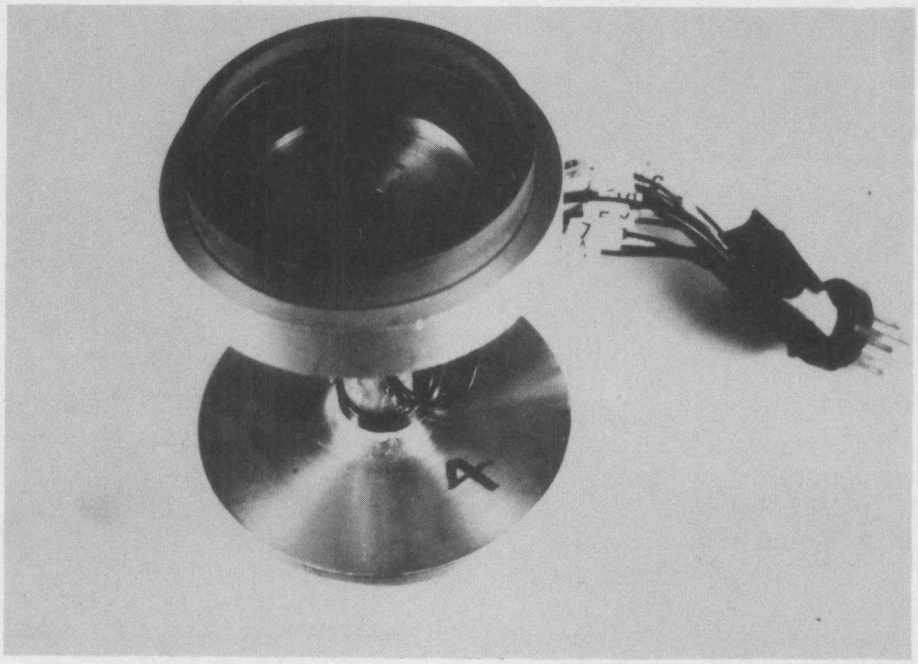

Figure 9. Photograph of Torque Tube.

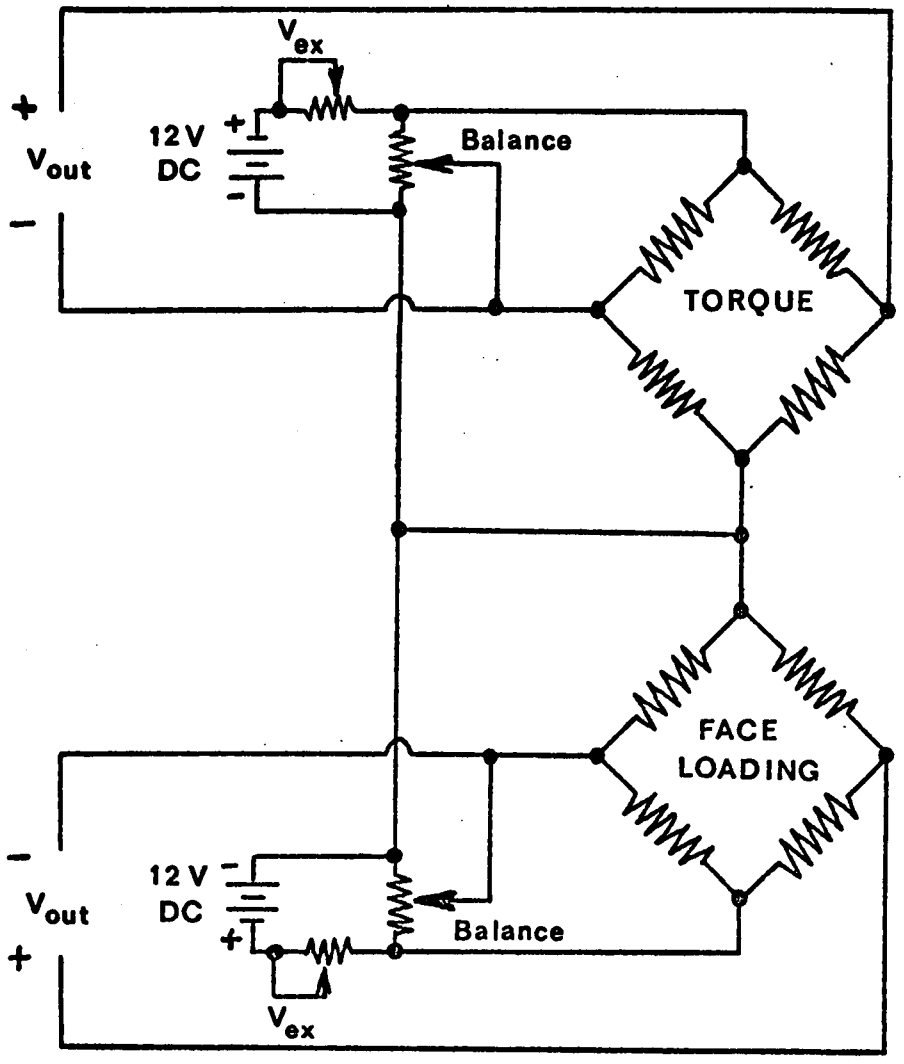

Figure 10. Wheatstone Bridge Circuits Used to Measure Face Loading and Torque.

mechanical strain of a known amount. Actual calibration of the torque tube was performed by applying a torque of known value to the tube and noting galvanometer deflection at a given amplification. Face Loading was calibrated in a similar manner by applying a known normal load to the tube.

Chromel-alumel thermocouples were spot-welded onto the side of the stators and covered with epoxy to insure their remaining in place. For tests in which more than one thermocouple was used, thermocouples were spaced approximately 120 degrees apart at varying depths on the ring. The output from the thermocouples was fed into a Honeywell Accudata 106 Thermocouple Millivolt Control Unit. Amplification for the thermocouple, face loading, and torsional signals was provided utilizing a Honeywell model A20B D.C. Amplifier and an Accudata 117 Multichannel D.C. Amplifier in series. This arrangement allowed almost continuous control of the amplification from a gain of one to a gain of 5000.

A Honeywell 1508 visicorder oscillograph recorder was used to obtain a continuous record of temperature, torque, and face loading for each test made. In future work, the use of a magnetic tape recorder to obtain data should be considered. A high speed recorder would allow the data to be reproduced at any speed desirable, lending greater analytical flexibility. Presently, a tremendous volume of paper is necessary to record a single test run. Magnetic tape alleviates this problem and has the advantage of re-use.

Difficulty was experienced in attaining repeatable alignment of seal rings. Previous work had resulted in the construction of a pair

of air bearings with design modifications made as necessary on the test rig. In the hopes of solving alignment problems, these bearings were installed only to result in compounded problems of test operation. Negative results regarding seal alignment resulted in the discontinuance of this approach. Much work is needed still in perfecting the test rig and instrumentation if repeatable results are to be obtained.

II. PROCEDURE

Specimen Preparation

Alloys to be used for the test rings were cast (in the form of discs approximately three inches in diameter and three-fourths of an inch thick) into a water-cooled copper mold, using a Balzer induction furnace. Commercial nickel 270 and swaged molybdenum rods were used as base materials. Spectrographic analysis of the molybdenum is given as .00x % Fe, .00x % Si. The material was checked for Mn, Cu, Ag, Ni, Cr, Co, V, W, Bi, Sb, As, Zn, Cd, In, Pb, and Sn, with no traces found. Material was well cleaned and pickled prior to use.

The castings were then machined into stators and rotors. Test rings were needed both in the ordered and the disordered condition. Following machining, the rings to be ordered were held at 775°C for one hour and quenched. Disordered rings received no further heat treatment following homogenization. Those rings receiving the disorder-order heat treatment after machining were pickled in a hot 20 percent HCl solution to remove any surface oxide present.

Some difficulty in the form of material cracking was experienced on ordering the test rings. Cracks were intergranular and were found

to lie along original alpha grain boundaries. It was felt that they were formed either as the material ordered or on cooling. Residual stresses induced by machining could have had a contributory effect on crack formation. As time did not permit, the subject was not pursued and tests were run using the ordered rings prepared in spite of surface cracks, realizing full well that the presence of surface cracks would be a complicating feature in the wear of the test rings.

Mating faces were then lapped to obtain optically flat surfaces. A flatness of within two helium light bands (23.2 millionths of an inch) was desired. Initial surface characterization included scanning electron microscopy and the use of a Talysurf profilometer to provide both qualitative and quantitative information regarding asperity height and general surface quality.

In Figure 11 is shown a scanning electron micrograph of the surface in an as ground condition. It is characterized by straight parallel sided grooves as a result of the grinding operation. (Note on micrograph: The designation "11-OD" indicates ordered test ring 11, run or to be run against disordered test ring 11. This convention will be followed throughout the paper. In addition, arrows will be used to note the relative direction of sliding of the mating test ring where this information is deemed of importance.) Figure 12 shows the same surface after lapping. Lapping was performed on a cast iron lap charged with 1450 grit aluminum oxide powder, light machine oil was used to lubricate the work piece during lapping. Note from Figure 12 that the surface is no longer characterized by the straight parallel abrasive grooves, but one can see that asperities now have

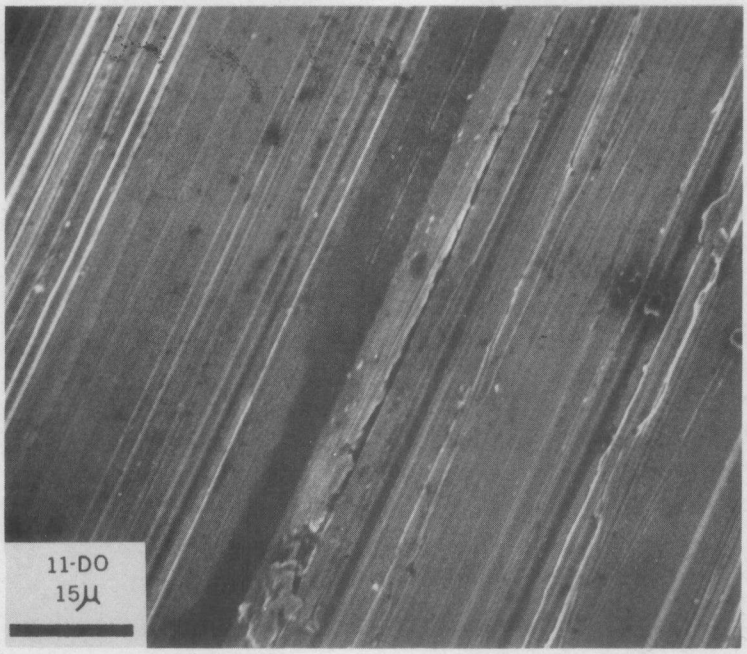

Figure 11. Scanning Electron Micrograph of the Ground Surface of a Test Ring.

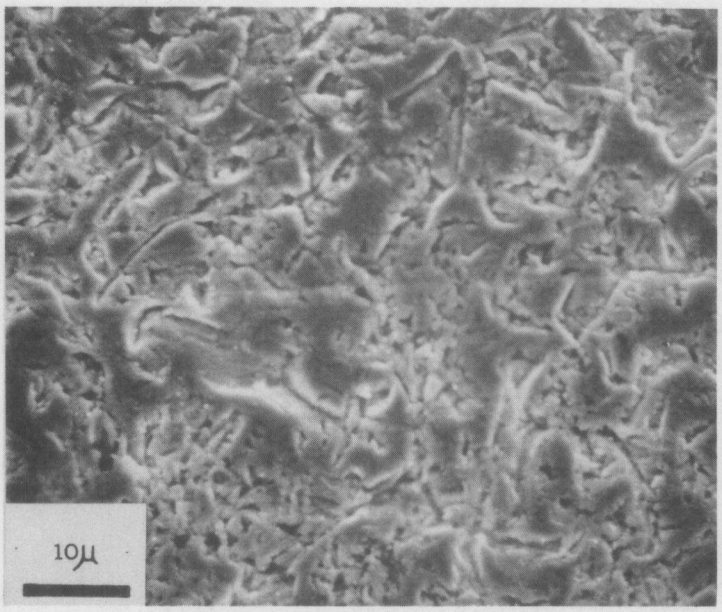

Figure 12. Scanning Electron Micrograph of the Lapped Surface of a Test Ring.

been flattened to produce a very uniform surface, marred only by a trace of random scratches. Individual asperities and surrounding low areas are clearly visible.

In Table I are presented the mean averages of at least four hardness readings taken per test ring prior to the actual test run. Note that tests include materials having three different hardness values: (1) nickel (R_B = 28-31); (2) disordered nickel-20 atomic percent molybdenum (R_B = 85-88); and (3) ordered nickel-20 atomic percent molybdenum (R_C = 32.5-42). The composition of the nickel-molybdenum test rings was assumed to be equal to the weighed composition of the heats. Nondispersive x-ray analysis showed that nickel and molybdenum were indeed the major constituents.

Scanning Electron Microscopy

Scanning microscopy was performed using an AMR 900 scanning electron microscope. Samples required no special preparation other than careful cleaning to remove any oil or lint that may have accumulated on the surface. This particular microscope has a large specimen chamber which allowed the test rings to be viewed whole without any sectioning. The only real disadvantages encountered with this practice are associated with the limited maneuverability of the test specimen. But the non-destructable nature and the ability to view the entire sample at one time are distinct advantages.

Transmission Electron Microscopy

Thin film electron microscopy was performed on several samples. Slices 20 mils thick were cut in test rings parallel to the surface of

TABLE I

HARDNESS DATA (MEAN AVERAGE OF AT LEAST THREE READINGS TAKEN PER SAMPLE)

Test No.	Type of Ring	Material	Average Hardness
1	Stator	Nickel	28.8 R_B
	Rotor	Nickel	28.0 R_B
2	Stator	Nickel	31.0 R_B
	Rotor	Disordered Ni_4Mo	84.9 R_B
3	Stator	Nickel	28.3 R_B
	Rotor	Ordered Ni_4Mo	32.5 R_C
4	Stator	Disordered Ni_4Mo	85.1 R_B
	Rotor	Disordered Ni_4Mo	87.0 R_B
8	Stator	Disordered Ni_4Mo	87.1 R_B
	Rotor	Nickel	29.5 R_B
9	Stator	Disordered Ni_4Mo	86.2 R_B
	Rotor	Disordered Ni_4Mo	87.9 R_B
10	Stator	Ordered Ni_4Mo	34.6 R_C
	Rotor	Ordered Ni_4Mo	42.0 R_C
11	Stator	Disordered Ni_4Mo	85.8 R_B
	Rotor	Ordered Ni_4Mo	41.6 R_C

the wear track as shown in Figure 13 and electrochemically dimpled to about 2 mils using the procedure outlined by Dubose and Steigler (23). Samples were kept carefully water cooled when cutting to minimize the effect that heat generation could have on the thin sections. The electrochemical thinning process is a two-step process. In step one, a jet of electrolyte is sprayed against the sample using air pressure. A platinum wire within the jet acts as one electrode, while the sample, held in platinum-tipped tweezers, is the other. The result is a saucer shaped dimple approximately a sixteenth of an inch in diameter. On the first or surface slice, dimpling is performed only on the side of the slice opposite the wear track to insure that the material observed in the electron microscope is as near the wear track as possible. After dimpling, the sample is placed in another electrolytic solution for further thinning. A photo cell is used to detect the presence of a hole and to shut off the voltage as soon as one appears. This is the most critical part of the procedure because to obtain a sufficiently thin area for study requires (1) for the bottom of the saucer to be uniformly thin and (2) for the thinning process to be stopped as soon as possible after the initial appearance of the hole. Failure to curtail thinning at the critical moment can result in destruction of all the usable portion of the sample. It is suggested that some way be found to protect the side of the sample on which the wear track is found from chemical attack by the electrolyte. Possibly a plastic soluble in acetone can be used to coat that side of the sample one wishes to defend from chemical attack.

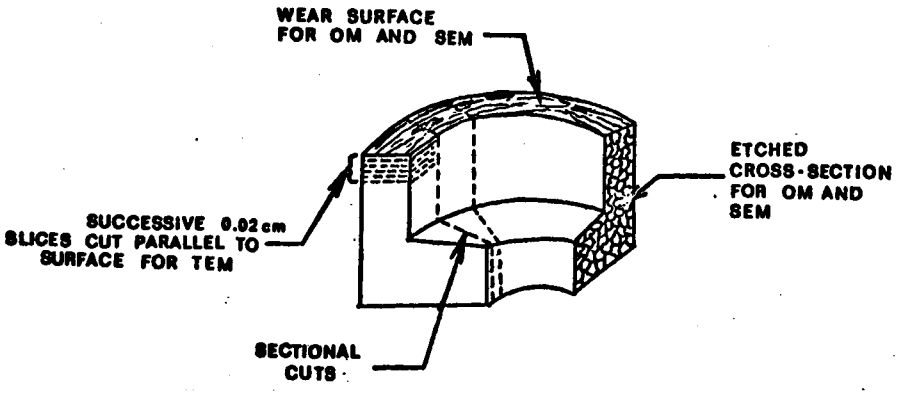

Figure 13. Schematic Diagram Showing Origin of Specimens for Microstructural Observations of the Test Rings.

CHAPTER III

DISCUSSION OF RESULTS

Due to the limited number of tests run and the mechanical problems associated with the performance of the test machine, it was impossible to obtain anything but qualitative results from the present research. At this time it can be said that the tests are statistically unreliable and care should be exercised when interpreting metallography. This chapter is divided into three sections, discussing in succession the test data, the characterization of interfacial wear reactions by optical and scanning electron microscopy, and examination of substructure with transmission electron microscopy.

I. TEST DATA

Argon was used to provide face loading and to act as a system "lubricant." Tests were run at a rotational speed of 3490 revolutions per minute which corresponds to an average relative sliding velocity of 975 centimeters per second. An attempt was made to run tests for a minimum of two minutes each, but as can be seen from Table II, this was not always possible. In the shorter tests, termination was in each case required due to the onset of noticeable seal chatter, indicating imminent seizure of the seal rings.

Temperature Data

Much effort in the literature is devoted to obtaining information

TABLE II

MAXIMUM BULK AND INTERFACIAL TEMPERATURE DATA

Test Run (No.)	Test Duration (sec)	Maximum T_B* (°C)	Time T_B Noted (sec)	Maximum T_i** (°C)
1	64	105	61	109
3	115	52	115	54.5
4	17	139.5	15	168.1
8	42	135	39	150.0
10	129	146	129	154.0
11	132	235	75	270.0

*T_B = Bulk temperature as measured at closest thermocouple to interface.

**T_i = Mean interfacial temperature.

on the rise in surface temperature at sliding interfaces due to frictional heating. Most efforts result at best in a rough estimate of the temperature increase. Recall the nature of two surfaces in contact and the fact that intimate contact occurs only at a few asperity tips which in most cases represents a small fraction of total surface area. It is at the tips of the asperities that frictional energy is dissipated as frictional heat or in some other form such as plastic deformation. The temperatures developed at these points of intimate contact are called flash temperatures since, as sliding occurs between the surfaces, the points of contact are continually changing. At asperity tips, flash temperatures can reach very high values and remain high for a very short time. The area of intimate contact, relative sliding velocity, thermal conductivity of the two materials, and the coefficient of friction are a few of the variables responsible for this effect. It is impossible at the present time to measure directly the flash temperature. Efforts to obtain flash temperature data are presently limited to the indirect method of noting the temperature of formation of surface oxides (14) and/or the temperatures at which phase changes or transformations might occur at the surface.

Difficulties also are encountered when trying to measure the mean interfacial temperature, that is, the average surface temperature. If the situation permits, pyrometric techniques are found useful. In some cases, if the sliding surfaces are of two different metals, the thermo-electric potential developed on sliding can serve as a measurement of temperature increase.

Practical considerations, however, excluded the afore-mentioned

techniques in the present study and thermocouples were used to measure bulk specimen temperature. In Figures 14 through 19 is presented the measured bulk specimen temperature as a function of test time for several of the test runs. In Figures 14, 15, and 16 note that three thermocouples were used. (One of the thermocouples in test three Figure 15 was inoperable.) The thermocouples were placed approximately 120 degrees apart on the stator at varying depths. In test four (Figure 16) a seeming inconsistency exists in that the intermediate thermocouple achieves a higher temperature at one point than the thermocouple closest to the interface. This point is easily rationalized when one realizes that the bulk specimen temperature at any one point is a direct function of interfacial reactions occurring nearest it. It is quite evident then that during the test period from five to nine seconds, considerably more surface interaction was occurring at the location of the second thermocouple than at the first, and after an initial period of running the test data assumed a more "normal" appearance. This effect is also seen in test three (Figure 15). The localized influence of surface interactions on bulk specimen temperatures can also be illustrated by considering any of the other tests. Noting the fluctuations in temperature as the tests proceed, one has the impression that the random rise in temperature is due to an increase in the amount of real activity in the area of the thermocouple possibly in the form of increased area of contact as asperities are worn away. One could attribute the decreases in temperature to a decrease in area of contact due to localized seal separation by wedge or prow formation, welded material, or possibly due to the conservation

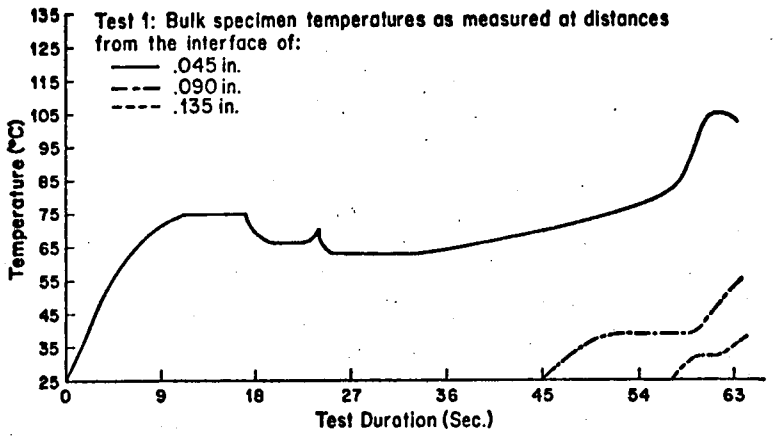

Figure 14. Temperature versus Test Time for Test 1.

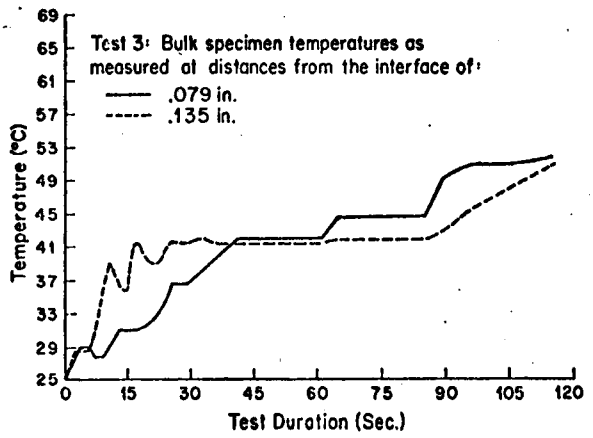

Figure 15. Temperature versus Test Time for Test 3.

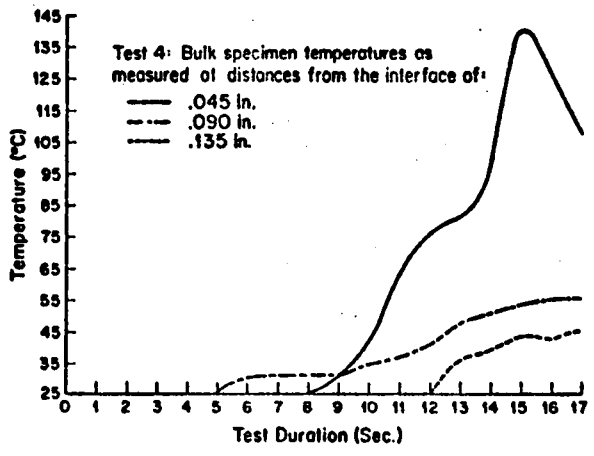

Figure 16. Temperature versus Test Time for Test 4.

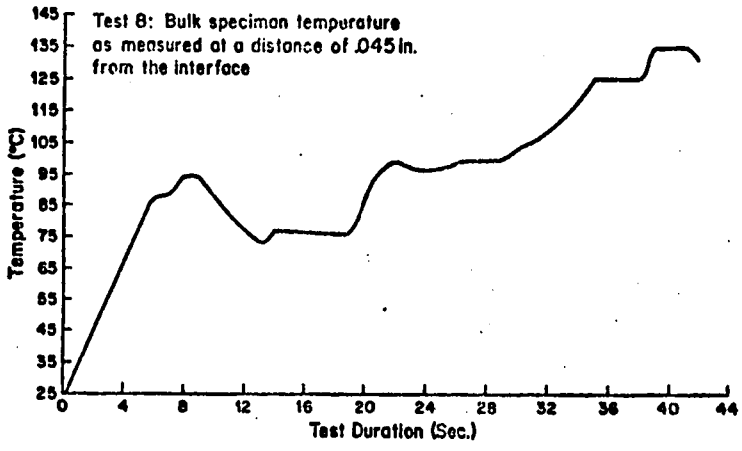

Figure 17. Temperature versus Test Time for Test 8.

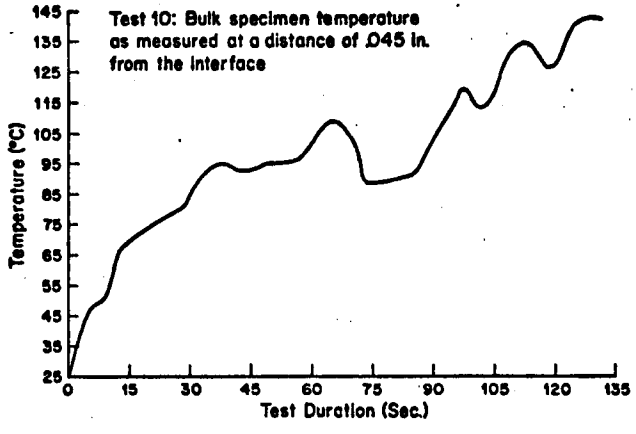

Figure 18. Temperature versus Test Time for Test 10.

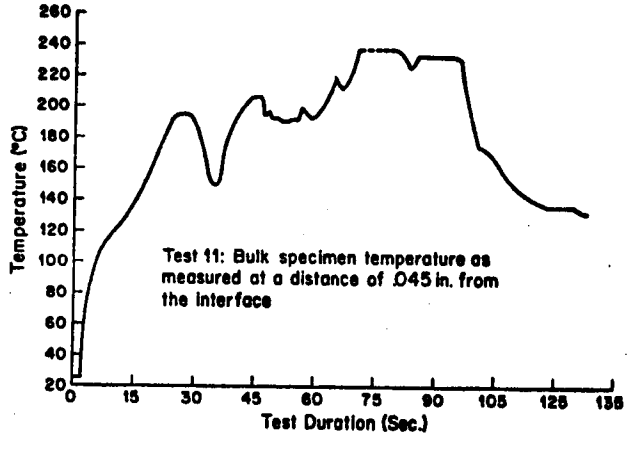

Figure 19. Temperature versus Test Time for Test 11.

of frictional energy as energy of plastic deformation due to thermal softening and flow rather than dissipation in the form of frictional heat.

In Table II (page 51) is noted the highest bulk temperature reached for each test run. In order to estimate the mean interfacial temperature, an error function solution to the Fourier series analysis was used (24). It should be stated that this is a very rough estimate in that radiation and geometrical effects were neglected. The solution used assumed a one-dimensional situation in which the interface was at some temperature T_0, T_B being the bulk temperature measured at a distance x from the interface at some time t. It was also assumed that at some finite distance from the interface the temperature was equal to room temperature and that at t = 0, T_B was equal to T_0 which was equal to room temperature. Values for T_0 calculated in this manner are noted in Table II (page 51). In Figures 20 and 21 is shown the thermal gradient at several times for tests one and four, respectively, as determined from these tests in which more than one thermocouple was used. The important point made here is that good agreement is obtained between the calculated maximum values and those attained graphically.

Finally, one would like to have an estimate for the maximum flash temperatures to expect under present test conditions. Archard (25) presented a theoretical model for calculating a value of the maximum attainable flash temperature. Although his model is rather unrealistic in that it assumes contact at only one point, it does serve as a method for calculating an upper limit on the flash temperature under given operating conditions. Maximum flash temperature will

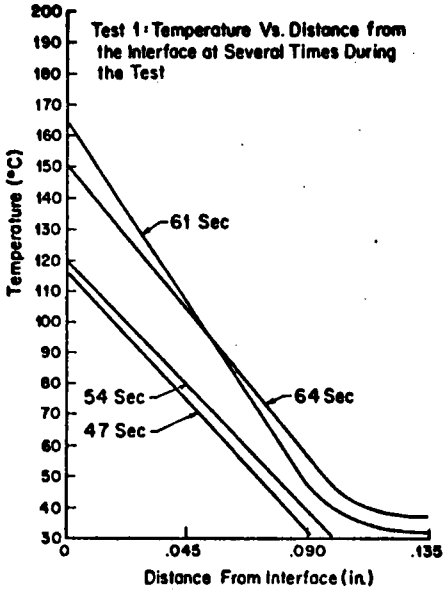

Figure 20. Thermal Gradient for Test 1.

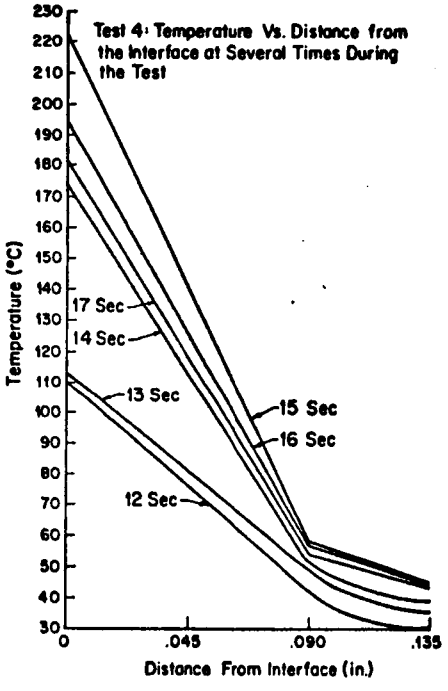

Figure 21. Thermal Gradient for Test 4.

be attained when the entire applied load is borne by a single asperity undergoing plastic deformation. For moderately high speed:

$$T_{max} = 0.435\ \gamma\ NL^{1/2} \qquad (10)$$

where $N = \frac{ug}{J}\frac{\pi p_m}{\rho c}$

$$L = \frac{W^{1/2}\,V}{2N(\pi p_m)^{1/2}}$$

$$\gamma = \frac{1}{[1 + 0.87L^{-1/2}]}$$

N = a constant of proportionality

L = a dimensionless parameter that considers speed effect

u = coefficient of friction

g = acceleration due to gravity

J = mechanical equivalent of heat

p_m = hardness or yield pressure

ρ = density of the material

c = specific heat

W = normal load

V = velocity of heat source or speed of sliding

n = thermal diffusivity

Using the above expression and appropriate values, a maximum attainable flash temperature of 435°C is calculated for test run number eleven. This value does not seem unrealistic since flash temperatures could be two or three hundred degrees higher than mean interfacial

temperatures. Time at these temperatures is extremely short, on the order of 10^{-6} second. Consequently, although flash temperatures could be in excess of 435°C, as this value is at best a crude approximation, observation of the disorder-order transformation is unlikely. (See the section discussing disorder-order transformation in Chapter I.)

Face Loading and Torque Data

No correlation was made between post-test topography or thermal fluctuations during the tests and frictional data. The natural frequency of the apparatus was calculated to be approximately 760 hertz by considering the torque tube and stator as a lumped spring-mass system. The torque and face loading data, an example of which is shown in Figure 22, assumed a cyclic nature very near to the natural frequency of the test apparatus. The system was thus operating in an unstable manner, vibrating for most of the tests at its own natural frequency. Under these conditions, the boundary lubricated wear regime is not possible.

This effect was observed also by Strom, et al. (26). Studying the vibration of face seals and the stabilizing effect of viscous and frictional damping, they found that undamped face seals have a very strong tendency for the nosepiece to vibrate unstably at high frequency (about 400 hertz in their tests). Amplitude of the vibrations was observed to be high (.025 cm). Lubricated and unlubricated face seals, when provided with either viscous or friction damping, were seen to operate stably at high speeds.

In the present tests, vibration was probably induced to the

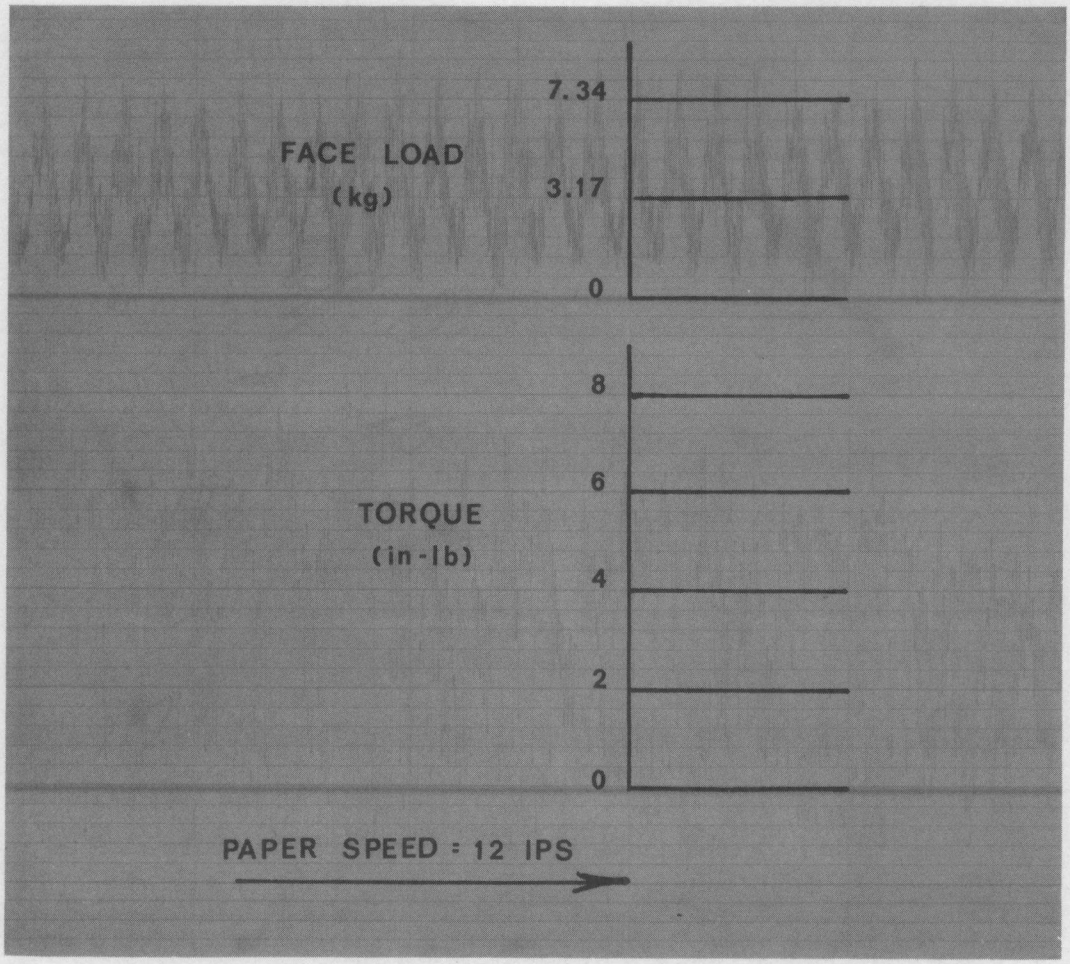

Figure 22. Cyclic Nature of Face Loading and Torque Data, from Test 11.

stator and torque tube from the rotor and shaft by frictional forces at the interface of the mechanical seals. It is obvious that some type of viscous damping of the test apparatus is needed in order to insure stable test conditions. The value of the torque tube is thus demonstrated to be considerable. Its use has indicated one area in which the test conditions must be improved if test results of a reliable nature are to be obtained.

II. CHARACTERIZATION OF INTERFACIAL WEAR REACTIONS

In a topographical study of wear surfaces there is a tendency to be attracted by unusual features and to overlook characteristic phenomena occurring on the surface. Much information on surface interaction and condition can, however, be attained by studying the unusual features encountered, so it is important that the inherent fundamental difference between characteristic and unusual features be kept in mind when interpreting results. This section will discuss the characteristic features of the wear observed on the nickel test rings, the disordered nickel-molybdenum test rings, and the ordered nickel-molybdenum test rings. Some of the unusual features will be reported. A hypothetical discussion of possible mechanisms involved will be presented where deemed appropriate.

Nickel Wear Surface

Figure 23 is a scanning electron micrograph of the surface of a nickel stator that has been run against an ordered nickel-molybdenum rotor. In this figure can be seen two differently worn areas. The

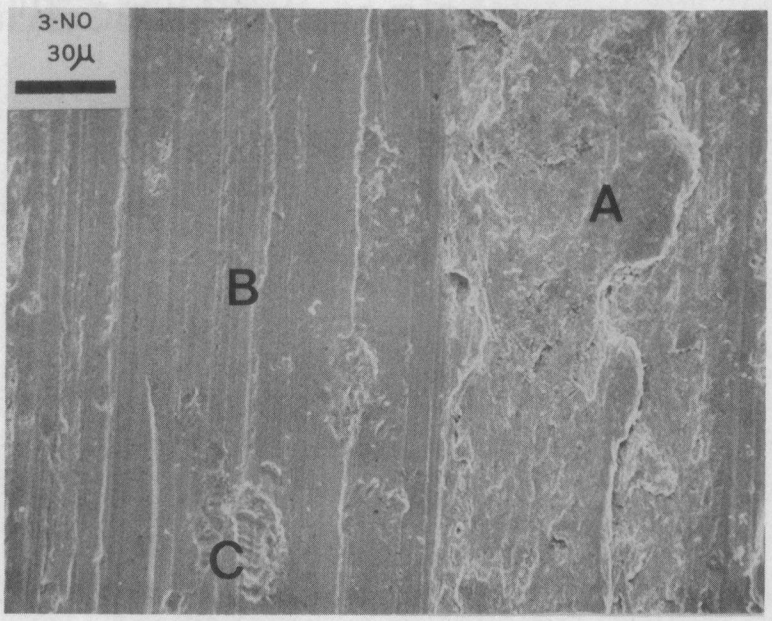

Figure 23. Scanning Electron Micrograph Showing Two Differently Worn Areas (A and B) on a Nickel Test Ring.

side marked A is a very highly distorted region, and adjacent to it (marked B) is a somewhat smoother region. These two areas are typical of the type of wear observed on the nickel test rings. Region A is characterized by smearing, much plastic deformation, and the formation of wear debris which can be seen as small bright specks on the darker background. Region B is similar in appearance to an abraded surface, as can be seen when one compares it to the scanning electron micrograph of the ground surface shown in Figure 11 (page 45). Figure 24 is a high magnification view of the area marked C in Figure 23. Note the highly deformed feature in the center, the formation of wear particles as indicated by arrows, and on either side of the center feature very finely spaced parallel grooves which lie parallel to the direction of travel.

To what mechanisms can these observations be attributed? The test rings were initially separated by high spots in area A of Figure 23. In the initial stages of the test, the real area of contact (a portion of which was area A) was small and contact pressure was high. Consequently, areas in contact initially became coldwelded and severely deformed. Plastic deformation of the nickel in area A resulted in the generation of much debris. As sliding continued, the high area was worn down, eventually allowing contact in the lower regions (one of which was probably region B of Figure 23). Region B has born less of the contact force resulting in less surface interaction and damage. The faint parallel grooves seen in Figure 24 were probably caused by the abrasive action of small microasperities on the surface of a larger asperity or particle on the mating test ring, while the

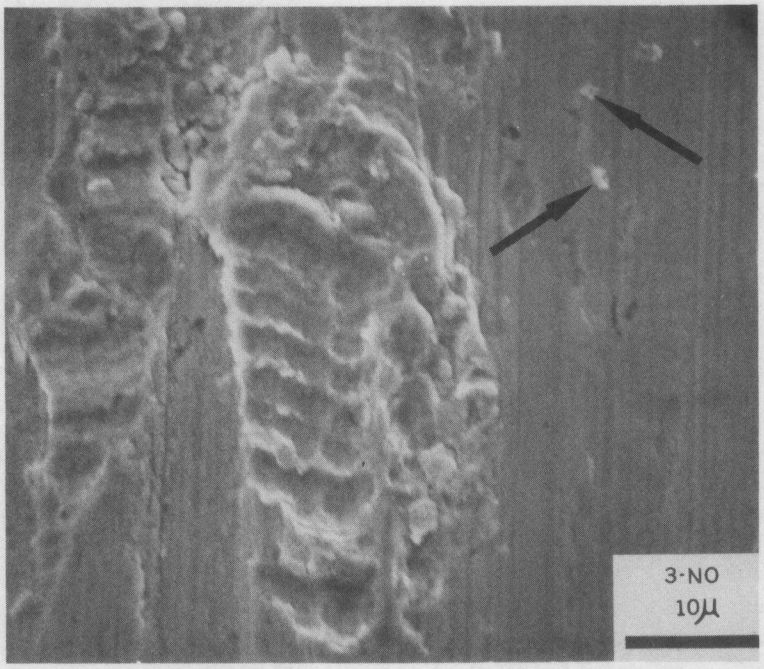

Figure 24. Scanning Electron Micrograph Showing Area C from Figure 23.

distorted area of Figure 24 can be attributed to some form of scuffing.

Figure 25, which shows a large particle (marked A) welded to the side of a well-defined wear groove (marked B), reinforces these conclusions. This is another area of the same groove shown as the relatively smooth region B in Figure 23 (page 63). The side of the particle nearest the groove (see arrow) has a sheared appearance as if at one time it was part of a larger particle, the remaining portion of which continued on its destructive journey around the test ring, gouging as it went the wear track shown as B. Note the layered appearance of the particle and the many jagged perturbations of its surface. If the mating portion of the particle had the same characteristics, it is easy to understand the fine parallel grooves of Figure 24.

Figure 26 is a high magnification view in another area of a very small, approximately 2.0 micron wide groove (marked A). Random asperities are visible in area B, while on the other side of the groove in area C can be seen very fine scratches which are probably comparable to the parallel grooves of Figure 24. There is some fine wear debris at the bottom of the groove.

Figures 27 and 28 are optical micrographs of a different area of this ring. Note in Figure 27 the presence of two large abrasive grooves (see arrows) and pre-test lap scratches indicative of incomplete mating on the left-hand side. The bright polished-looking region (marked A) in Figure 28 consists of several layers that by welding and smearing formed a raised "island" of material. At the upper edge of the "island" (see arrow) is an area in which the welded material has separated slightly from the original load bearing surface. Possibly

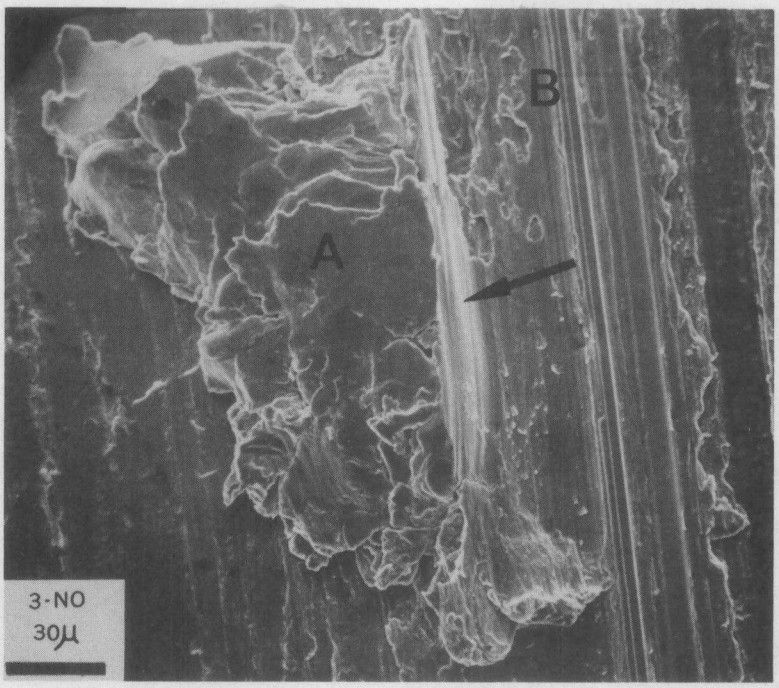

Figure 25. Scanning Electron Micrograph Showing a Large Particle (A) Welded to the Side of a Groove (B).

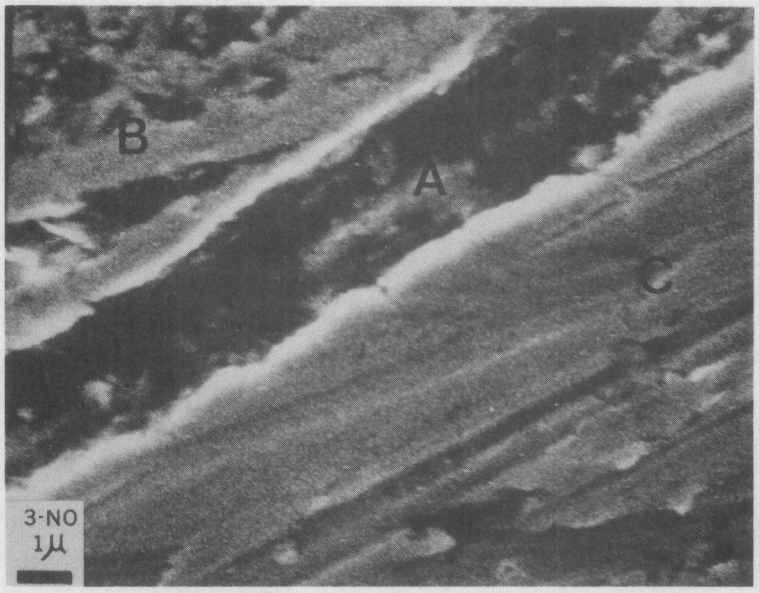

Figure 26. Scanning Electron Micrograph of a Small Groove (A) and Microasperities (B).

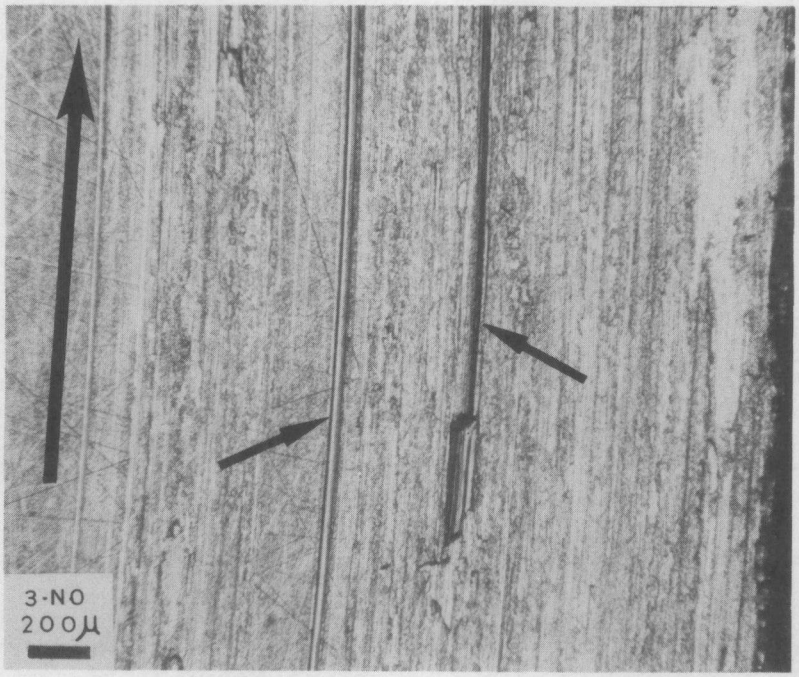

Figure 27. Optical Micrograph of Two Deep Abrasive Grooves (Small Arrows).

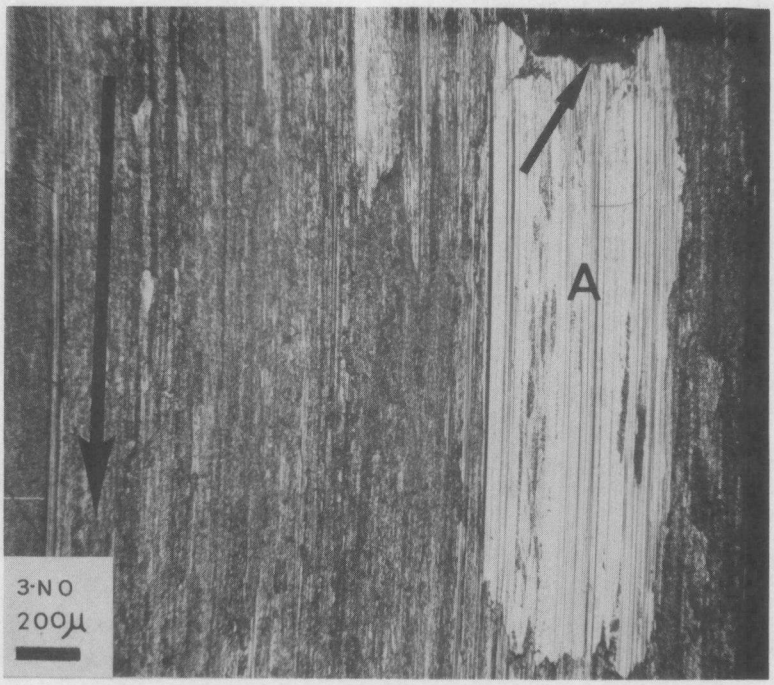

Figure 28. Optical Micrograph of an Island (A) of Welded Material Showing an Up-raised Lip of Material at Top of Micrograph (see Small Arrow).

on termination of the test, when the rings were forced apart, this area was welded more securely to the surface of the mating test ring than to the surface of the ring shown here and was pulled loose. More probably, however, it was "pulled" or "pushed" loose by repeated interaction and welding with material of the opposite surface. Figure 29 is a scanning electron micrograph of the "island" in Figure 28. Figure 30, at higher magnification, shows the layered appearance of the "island." Nondispersive x-ray analysis of this feature showed no evidence of molybdenum, indicating that material used in its formation was generated by the nickel ring and not from the mating nickel-molybdenum test ring.

In Figure 31 is an optical micrograph showing another area in which welding has occurred. Figure 32 is a scanning electron micrograph of the same area. (Note that Figure 32 is a mirror image of Figure 31.) There is a large unusual looking "island" of material below which can be seen the original lapped surface (A) with associated lapping scratches. In region B some semblance of uniform mating of the surfaces of the test rings has occurred and the "familiar" gross wear of the nickel surface is observed. Nondispersive x-ray analysis showed the "island" to contain molybdenum and, hence, the material used in its formation is from its mate, the ordered nickel-molybdenum ring. It appears as if the formation of the island occurred in two stages. Initially, the area of the island marked C became welded and at some later time in the test the area marked D became fixed in place.

Figures 33 and 34 are higher magnified views of the rightmost edge of the island. Note the presence of "tire" marks on the lower

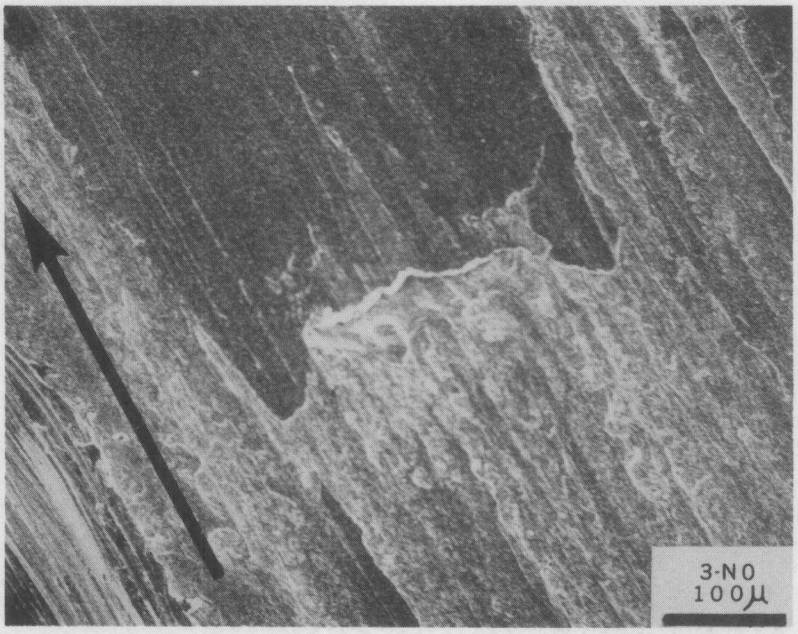

Figure 29. Scanning Electron Micrograph Showing Lip Noted in Figure 28.

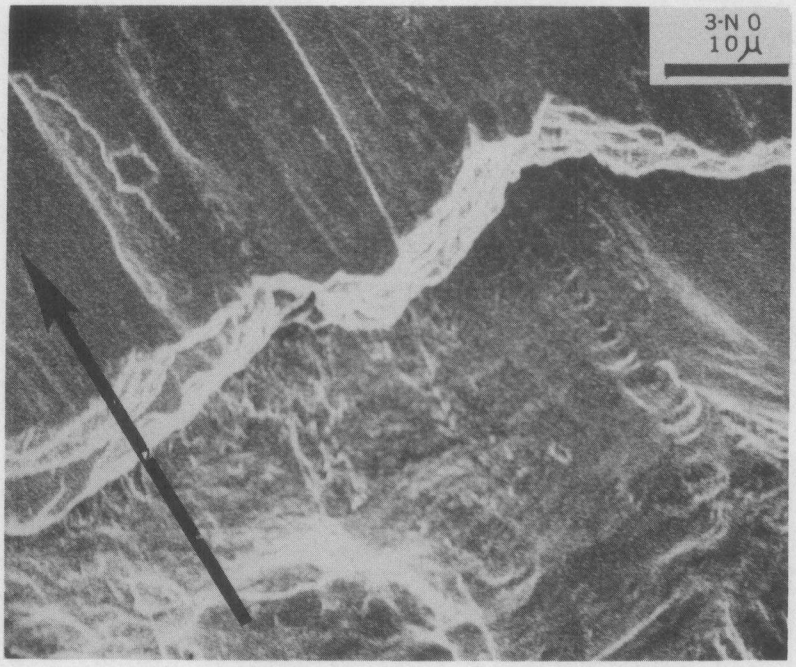

Figure 30. Higher Magnification View of Center of Lip in Figure 28.



Figure 31. Optical Micrograph Showing Island of Ordered Nickel-Molybdenum Alloy Welded to the Surface of Pure Nickel Test Ring.

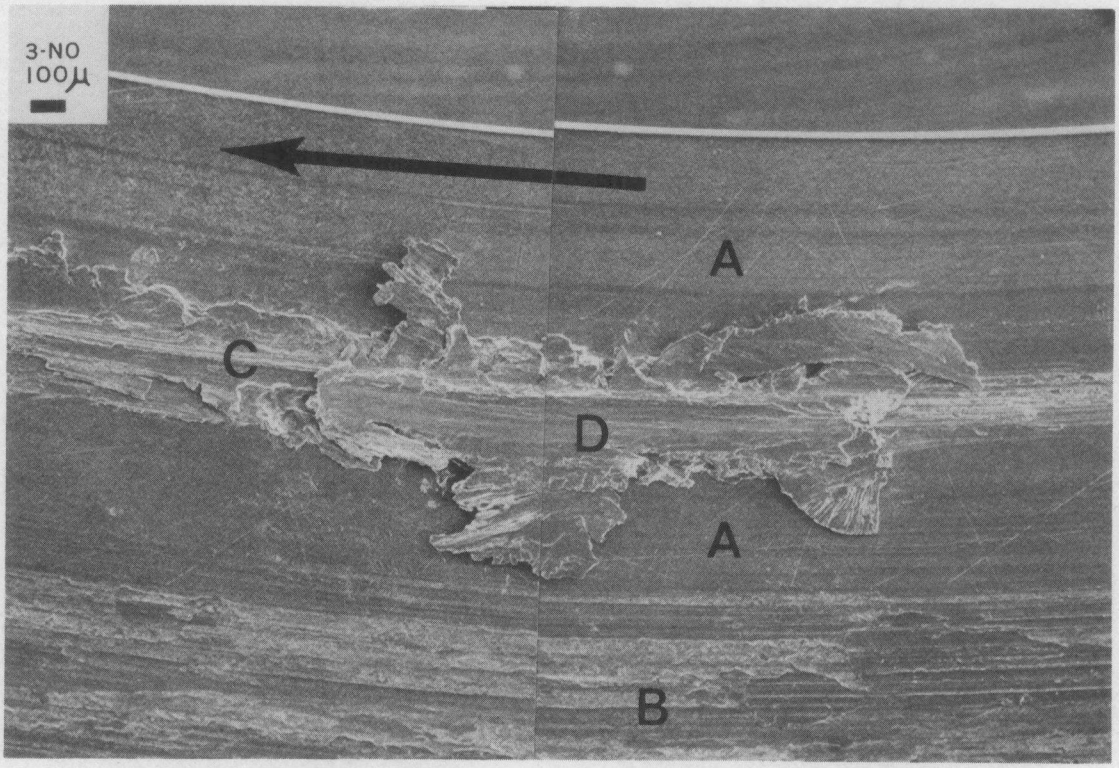

Figure 32. Scanning Micrograph of Feature Shown in Figure 31.

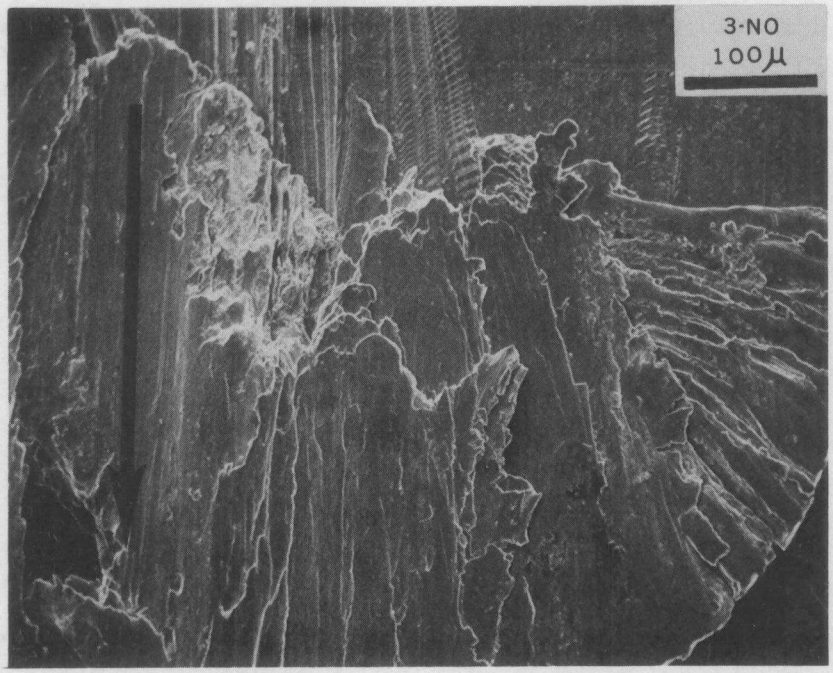

Figure 33. Scanning Micrograph of Right-Most Area of Figure 32.

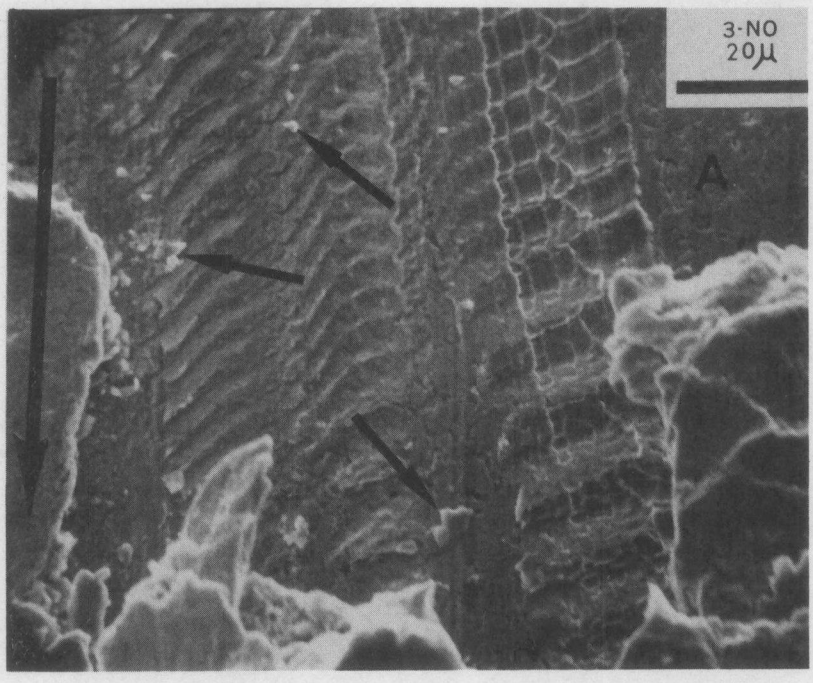

Figure 34. Higher Magnification of Area Shown in Figure 33.

Note particulate matter (small arrows), the layered appearance of the "island," cyclic deformation of the lower layer, and the lapped Area A.

level as if the particle stuck in one position momentarily and then was detached to become welded again, finally resting in the configuration shown. This all seems reminiscent of the stick-slip motion of friction (3). The lower level clearly shows the structure of the pre-test lapped surface (Figure 34, region A). Compare the layered appearance of the island with the particle in Figure 25 (page 67). Note in Figure 32 the presence of a well-defined wear track immediately ahead of the area shown as Figure 33, and in Figure 34 the presence of particles ranging in size from a few tenths of a micron to two or three microns (see arrows).

To illustrate the distribution of molybdenum atoms on the surface of the sample, an area map was made from the region shown in Figure 35. Figures 36 and 37 show the distribution of molybdenum and nickel atoms, respectively. For clarity and orientation purposes, corresponding points of interest are marked A, B, C, and D on the three figures. It has been shown that the dots in the region A of Figure 36 are a result of electronic noise. The areas marked B in Figures 35 and 36 correspond to the surface of the island. The point marked C on Figure 36 appears to exhibit an increased molybdenum content as evidenced by the greater density of dots when compared to the rest of the surface of the island. Note an absence of dots in the area marked C in Figure 37. The absence of dots in areas marked D of Figures 36 and 37 is due to the geometrical "shadowing" of x-rays from the x-ray detector. Note in Figure 35 that in each case the area marked D is characterized by holes or overhanding material. To summarize, then; a fairly even distribution of nickel is observed in Figure 37 except in area C where a possible depletion of

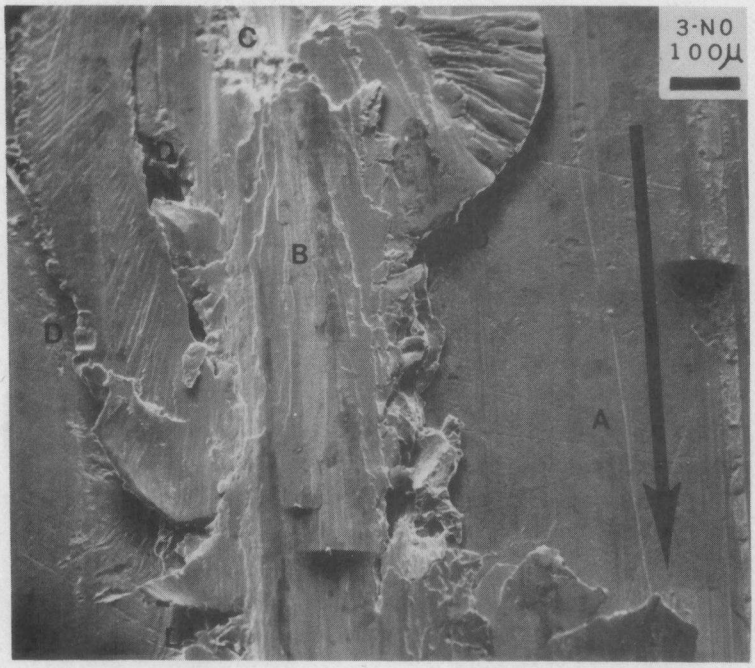

Figure 35. Portion of the "Island," Shown in Previous Figures, in Which Non-Dispersive X-Ray Analysis for Nickel and Molybdenum Was Performed.

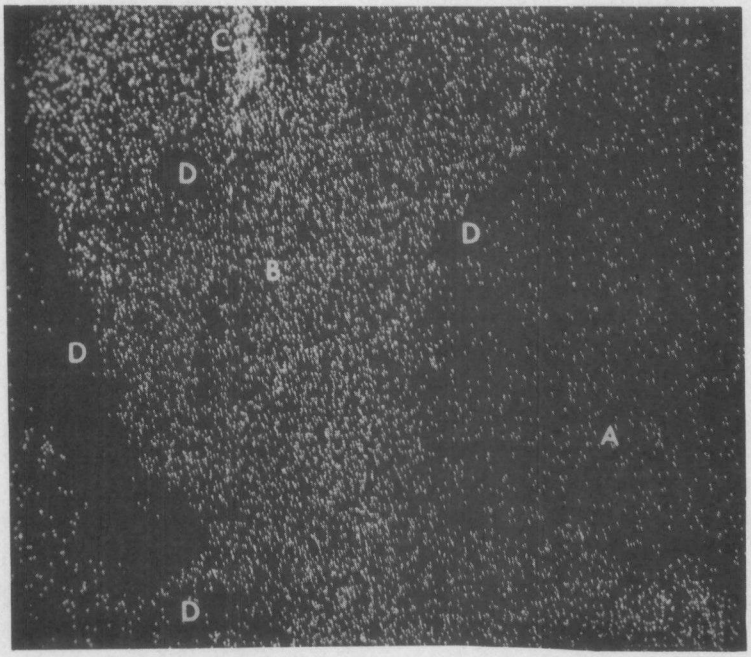

Figure 36. Area Map of Island in Figure 35 Showing Distribution of Molybdenum as Evidenced By Excitation of MoL_{α} X-Rays by the Electron Beam.

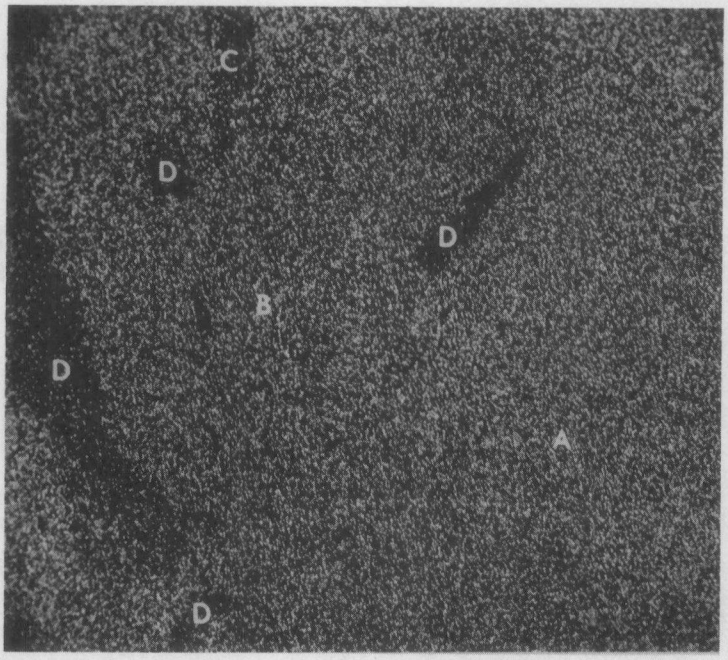

Figure 37. Area Map of Island in Figure 35 Showing Distribution of Nickel as Evidenced by Excitation of NiK_{α} X-Rays by the Electron Beam.

nickel content is observed. And, in Figure 36, molybdenum is distinctly present on the surface of the island, possibly in two different concentrations. Increased molybdenum content in the one area is not readily explainable.

A section was cut along the line marked A on Figure 31 (page 71), it was mounted in cross-section, polished, and then heavily etched for scanning electron microscopy. A scanning electron micrograph of the edge of the sample is shown in Figure 38. An arrow points to the wear track which runs perpendicular to the plane of the paper. Grain boundaries are clearly visible. The substrate was severely attacked by the etchant. Note the areas marked A appear not to have been attacked as severely by the etchant. This is an indication of severe coldworking in the surface and subsurface region of the test ring, supporting past work by Newman, et al. (27) on transmission electron microscopy of nickel wear rings. Their results showed high dislocation density and heavily cold worked material in such areas. It is apparent from Figure 38 that along the surface deformation and cold working were more severe in region A than at the point marked B illustrating the localized nature of surface interaction. The region A of Figure 38 seems to correspond to polished looking areas marked B in Figure 31 (page 71).

Figure 39 is an optical micrograph of layered material on another test ring. The lower level (marked A) is very much out of focus; the upper level or "island" (marked B) is approximately 25 microns higher than the surrounding surface. Figures 40 and 41 are higher magnification scanning electron micrographs of the area shown in Figure 39. The greater depth of field inherent in scanning electron microscopy is clearly

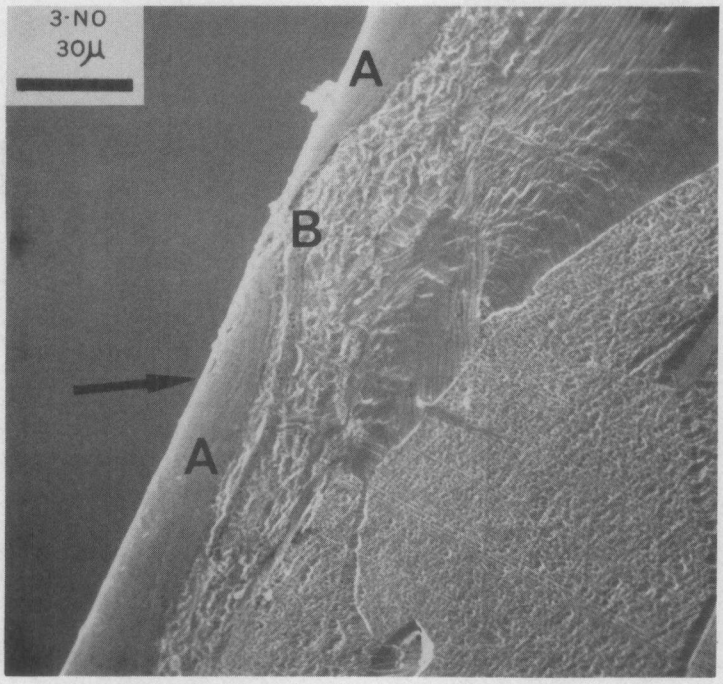

Figure 38. Scanning Electron Micrograph of Polished and Etched Cross-Section from Nickel Test Ring.

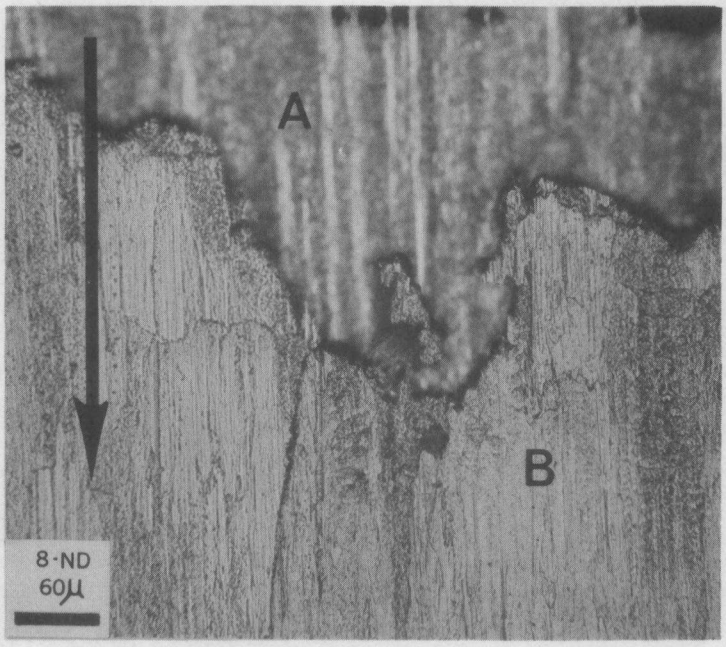

Figure 39. Optical Micrograph of Layered Material (B) on Test Ring 8.

The lower level is marked A.



Figure 40. Scanning Micrograph of Feature Shown in Figure 39.

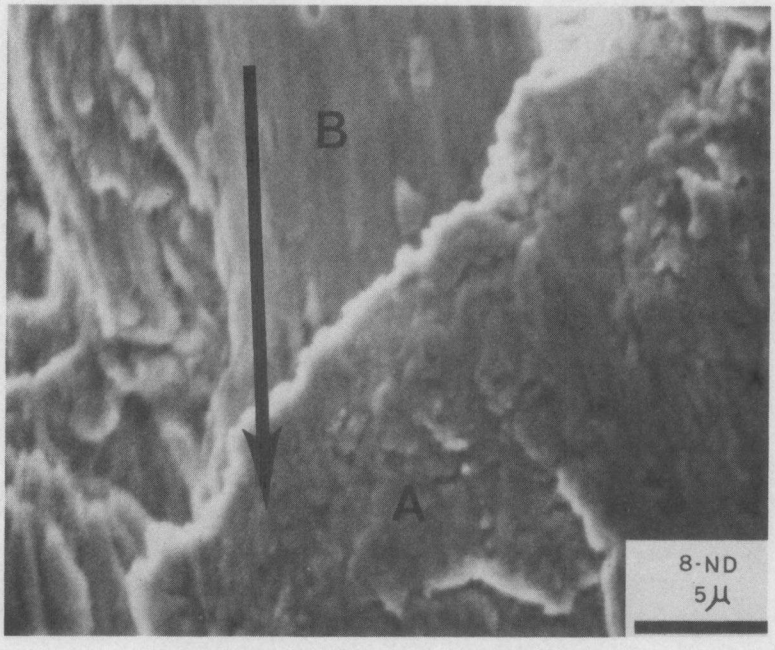

Figure 41. Higher Magnification of Edge of "Island" (A) Shown in Figure 39.

Note the differing appearance of the "island" and the lower level (B).

evident when Figure 40 is compared with Figure 39. Again, the edge of the island has a layered appearance (see Figure 40). The surface of the "island" has a random texture somewhat like that of a lapped surface (Figure 41, area A).

In sharp contrast to the surface of the island, the surrounding material or lower level as shown in Figure 42 has a very directional appearance. It should be evident at this point that in the absence of abrasion this ductile appearing smeared surface is characteristic of severe unlubricated wear in pure nickel. The appearance of the surface is very similar to that observed by Frey (28) on the wear of gold, and is related to the type of stress involved in breaking adhesive bonds. A uniform tensile stress will produce equiaxed uniform dimples, with a nonuniform tensile stress producing elongated or oblique dimples. If a shear stress is involved then the dimples will become more severely elongated as is the case in Figure 42.

Figures 43 and 44 are offered as final evidence of this. These are micrographs of a nickel test ring run against nickel. Note in the center of Figure 43, and slightly to the right of center, holes in the surface (see arrows). Figure 44 is a higher magnification of the center hole. Extremely severe smearing of material over the same area has caused it to be lapped over itself creating holes such as shown here.

Metal build-up on a surface has the effect of separating surfaces to preclude intimate uniform contact. The "islands" discussed up to now have been explained as being a result of welding and smearing material. Also observed on the nickel test rings was the development of wedges of material. The mechanism of their formation seems to be similar to

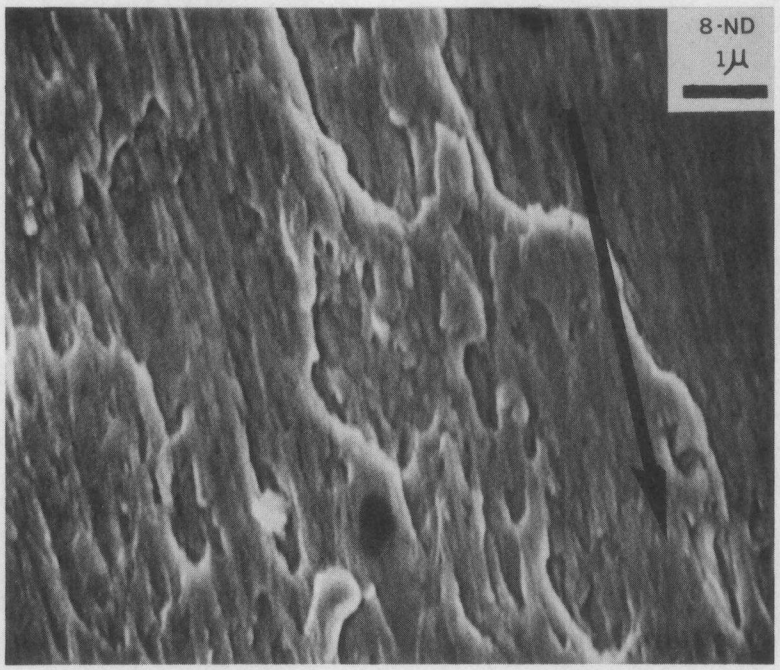

Figure 42. Area B of Figure 41 at Higher Magnification.

This shows the great amount of plastic deformation inherent in the adhesive wear of nickel test rings.

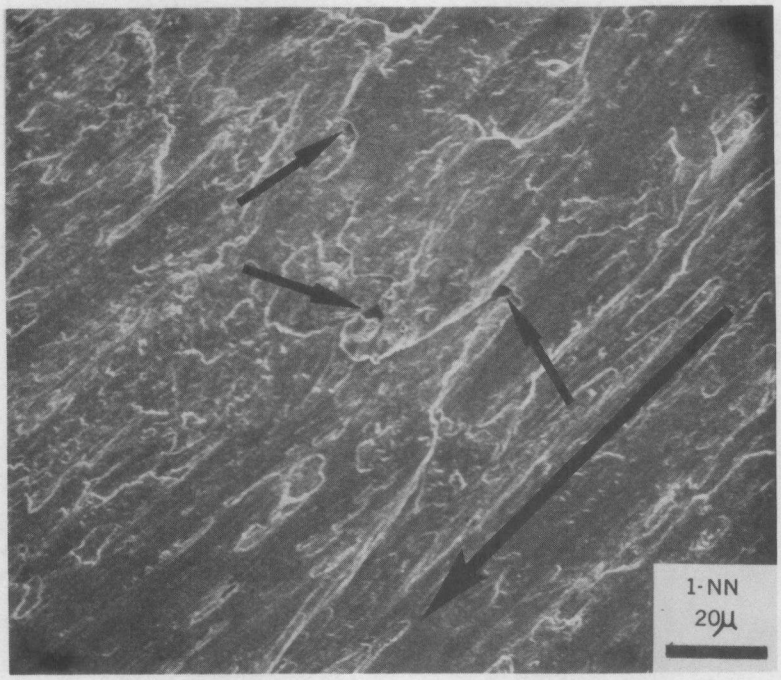

Figure 43. Smeared and Layered Appearance of Nickel Test Ring.

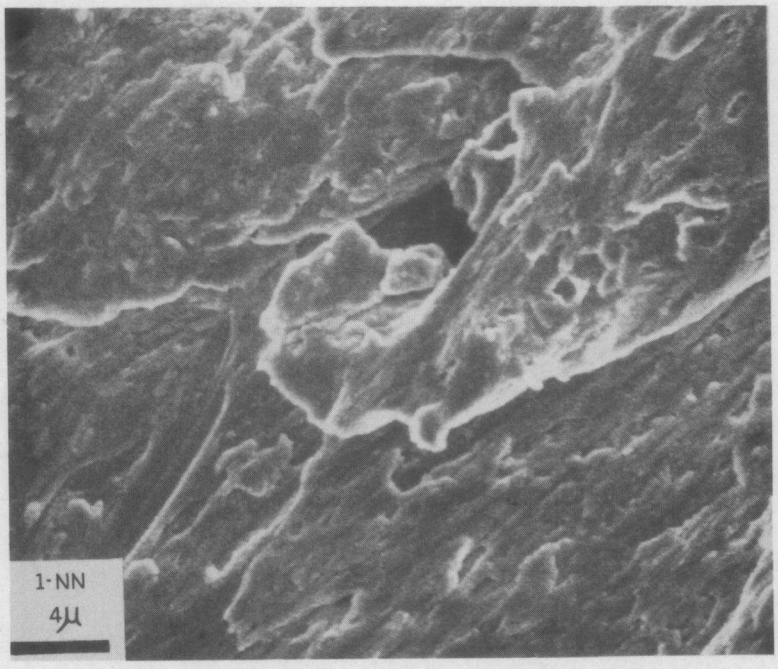

Figure 44. Hole Created by Smeared Material in Area Shown as Figure 43.

that discussed by Cocks (29). Cocks observed the wedge formation with nickel sliding on nickel using an experimental configuration very similar to that used in the present work, although sliding speeds in his work were very slow (0.033 cm/sec compared to 975 cm/sec). His test duration was, however, much longer, with normal loads of the same magnitude approximately as used in this study. Cocks found similar results using aluminum, copper, and steel. His observations with nickel indicated that wedge size grew to a maximum after sliding for five to 15 minutes and then decreased to a minimum after about three hours of sliding, an indication that as sliding progressed the wedges were severely work-hardened, broken-up, and worn away. A primary difference between his tests and those of this research would be in the higher interfacial temperatures reached here.

The effect of these high temperatures can be seen if we compare micrographs of a nickel stator and rotor run against each other, Figures 45 and 46, respectively. Wedge formation and the characteristic abrasion and plastic deformation were observed on the rotor (Figure 46). While on the stator something very different has occurred. The surface of the stator (Figure 45) appears very distorted, a jumble of random swirls similar to waves on a rough sea. A possible explanation lies in the relative mass and available heat sink present for each piece. The rotor is a much more massive piece, fixed securely to a large massive stainless steel shaft; thus, its surface has a very large heat sink conducting heat readily away from it. A very different situation exists for the stator; it is relatively small and is attached loosely to the torque tube. Thus, one would expect surface and subsurface

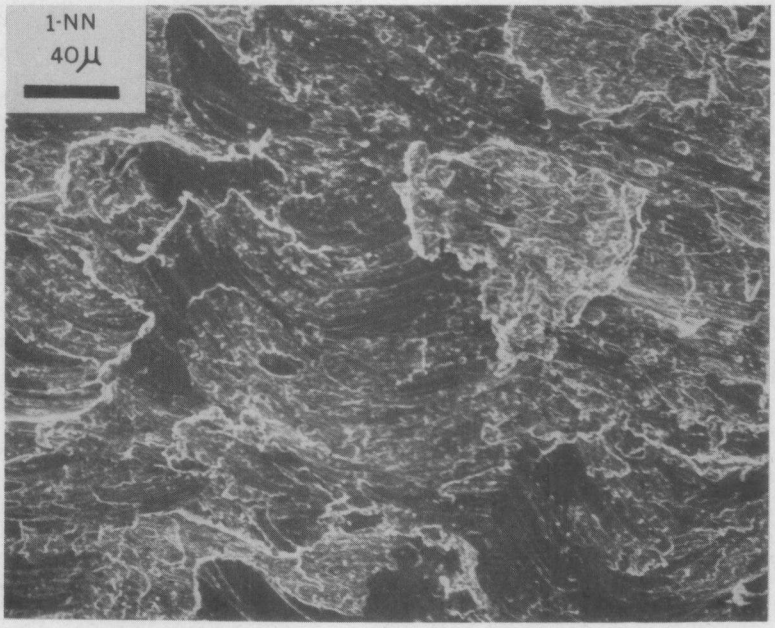

Figure 45. Deformation on the Surface of the Nickel Stator of Test 1.

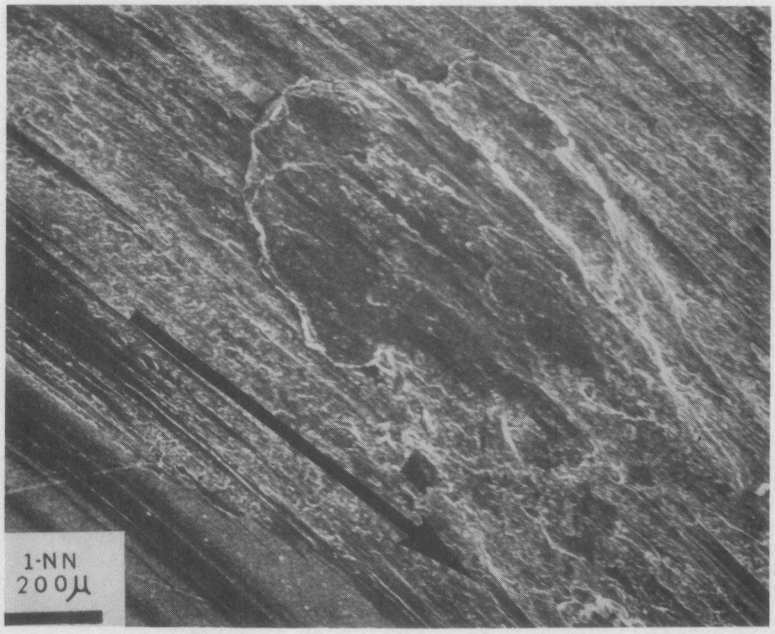

Figure 46. Initial Stages of Wedge Formation.

This micrograph shows the rotor which was run against the surface characterized by Figure 45.

temperatures to be very high accounting for the extremely large amount of distortion.

Figures 46, 47, and 48 show several different views of the wedges under discussion. Figure 49 is a hole apparently left when the wedge formed there was plucked out and carried away as a wear particle. Note in Figure 48, in the spall cavity being formed, the presence of cyclic fatigue type markings (see arrow). Cocks' experiments (29) indicated that the junctions formed when the surfaces were first brought into contact did not break upon initiation of sliding and that the relative motion is taken up by plastic deformation near the junctions. Shearing of the metal occurs at an angle slightly inclined to the surface, the sheared metal emerges from the surface and wedges are formed. The cyclic nature of the bottom of the cavity being formed in Figure 48 indicates that stresses causing shearing of the wedge from the substrate are being relieved in a regular manner by the relatively easy plastic deformation of the mating ring due to thermal softening of that surface. The wedge is being continually work hardened and if it is not sheared off or rolled away it could act as a hard prow to cause severe elongated scuffs on the surface.

In Figure 50 is another spall cavity. This one seems to have been formed as a result of perhaps several related instances of spalling. One wedge originated at point A and a second at point B with both cavities ending near point C. The surface is repleat with fatigue-like striations indicating varying lengths of crack propagation. Many striations were undoubtedly destroyed as the wedge was sheared out of the cavity. Figures 51, 52, and 53 are higher magnification views of areas A, D,

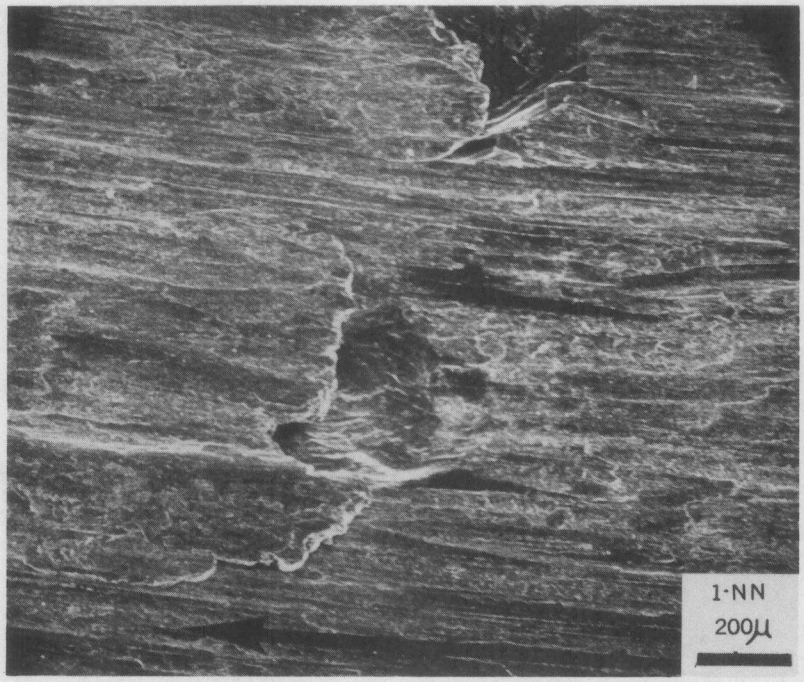

Figure 47. Another View of Wedge Formation on the Surface Shown in Figure 46.

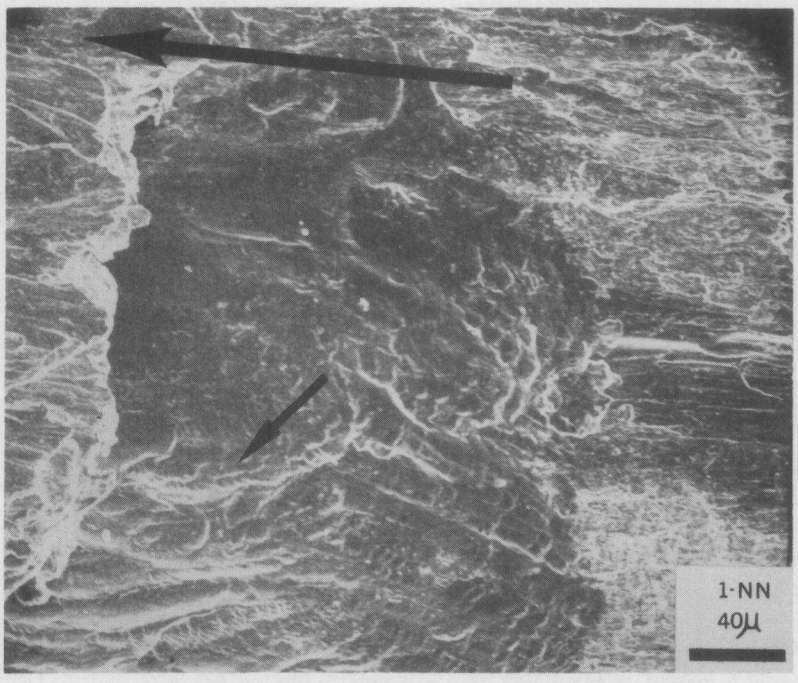

Figure 48. Trailing Edge of Another Wedge and Hole Being Formed as Material is Removed.

Note the presence of fatigue markings (small arrow).

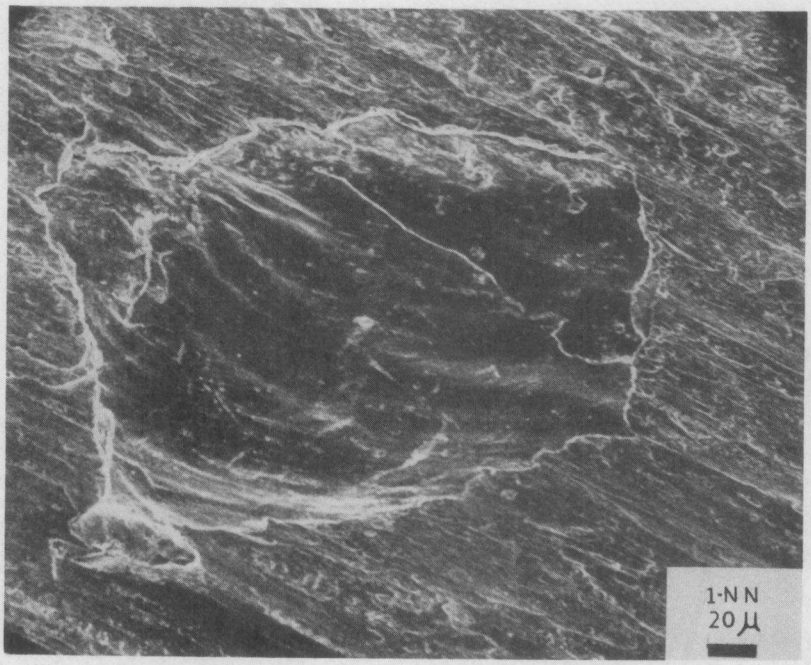

Figure 49. Spall Cavity or Hole Formed on Wedge Removal.

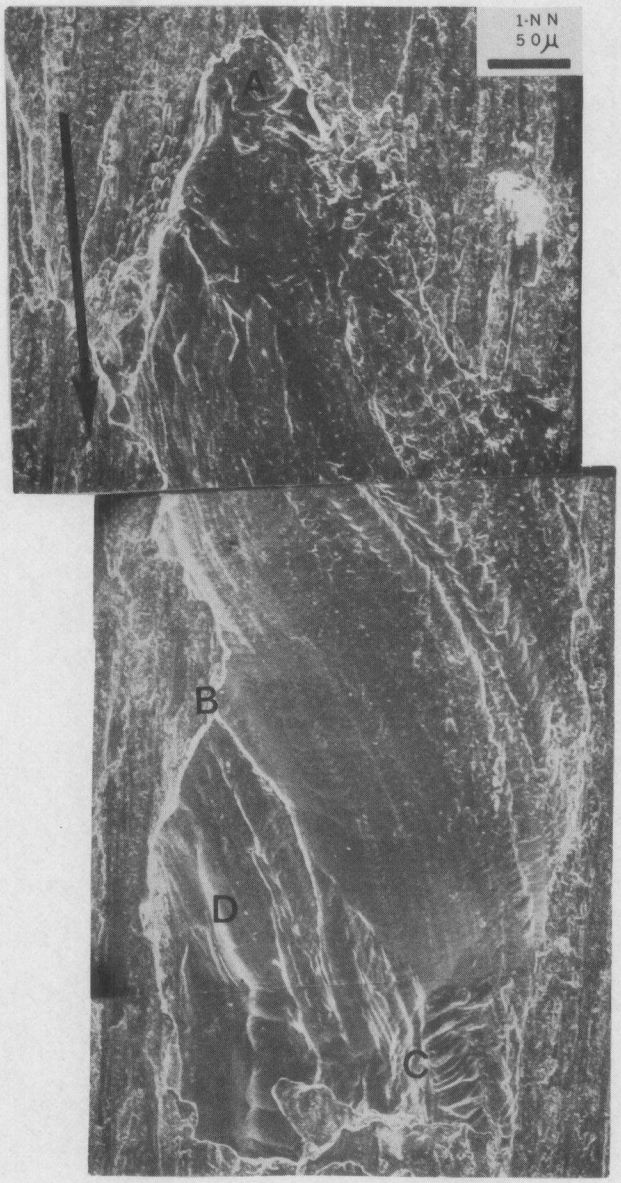

Figure 50. Spall Cavity Left as a Result of Perhaps Several Related Instances of Wedge Formation.

Wedges initiated at points A and B.

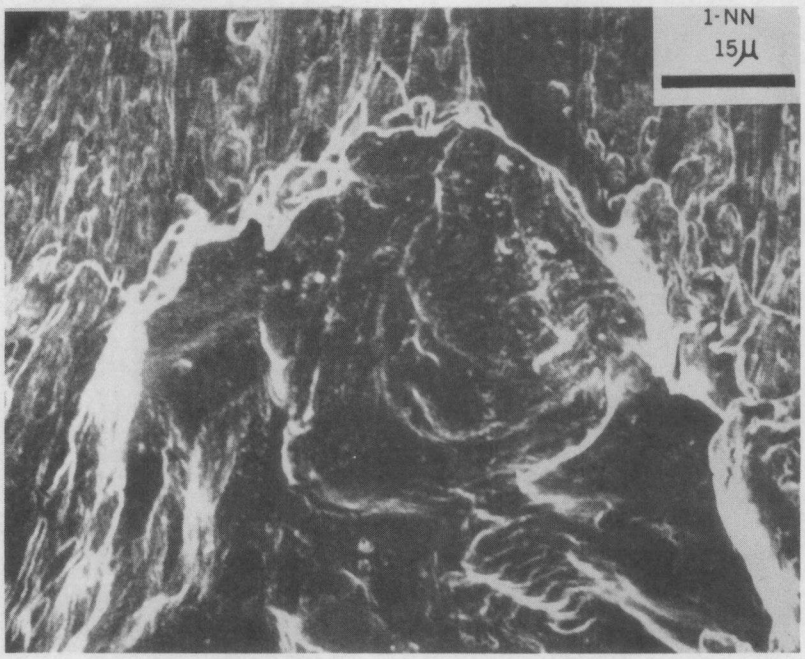

Figure 51. Magnified View of Area A Shown in Figure 50.

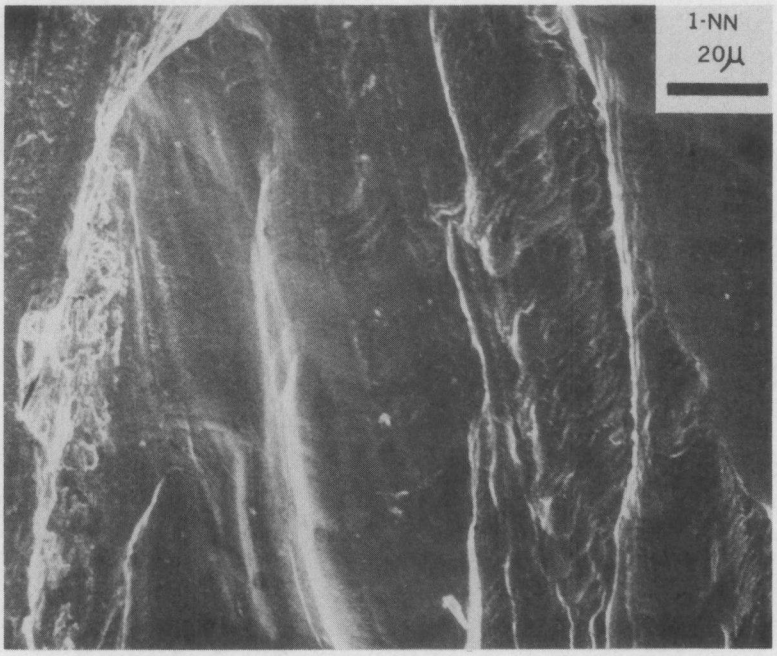

Figure 52. Magnified View of Area D Shown in Figure 50.

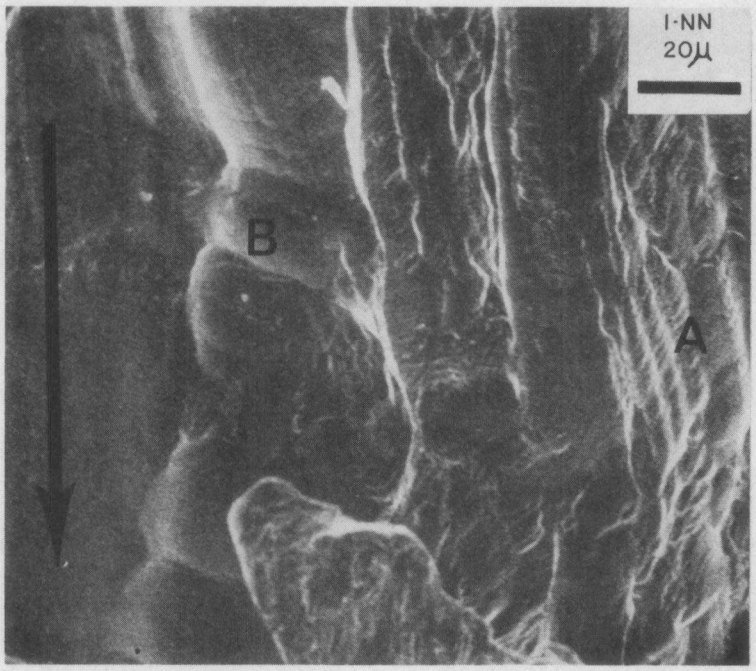

Figure 53. Magnified View of Area C Shown in Figure 50.

and C, respectively, of Figure 50. Note the short length of crack propagation in area A of Figure 53 versus the distance of propagation in area B. Figure 54 shows details of the center portion of Figure 53, and Figure 55 gives a better view of area A. Note the holes or voids present in Figures 54 and 55. In Figure 55 they lie in the bottoms of the fatigue marks. Their origin is not known at this time.

Disordered Nickel-Molybdenum Wear Surface

Figure 56 is an optical micrograph showing what seems to be fairly typical of the type of worn surface observed on the disordered test rings. It is characterized by very uniform plastic flow with little or no abrasion or creation of wear debris. Figure 57 is a scanning electron micrograph of an area similar to that shown in Figure 56. Note the layered appearance of the surface, a portion of which is shown at higher magnification in Figure 58. Figure 59 is another area with what appears to be a uniform abrasive groove (marked A) barely visible, running through the center of it. At the top portion of Figure 60, area A, note what appears to be a gouged or scuffed area. Again, evidence is seen of the material being lapped over itself.

Figure 61 is a scanning electron micrograph of a portion of test ring eight showing a comparatively large wear particle with the wear track (marked A) it has obviously created, trailing behind. The surrounding surface shows no evidence of the original pre-test lapped structure and is very similar in appearance to that observed on specimen eleven. One difference between the two surfaces is shown in Figure 62.

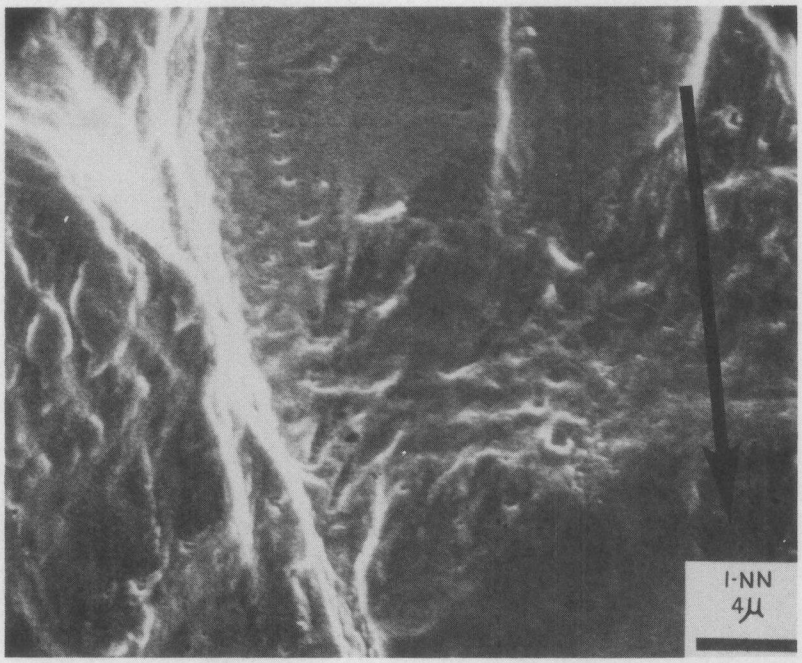

Figure 54. Higher Magnification of Center of Figure 53.

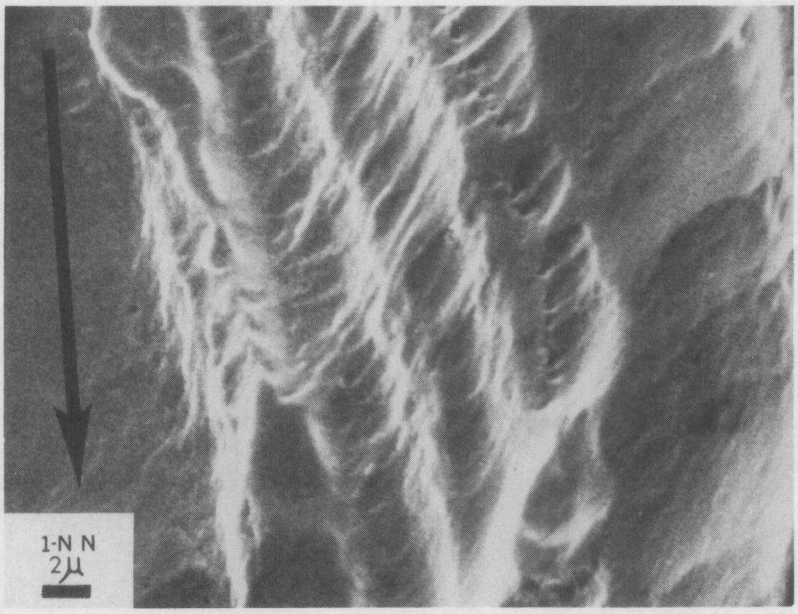

Figure 55. Area A of Figure 53.

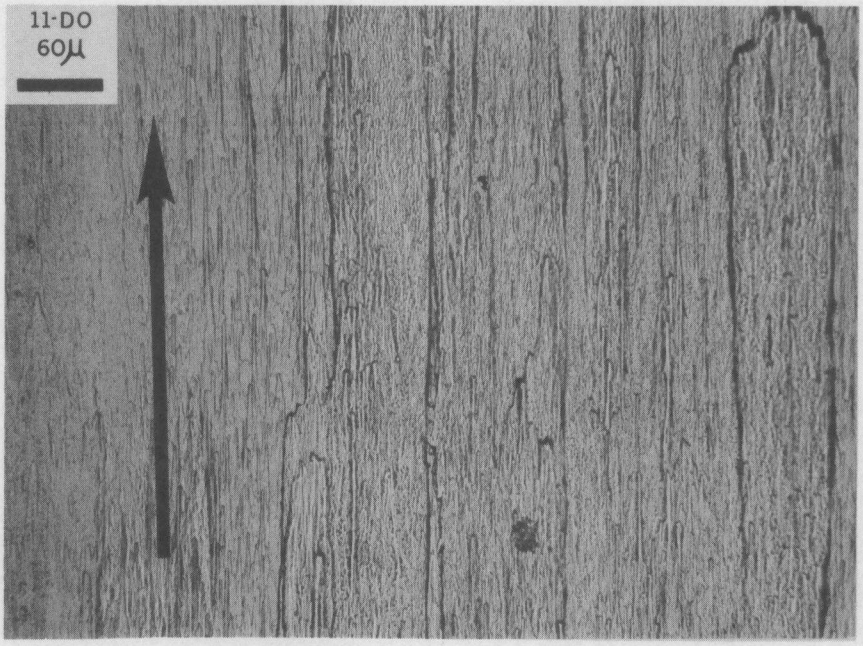

Figure 56. Optical Micrograph Showing the Surface of a Disordered Test Ring.

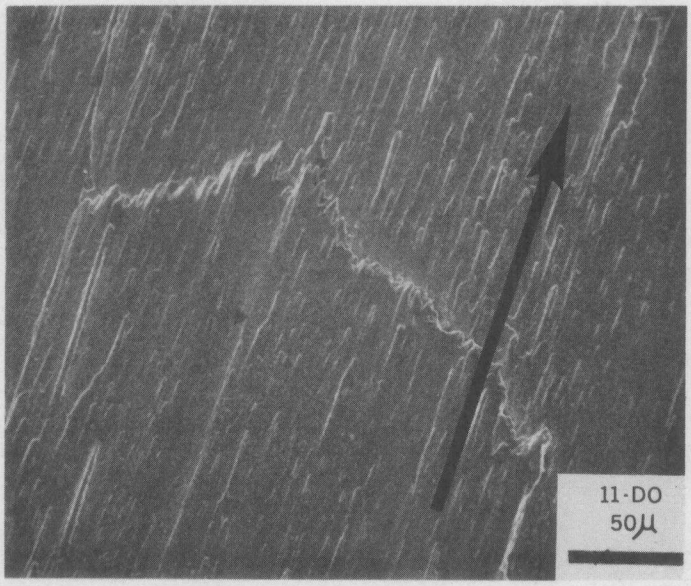

Figure 57. Scanning Micrograph of the Surface of a Disordered Test Ring.

The surface is uniform in appearance and is characterized by much smeared material.

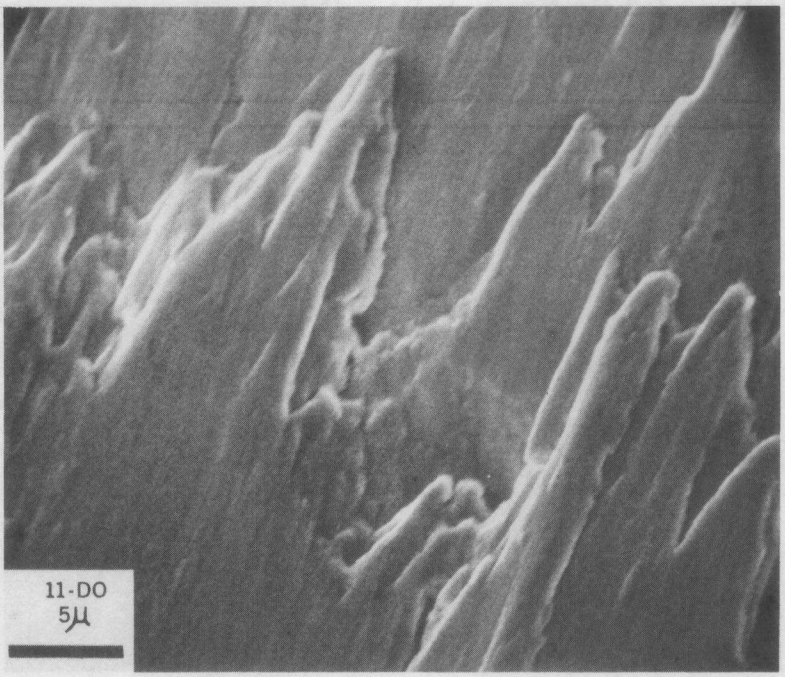

Figure 58. Higher Magnification Showing the Edge of the Raised Area Shown in Figure 57.

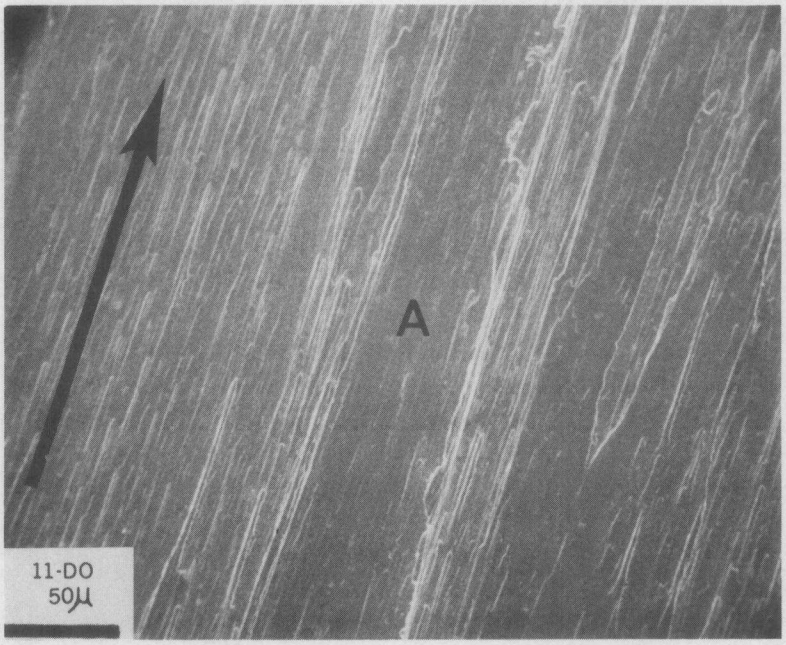

Figure 59. Characteristic Surface Flow of Disordered Material.

Running from bottom to top of the micrograph can be seen a faint abrasive groove (A).

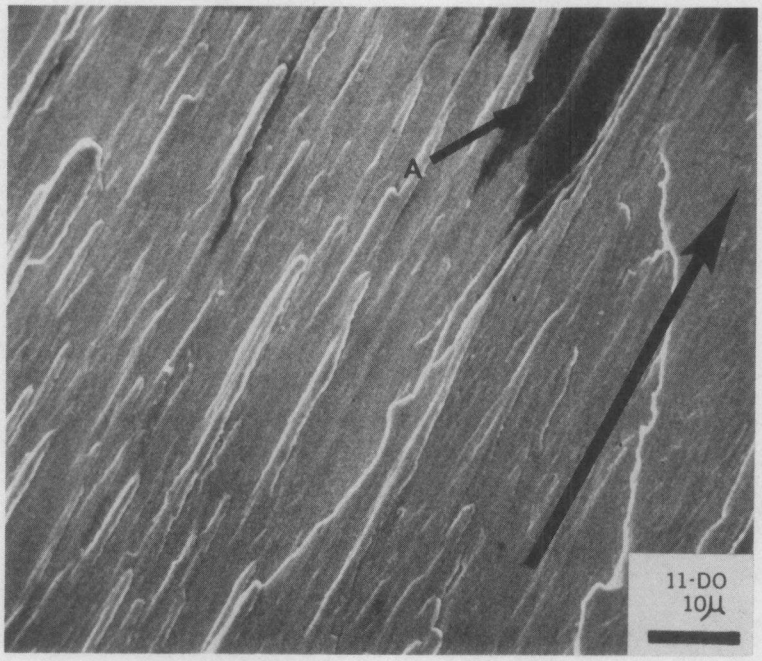

Figure 60. Scuffed Region (A), Surrounded by the Layering and Surface Flow of a Disordered Test Ring.

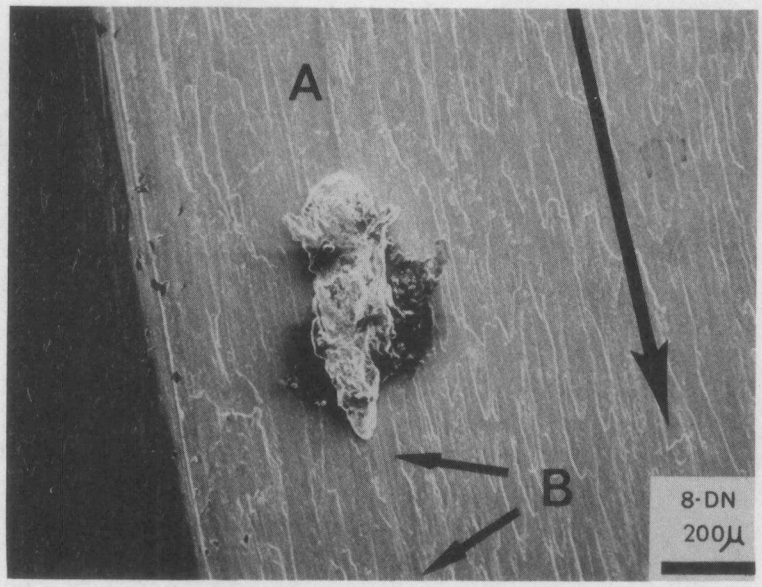

Figure 61. Another Test Ring (8) Showing a Large Particle with an Abrasive Groove (Marked A and B) It Has Created.

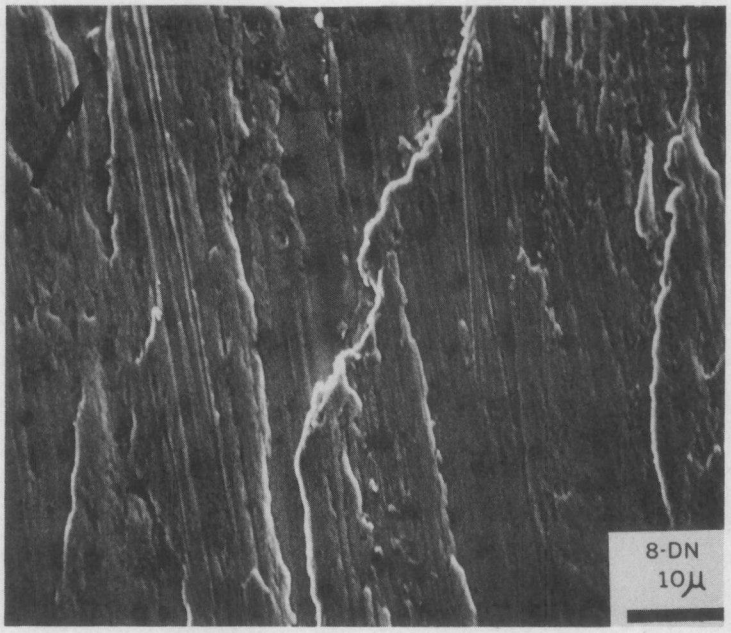

Figure 62. Magnified View of the Surface of Test Ring 8.

Evidence of abrasion and scuffing can be seen; also note small holes covering the surface.

Note the presence of many tiny holes which are not in evidence on micrographs of specimen eleven (compare Figures 60 and 62). These holes cover the entire surface and are possibly attributable to the lowest areas between asperities in the original lapped surface. The smearing appears somewhat more uniform on specimen eleven and thus could have masked holes present on it. Temperature measurements (Figures 17 and 19, pages 55 and 56) show that temperatures were considerably higher in test eleven than in eight. Thus, plastic deformation in the form of surface flow would have been considerably easier due to the thermal softening of the material associated with higher temperatures in test eleven.

Figure 63, however, would seem to void the above hypothesis concerning the origin of the holes. This micrograph was taken of the bottom of the wear track formed by the particle in Figure 61 (area A). It, too, clearly shows the presence of these holes. Since they are present here in the bottom of a groove, it is unlikely that they can be attributed to the lapped structure. Note in Figure 63 the fine parallel sided abrasive groove marks. They were undoubtedly caused by small asperities on the particle of Figure 61. After this particle became welded, a portion of it was torn loose, adhering to the mating surface to form fairly evenly spaced gouge marks shown as B in Figure 61. Note in Figure 62 the appearance of scuffed regions (see arrow). The mechanism of scuffing is similar in nature to prow formation and is discussed by Macdonald (30).

Figure 64 is a higher magnification of the side of the particle shown in Figure 61. There are several points of interest that can be

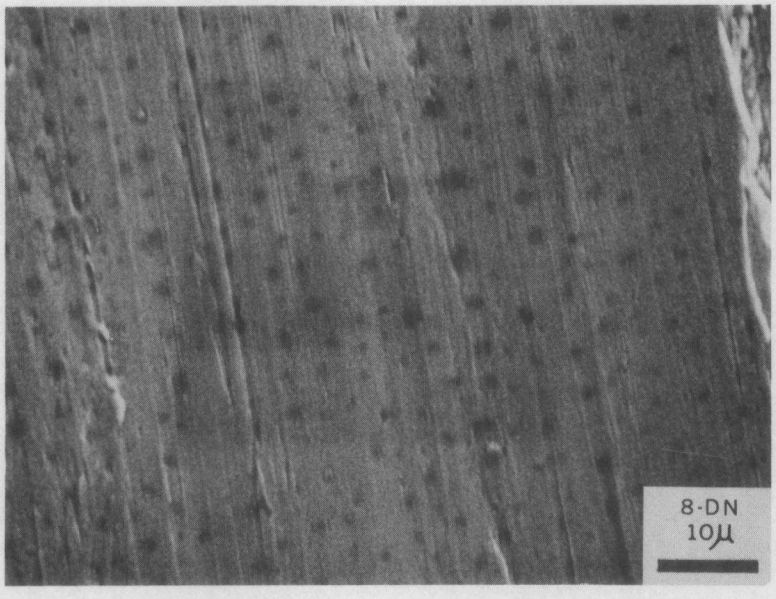

Figure 63. Bottom of Groove Shown as Area A in Figure 61.

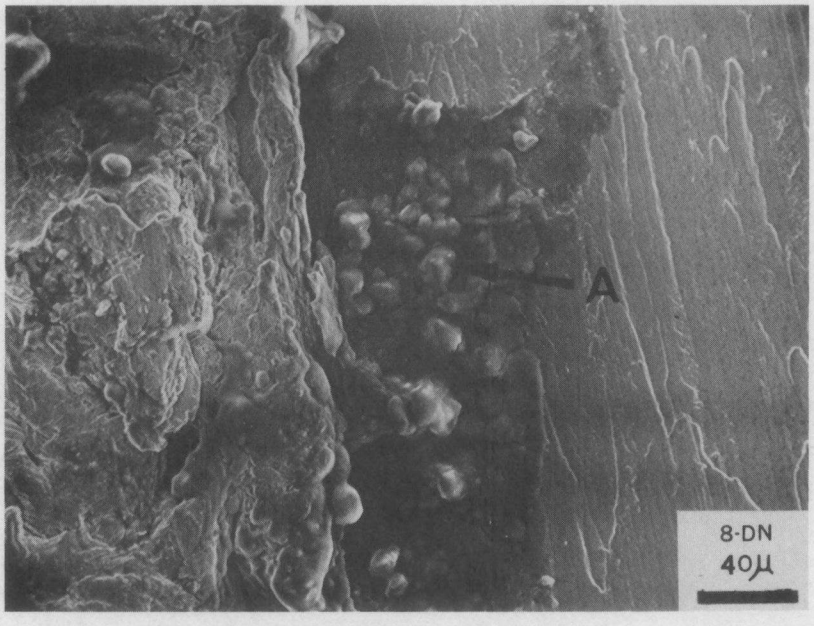

Figure 64. Side of Particle Shown in Figure 61.

In Area A is what appears to be an oxide.

made. Note in the center of the micrograph an area A that has the cake-like appearance of an oxide. There is no apparent explanation for the presence of an oxide as tests were run in an argon atmosphere. The particle itself is very rough and irregular, almost as if it was in the process of being broken up or fragmented, to be spun out of the system at some later time. Note the presence of a dendritic-like structure (see arrows) in Figures 65 and 66 (magnified views of an area of the particle shown in Figure 61 on page 95). It is possible that the particle was once a molten ball of material that solidified quickly on cooling to give the structure shown. If so, then what prevented the material from being smeared out? Perhaps it was formed and solidified during momentary separation of the test surfaces. Non-dispersive x-ray analysis of the particle revealed no molybdenum. Thus the material for the particle must have originated on the mating nickel test ring.

In Figures 67 through 70 are shown shots of a similar particle on another sample. This particle was responsible for grooves on both test surfaces. The surface of the particle is similar in appearance to a lapped surface in places (Figure 70). Again, note the presence of what appears to be a dendritic structure. In Figure 68 can be seen a large number of abrasive grooves and many fine particles (see arrow). The dominant operating wear mechanism seems to be abrasion with some smearing, although not so pronounced as in tests eight and eleven (other disordered samples) in which the complicating effect of particulate matter was not so much in evidence.

Figures 71 through 73 are optical micrographs showing a

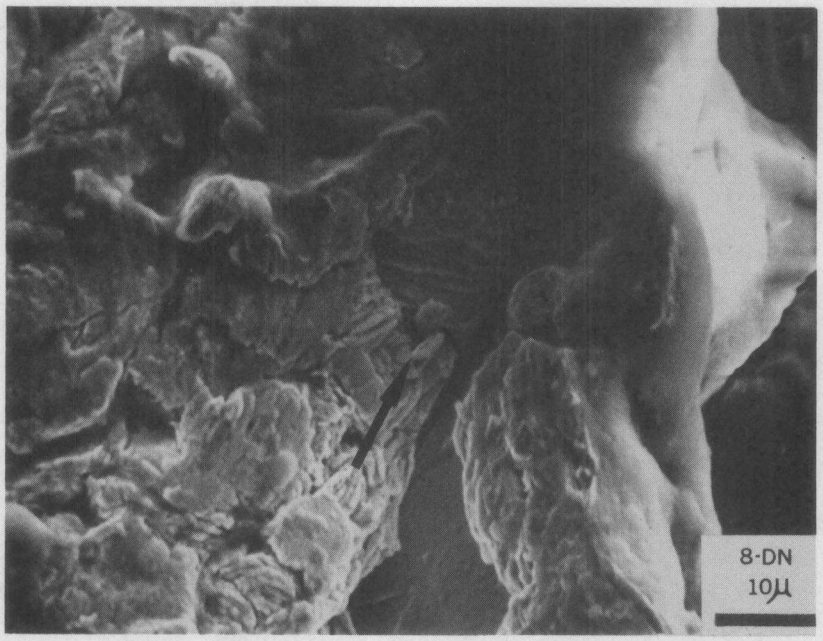

Figure 65. Another Area on the Side of the Particle Shown in Figure 61.

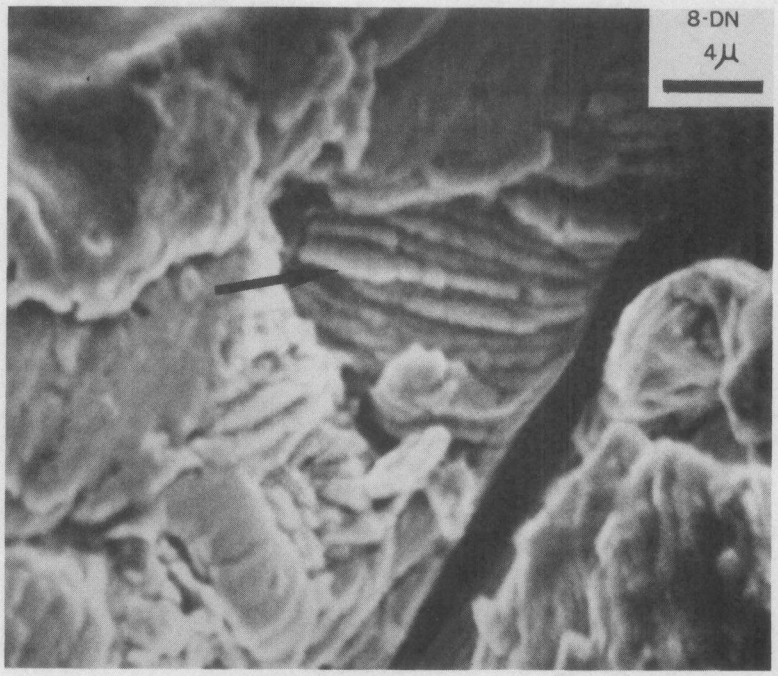

Figure 66. Magnified View of Center of Figure 65.

Arrow points to what appears to be a dendritic-like structure.

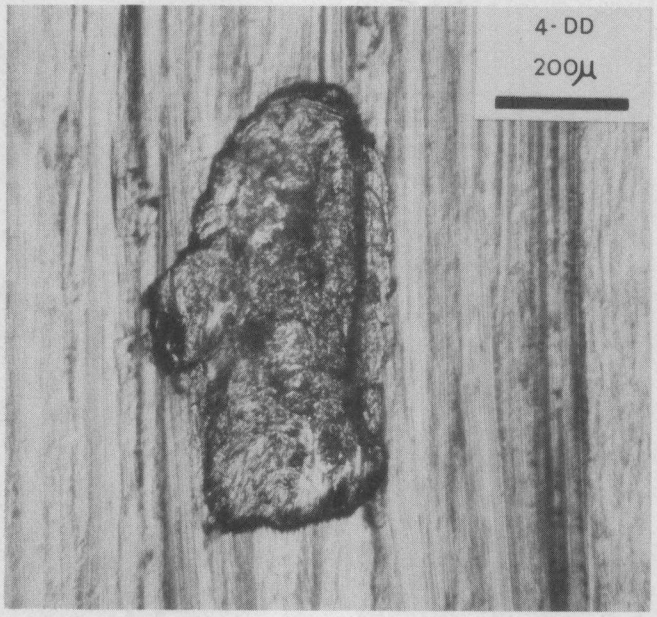

Figure 67. Optical Micrograph Showing a Particle on Disordered Test Ring 4.

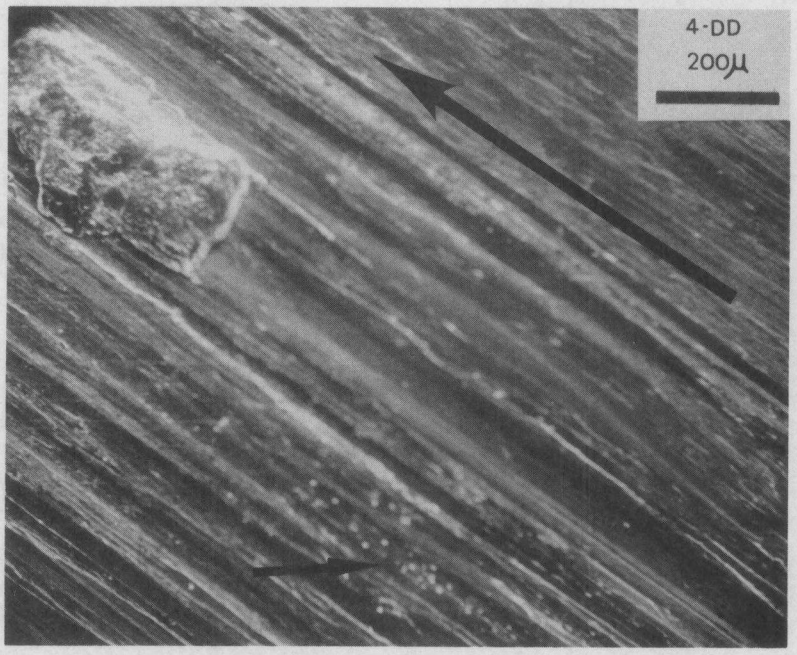

Figure 68. Scanning Electron Micrograph Showing Particle Noted in Figure 67.

Note the rather deep groove it has created and particles on the surface (arrow).

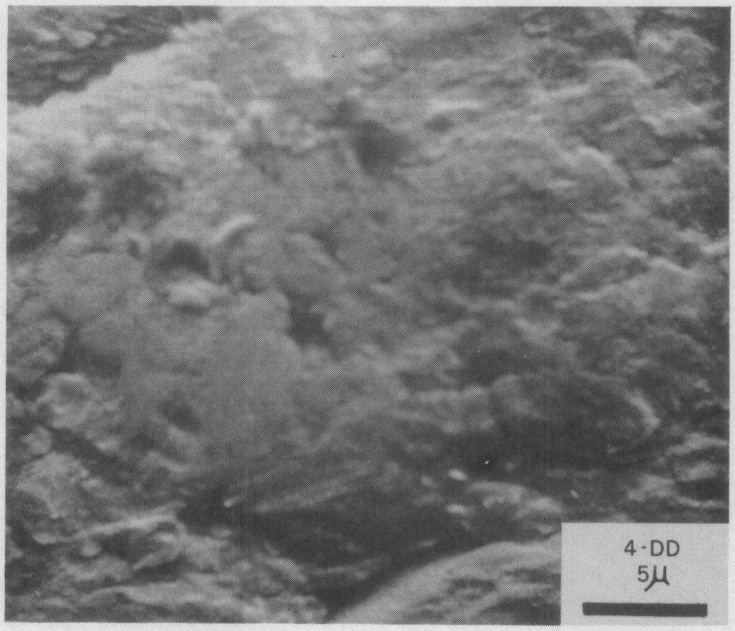

Figure 69. Surface of Particle in Figure 67.

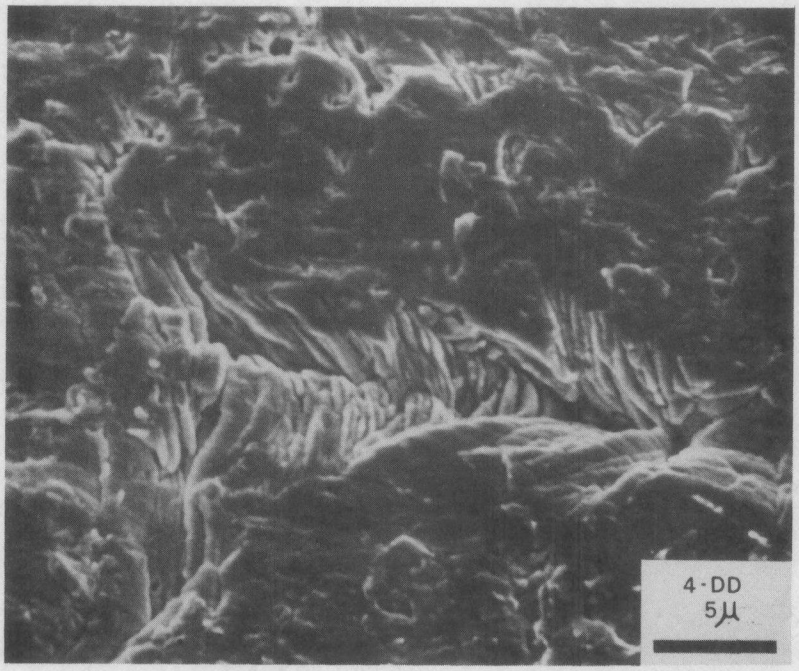

Figure 70. A Different Area on the Surface of the Particle in Figure 67.

Note the dendritic-like structure and that the surface is similar in appearance to that of the pre-test lapped surface.

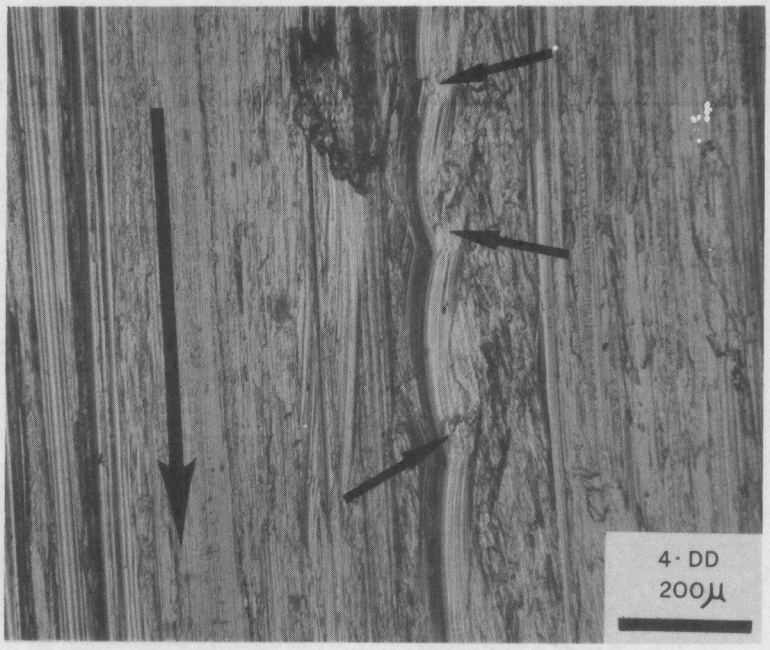

Figure 71. Optical Micrograph Showing Large Groove.

The particle or asperity that has created this groove has been interrupted from its straight line path parallel to the wear direction at several points (small arrows).

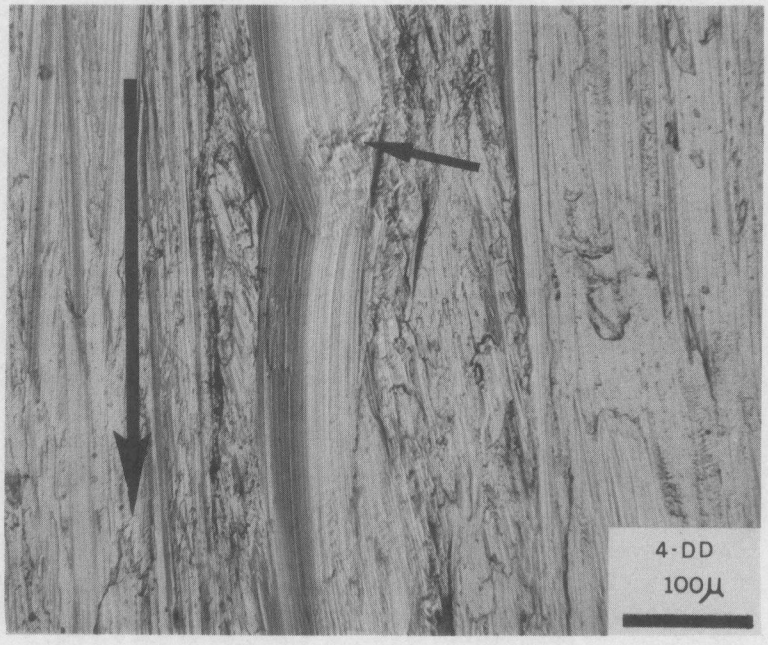

Figure 72. Optical Micrograph Showing a Magnified View of One of the Changes of Direction in Figure 71.

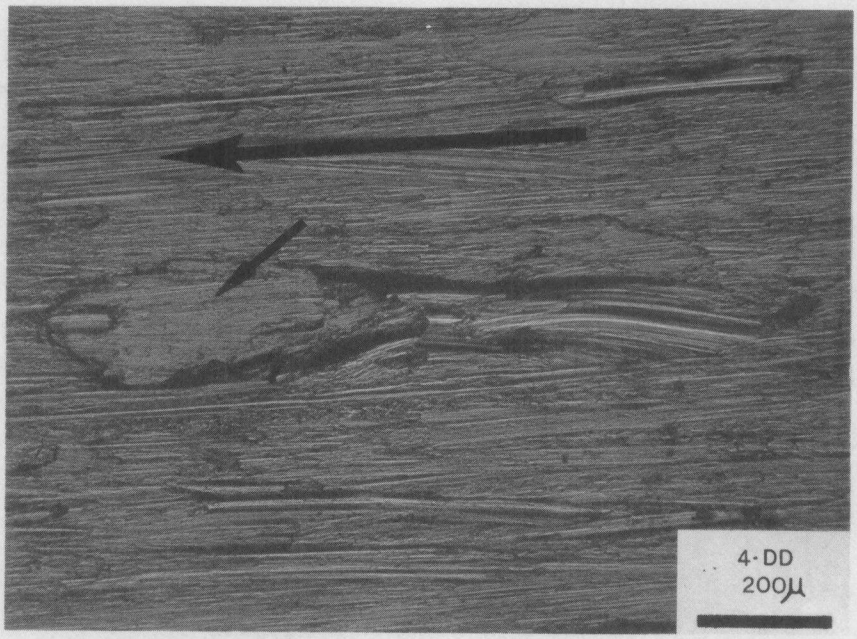

Figure 73. The Wedge, or Portion of the Asperity that Created the Groove Shown in Figures 71 and 72.

different region of the surface and a very unusual feature. Here is seen not the typical straight parallel sided abrasive grooves, but a long groove which in a very uniform manner is constantly changing direction. Figure 71 is a low magnification optical micrograph showing several such changes of direction (see arrows), and Figure 72 is a magnified view of one of the areas in which the change of direction occurred. At a point out of view of Figure 72, the "chain" broke up, becoming a series of evenly spaced gouge marks ending in the feature (see arrow) shown in Figure 73. This is apparently the particle that caused the damage, a prow or wedge of material probably gouged loose in the last revolution or so of the test. For some reason it had a tendency to veer away from the normal direction of sliding. Possibly it was coming into contact with local hard spots on the surface, causing it to deviate in the manner shown; perhaps its shape was a critical factor.

Figure 74 is an optical micrograph showing one of several particles (see arrow) approximately 10 to 20 microns high which were plucked out of the surface of test ring nine at an early point in the test. Note the extremely low wear of the surrounding surface; lapping marks are clearly visible. The presence of a large number of these particles on the surface indicates that early in the test the rings were separated by, and sliding on, their tops, giving rise to incomplete mating and uneven wear of the surfaces. If the test had proceeded further, the particles could have been broken up to act as an abrading media and allow more complete mating. It is even possible that the localization of interfacial temperatures at these particles

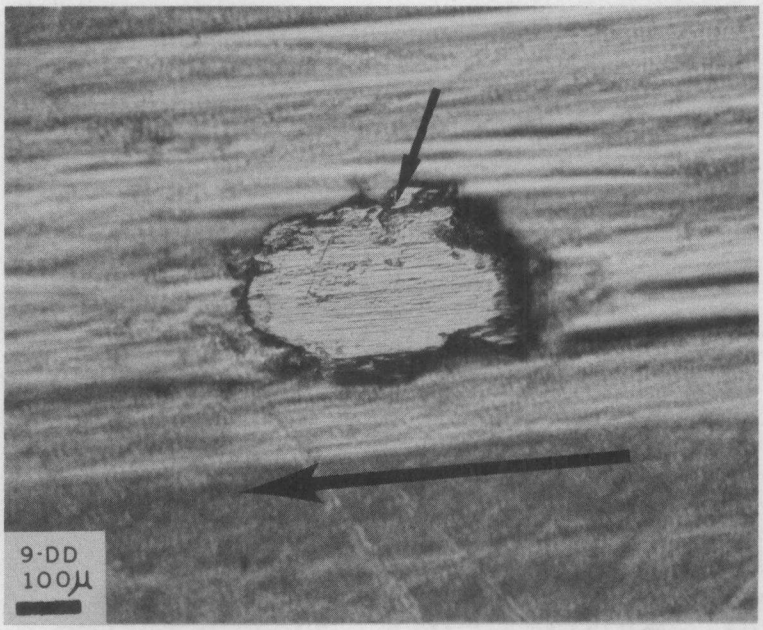

Figure 74. One of Many Particles Welded to the Surface of Test Ring 9.

could have induced the disorder-order transformation in them.

Ordered Nickel-Molybdenum Wear Surface

Figure 75 is a scanning electron micrograph of the surface of the ordered test ring of test eleven. Figures 76 through 79 are higher magnification views of regions shown in Figure 75. Note in Figure 76 there are three clearly different areas with a fourth area out of view slightly to the right; each area exhibits a different degree of wear. These areas are shown at higher magnification in Figures 77, 78, and 79. In Figure 77 can be seen the structure of the original lapped surface. Wear in this area is evidenced by the presence of faint abrasive grooves. Immediately to the right of this area wear has been of a more severe nature (see Figure 78) almost eradicating all trace of the pre-test structure. Flattened asperities are, however, still in evidence and on the right can be seen a very pronounced groove. In Figure 79 the wear is more severe; here can be seen one of several wear grooves (marked A), and what appears to be a scuff (marked B). In area B is a quantity of what seems to be debris. This example is typical of the wear observed on the ordered samples on which the degree of wear ranges from the mild abrasion shown in Figure 77 to the severe surface destruction shown in Figure 79.

The four areas discussed above can be hypothetically explained by considering the interaction of a large asperity on the mating surface, as was done in the discussion of the nickel wear surface. The highest portion of the asperity was in initial contact with the region shown in Figure 79, area B. High contact pressure due to the real

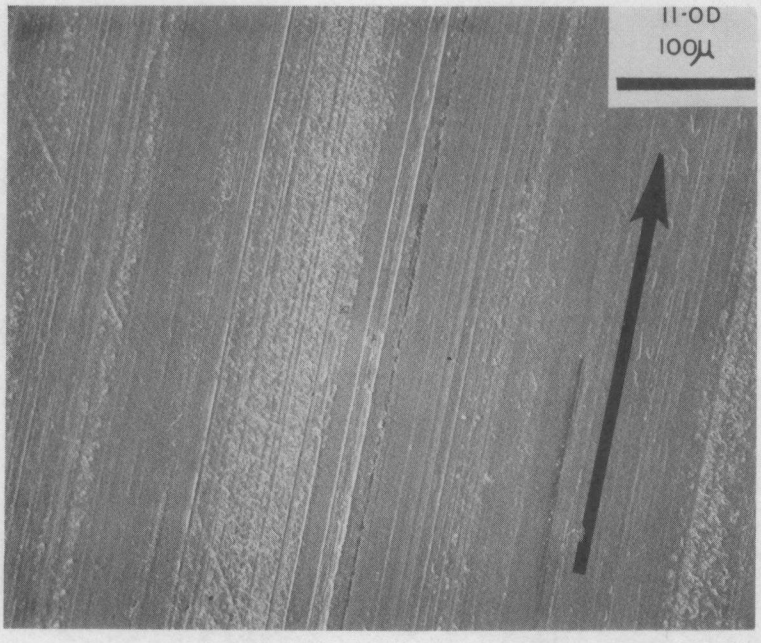

Figure 75. Scanning Electron Micrograph Showing Wear Typical of the Ordered Test Rings.

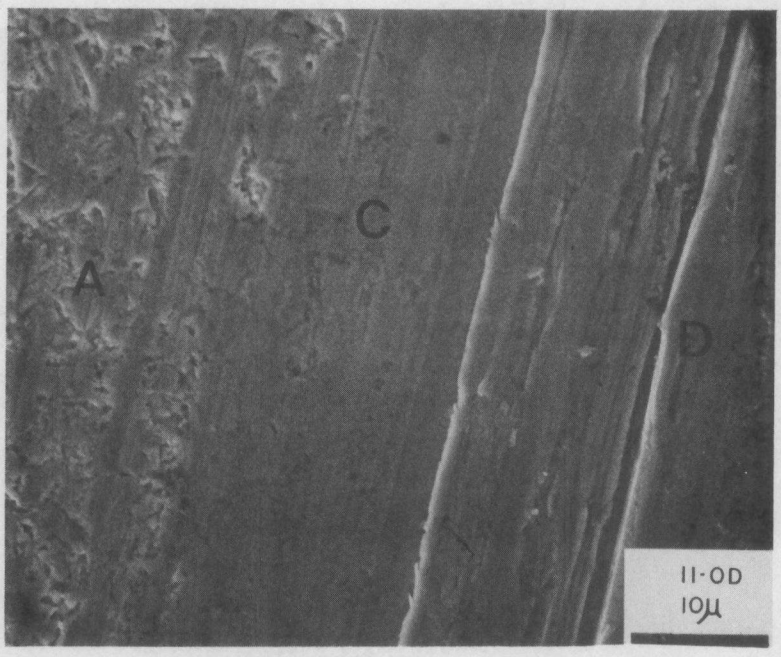

Figure 76. High Magnification View From the Center of Figure 75.

Showing three areas A, C, and D; each area exhibits a different degree of wear.

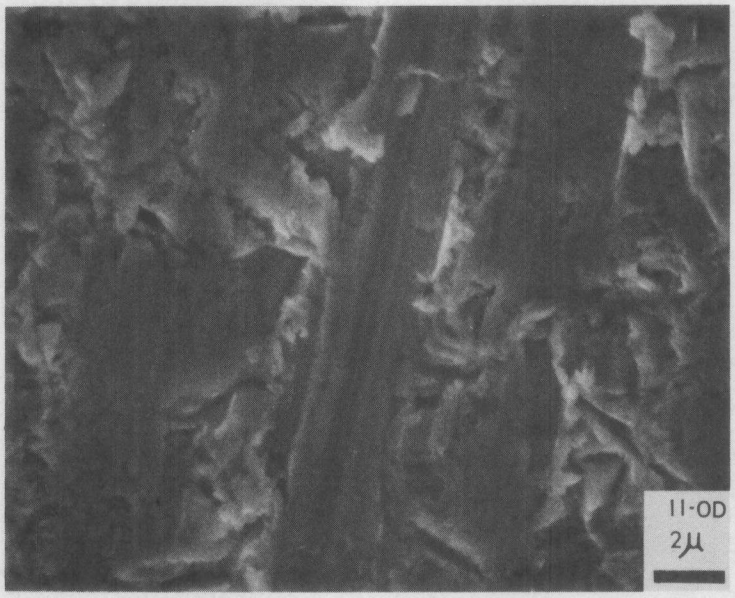

Figure 77. Area A from Figure 76.

Pre-test lapped structure is plainly visible.

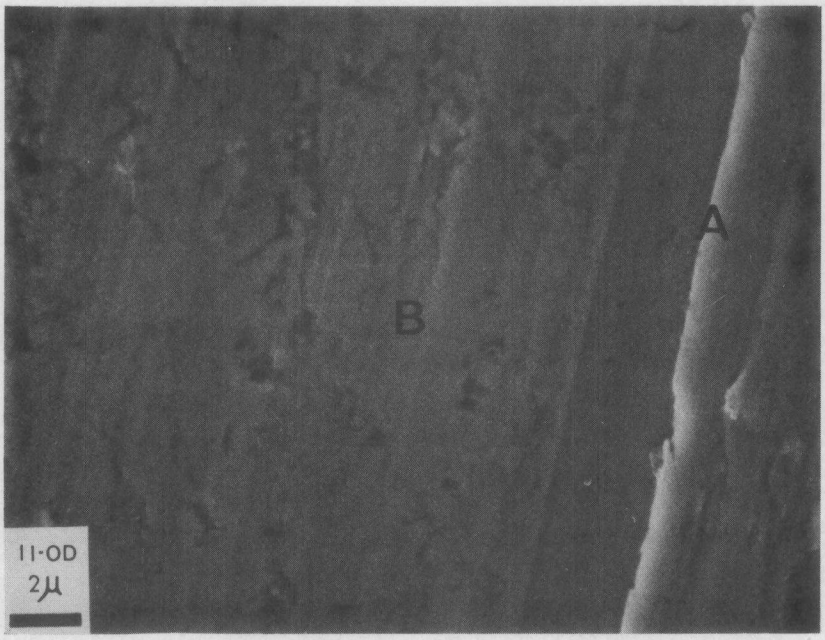

Figure 78. Area C from Figure 76.

Pre-test lapped structure (B) has almost been eradicated.

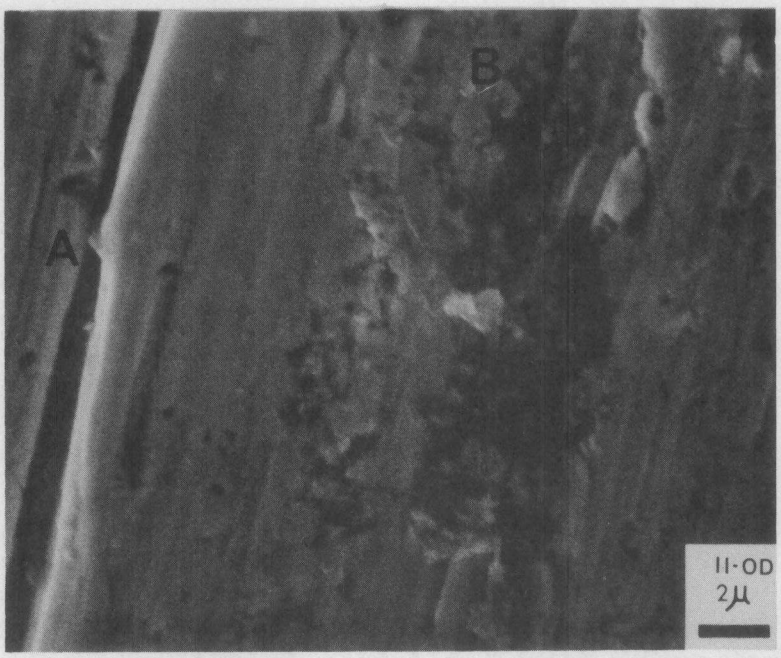

Figure 79. Area D from Figure 76.

A deep abrasive groove (A) and what appears to be a scuffed region (B) can be seen.

area of contact being small resulted in the scuffed area B. The deep score marks shown as A in Figures 78 and 79 and the milder abrasive grooves shown in Figure 78 (area B) were probably formed by wear particles or smaller asperities on the surface of the larger irregularity. As the test proceeded, large surface irregularities and asperities were worn away, resulting in more complete mating and greater surface interaction. The region in Figure 77 was the last area to make contact and thus has undergone less wear. The ordered samples serve to illustrate graphically the stages of the wear or run-in process of many machine elements.

Figures 80 through 83 show similar features as discussed above, observed on the sample from test three. Again is seen the transition from very mild wear in Figure 80 to the gross surface destruction caused by scuffing and increased surface interaction shown in Figures 81, 82, and 83.

Figures 84, 85, and 86 are scanning electron micrographs of a large particle welded to the surface of ordered test ring three. This particle is very similar in appearance to the one shown in Figure 61 (page 95). Nondispersive x-ray analysis of the particle itself shows it, too, to be nickel. Again is seen a pronounced dentritic structure along with a lap-like appearance of the surface of the particle, giving reason to believe that at some time in the test this particle could have been a molten ball of material.

Figure 87 is an optical micrograph of another area on ordered test ring eleven. There are several interesting features. Note the presence here of two relatively large raised "islands" of material

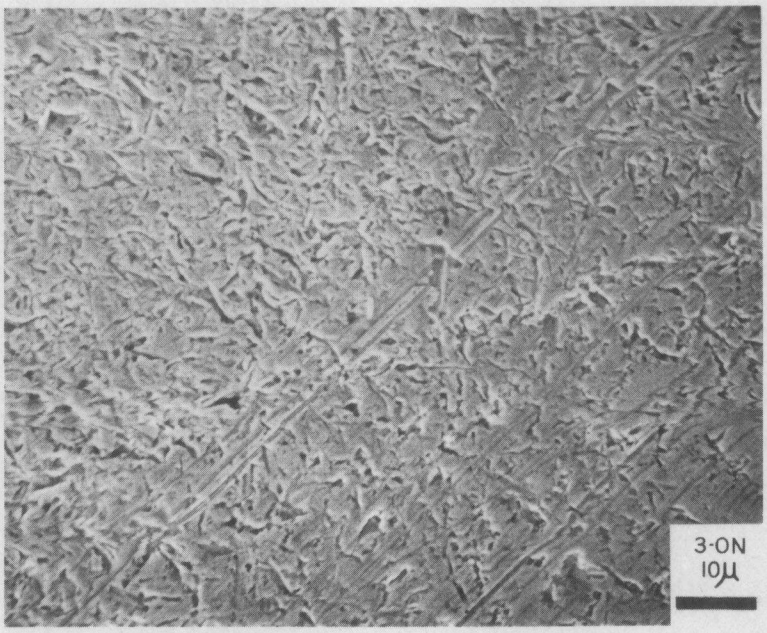

Figure 80. Mild Wear of Ordered Test Ring 3.

The pre-test lapped structure is clearly visible.

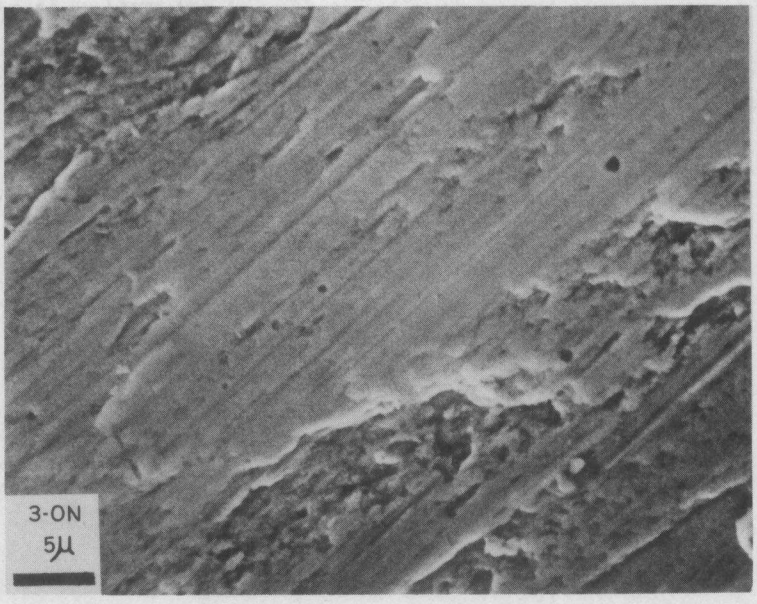

Figure 81. Abrasion and Scuffing on Ordered Test Ring 3.

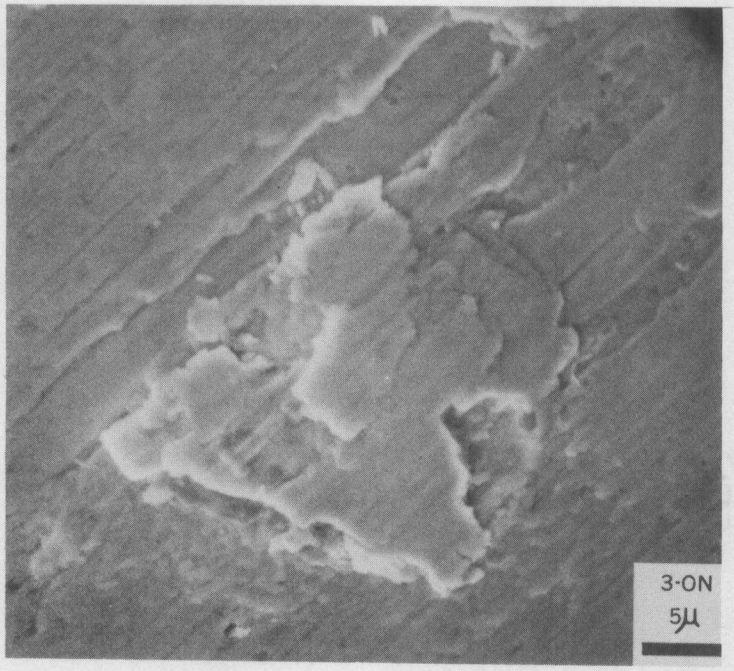

Figure 82. Initial Stages of Debris Formation on Ordered Test Ring 3.

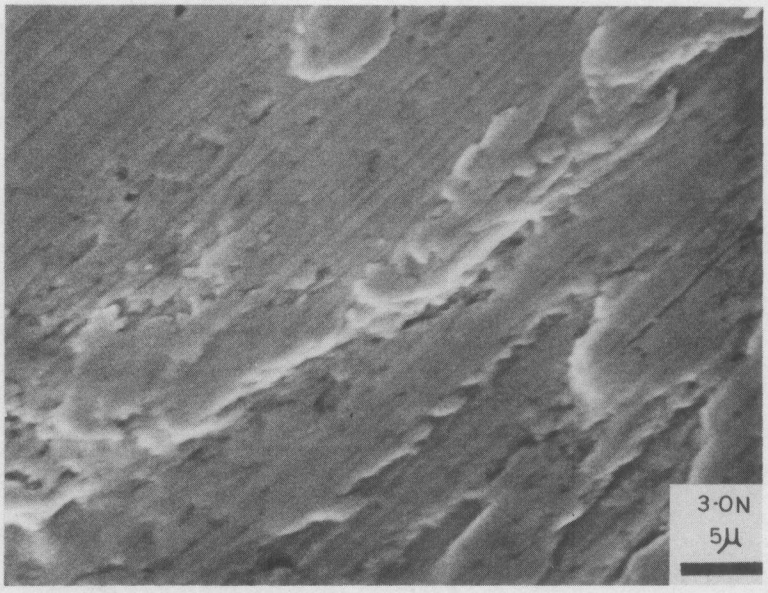

Figure 83. Abrasion and Scuffing.

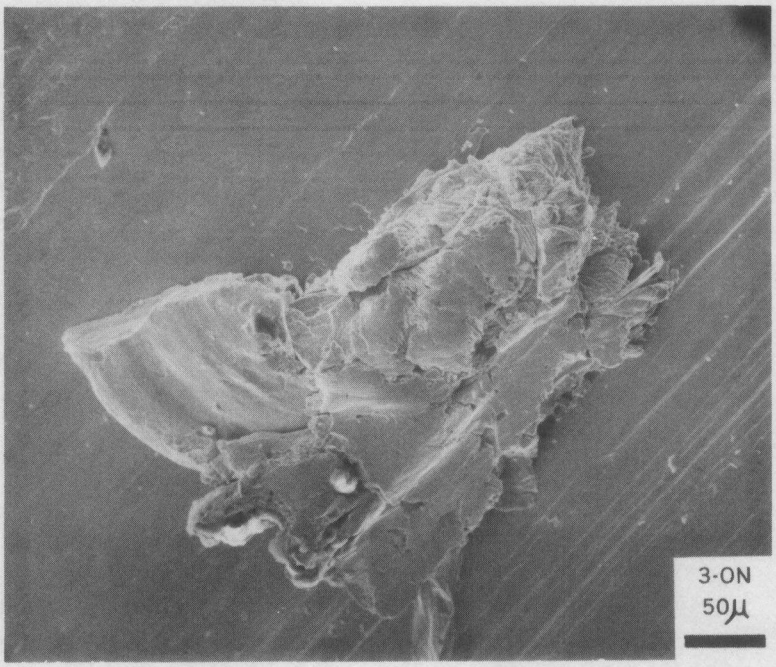

Figure 84. A Particle Welded to the Side of Ordered Test Ring 3.

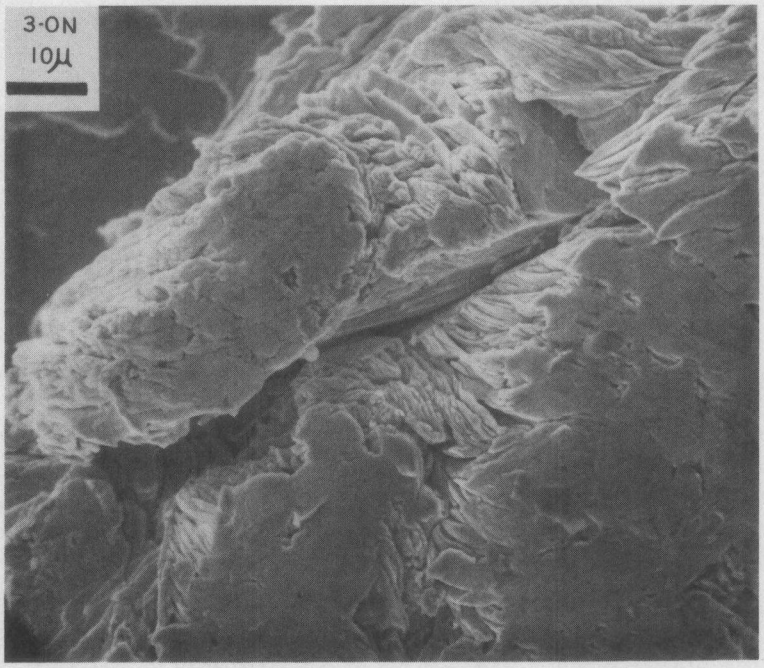

Figure 85. Magnified View of the Particle in Figure 84.

The surface is very irregular; it is similar in appearance to a lapped surface in areas and again can be seen a very pronounced dendritic-like structure.

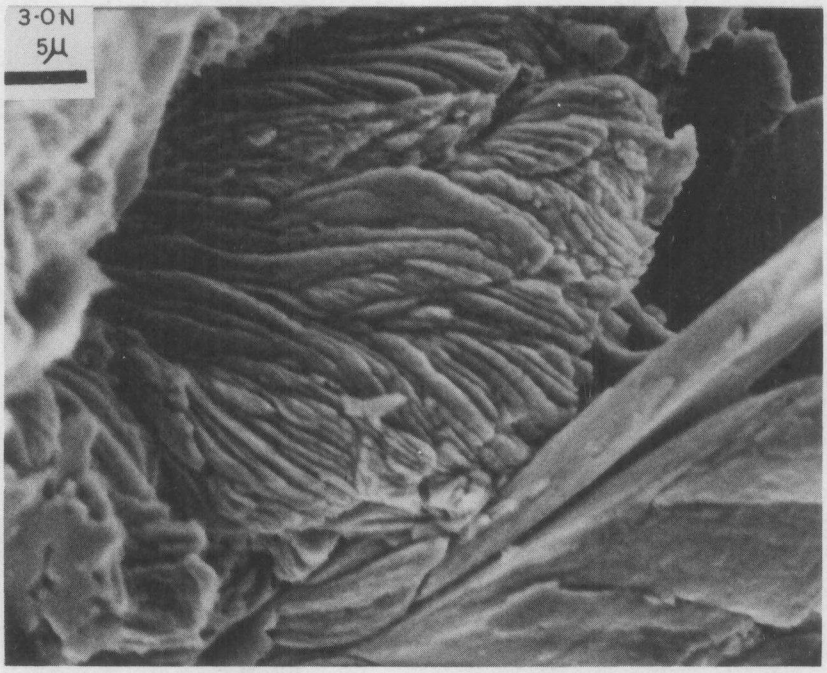

Figure 86. Close-Up of Dendritic-Like Structure Seen in Figure 85.

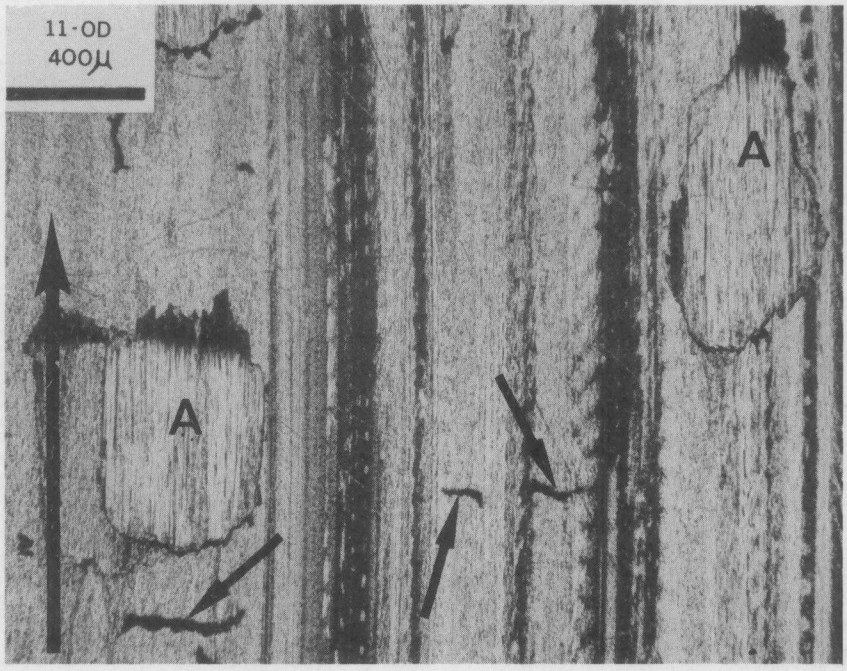

Figure 87. Optical Micrograph of "Islands" of Welded Material (A) and Surface Cracks (Small Arrows) on Ordered Test Ring 11.

(marked A). These are scattered over the entire surface of the test ring and were observed not only on this ring but on other ordered test rings as well. Figure 88 shows one on test ring ten. In Figure 87 note also the presence of surface cracks (see arrows) which, as discussed previously, are a result of the disorder-order heat treatment. Figure 89 is a scanning micrograph of one of these cracks. Now, referring to Figure 87, note that there is no apparent relationship between the location of these cracks and the presence of the raised "islands." Consequently, one can conclude that the presence of the cracks is not responsible for "island" formation.

Figure 90 is an optical micrograph of another "island" on specimen eleven. A scanning electron micrograph of this island is shown in Figure 91 and is very revealing. Several points can be made. The appearance of the island differs markedly from the material to which it is attached. On the lower level, marked A, is seen the characteristic wear surface of the ordered test ring. The surface of the "island" bears a marked resemblance to the smeared and layered appearance of the disordered wear surface (compare Figures 90, 91, and 93 to Figure 58, page 94). The edge of the island (marked B in Figure 91 and shown at higher magnification in Figure 92) has become separated from the material to which it was obviously adhered at one time. This is a characteristic of all the islands observed which adhered to ordered samples. Finally, note the presence of longitudinal cracks on the surface of the "islands" (see arrows). As can be seen in Figure 93,

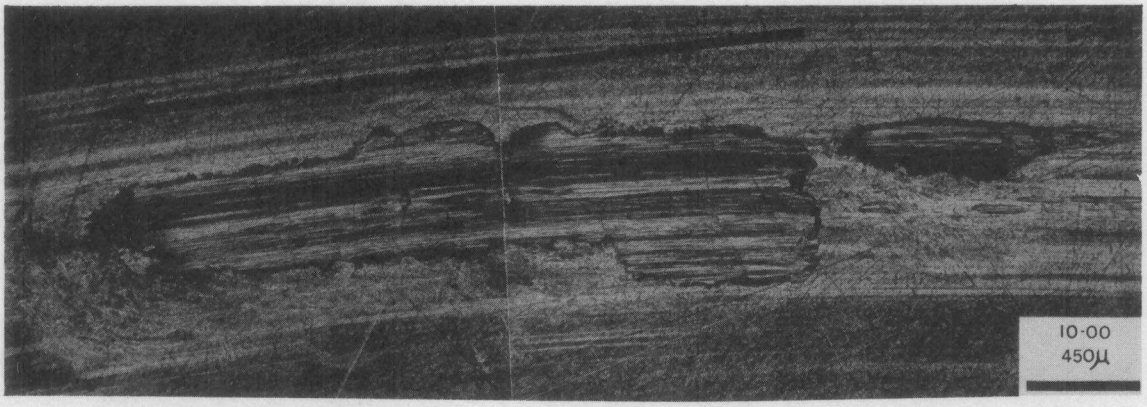

Figure 88. Welded "Islands" of Material Similar in Appearance to Those Observed in Figure 87.

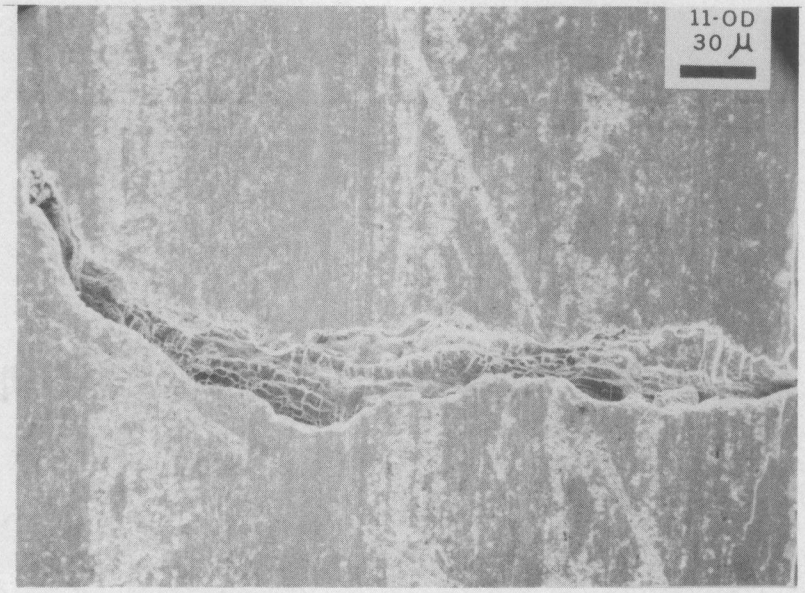

Figure 89. Scanning Electron Micrograph Showing Surface Crack, Probably Formed During the Disorder-Order Heat Treatment.

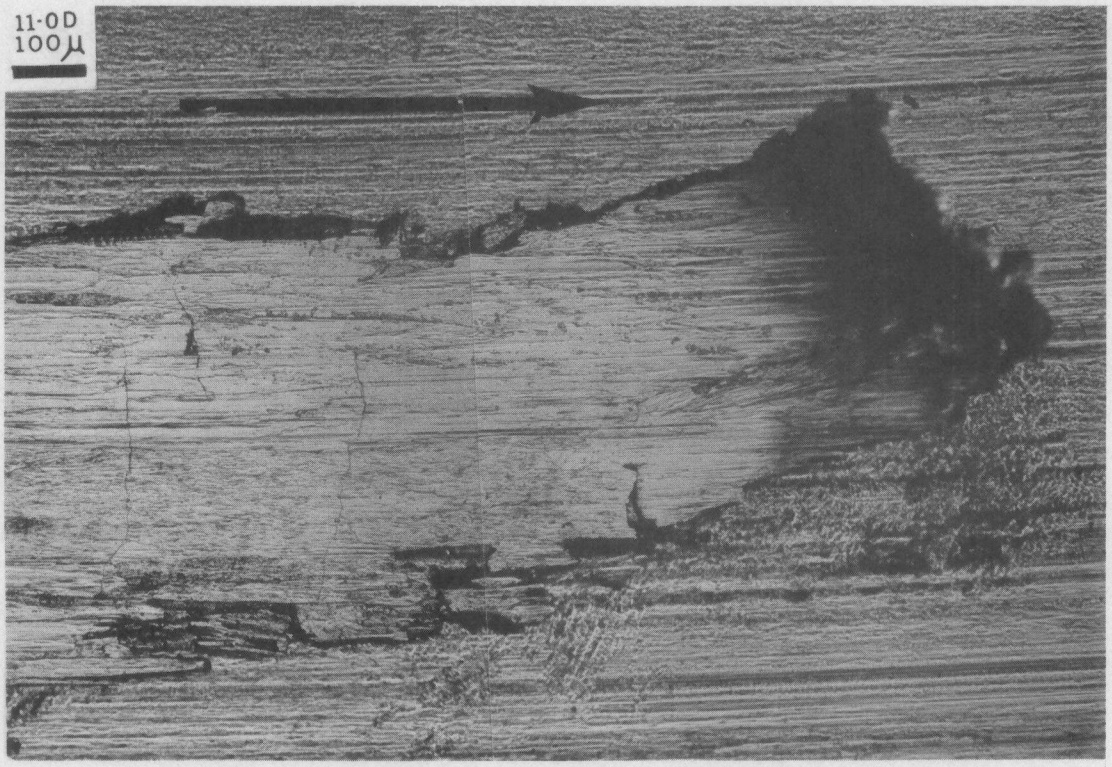

Figure 90. Optical Micrograph of Another Welded Island on Test Ring 11.

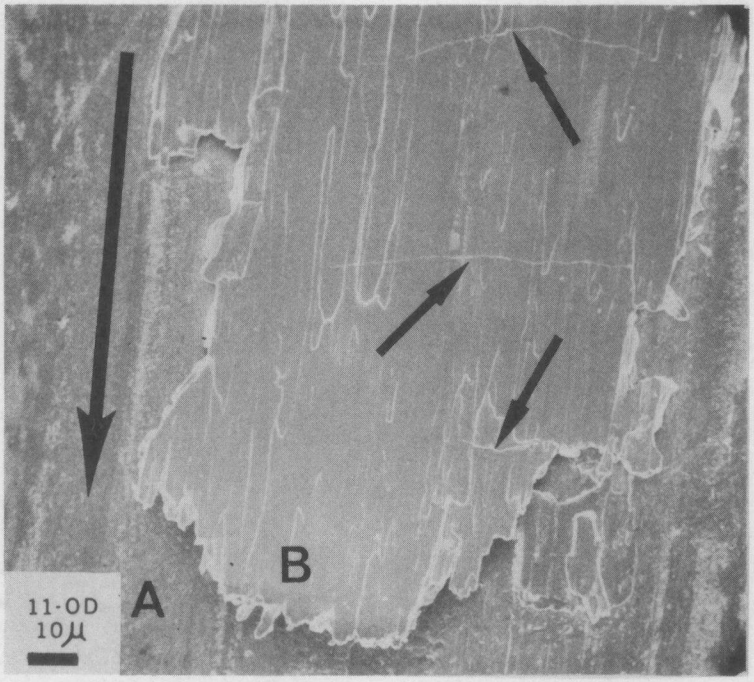

Figure 91. Scanning Electron Micrograph of "Isla
Shown in Figure 90.

Surface cracks on the island (small arrows) can be seen running perpendicular to the direction of relative rotation of the test rings (large arrow).

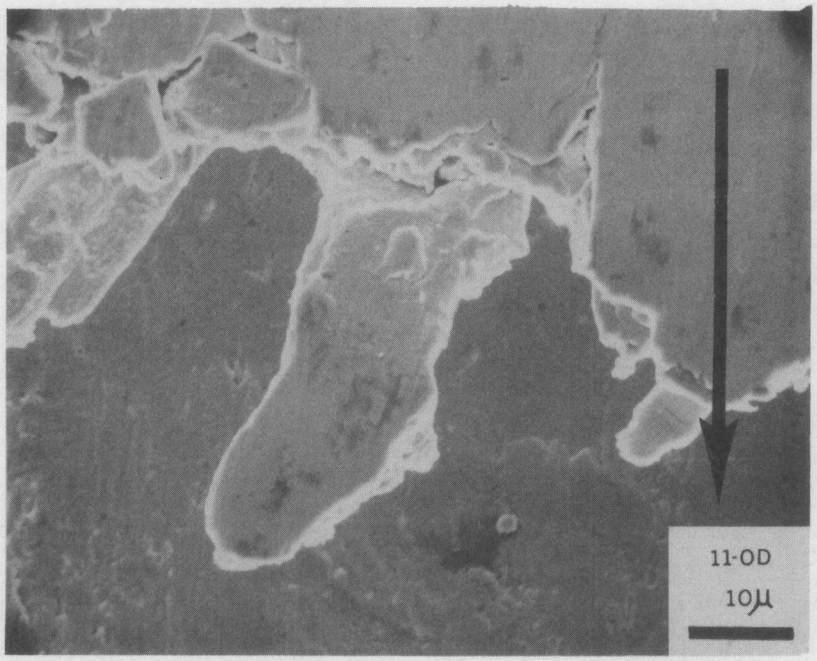

Figure 92. Magnification of the "Lip" (Area B in Figure 91) of the "Island."

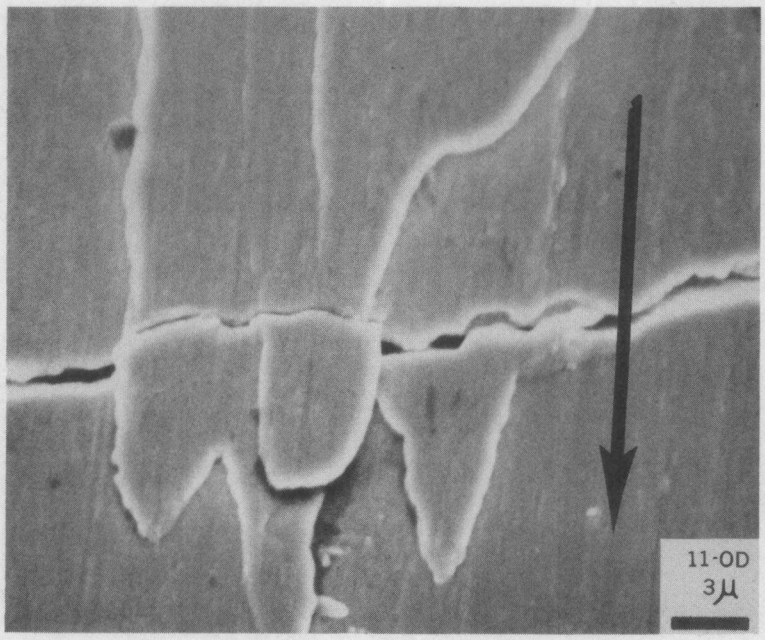

Figure 93. High Magnification of One of the Surface Cracks on the "Island" in Figure 91.

The crack formed after surface flow of the "island."

a magnified view of one of the cracks in Figure 91, cracking of the islands occurred after surface flow.

Raised "islands" similar to those discussed have been observed by Quinn (13). X-ray diffraction analysis in his work of wear tests in air indicated that the islands were oxide films. In the present study it is unlikely that islands observed are oxide. Due to their striking resemblance to the surface of the disordered test rings, it is quite possible that the "islands" are composed of disordered material. If one accepts this hypothesis, then the "island" on the specimen shown in Figure 88, which is the surface of an ordered ring tested against an ordered ring, is composed of material that has undergone an order-disorder transformation, not impossible in an area reaching high temperatures. The islands are real areas of contact, large but small in number as opposed to asperities which are small but large in number. Consequently, the presence of the "islands" has a very real effect on the heat flow characteristics of a surface.

Referring to Figure 91, mild wear of the lower level (marked A) occurred in the first few seconds of the test prior to the formation of the islands. There is no evidence that islands, once formed, shifted. After their initial formation all sliding occurred on the islands themselves. That is, for an ordered test ring running against a disordered test ring, after the first few seconds of the test, disordered material was sliding on disordered material. The cracks in the surface of the island occurred after surface flow, that is, after the test was completed and the test rings were cooling to room temperature. The cracks are quite possibly formed as a result of a difference

in the coefficient of thermal expansion/contraction between the ordered material of level A and the disordered material of the "island."

III. TRANSMISSION ELECTRON MICROSCOPIC EXAMINATION OF SUBSTRATE

Samples were prepared from the nickel-molybdenum ordered and disordered test rings and observed with the transmission electron microscope to obtain information on the mechanisms of plastic deformation operating during wear of the surfaces. Thin films directly at the surface and at some distance from it were studied. Sample designations on micrographs discussed in this section are followed by a letter and a number in order to orient the thin film to the surface. The letter designates an area of the test ring from which the slice was taken. The number tells which slice is being observed; i.e., 1 is the surface slice (ideally, material observed is only a mil or so from the surface), 2 is the second slice (material approximately 35 mils from the surface), and so on. Thus, the C1 designation in Figure 95 means that the micrograph was taken of a portion of the slice nearest the wear track in area C of the test ring.

Figures 94 through 97 are transmission electron micrographs of thin films taken from disordered test rings. Figure 94 shows a structure characteristic of undeformed disordered material. A few random dislocations can be seen, but otherwise the microstructure is clear of any evidence of effects from plastic deformation or from heating. Figures 95 through 97 are micrographs of material at the wear track. Note in Figure 95 the numerous tangles of dislocations and that the dislocations seem to arrange themselves in perpendicular and parallel

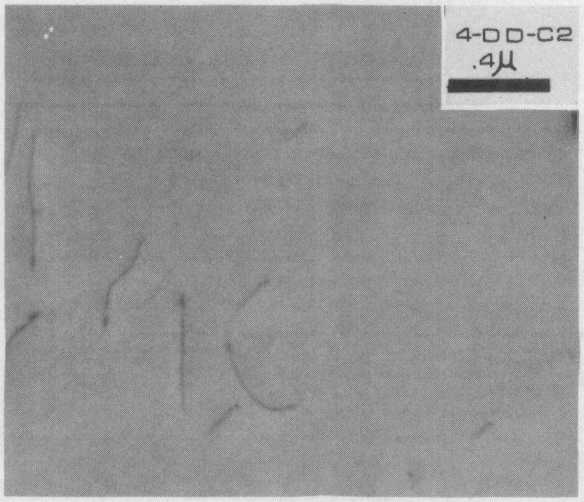

Figure 94. Transmission Electron Micrograph Illustrating the Microstructure of Undeformed Disordered Ni_4Mo.



Figure 95. Transmission Electron Micrograph of Disordered Ni_4Mo Observed Near the Wear Track.

Numerous dislocation tangles are in evidence.



Figure 96. Transmission Electron Micrograph of Disordered Ni_4Mo (Deformed); Bands are of Unexplained Origin.

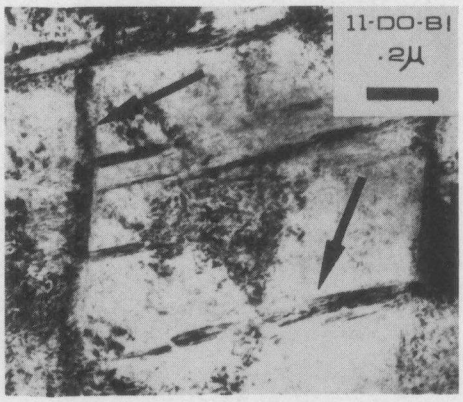

Figure 97. Deformed Material Near the Wear Track of a Disordered Test Ring.

The bands (arrows) are possibly due to contrast effects associated with twinning.

lines. Other researchers (31) have noted that the parallel arrangement of dislocation tangles is directionally associated with the wear track and separated by distances equal to the distance between microgrooves on the surface. The bands (see arrows) in Figures 96 and 97 are possibly due to contrast effects associated with twinning. As would be expected, selected area diffraction yielded very complex patterns in these areas and as of this writing have not been analyzed in detail.

In Figure 98 is shown the typical structure of undeformed ordered material. Figures 99 through 102 are examples of observations made on surface layers of the ordered wear samples. The dark ribbons seen in Figures 99, 100, and 101 (see arrows) are similar in appearance to those observed by Brooks, et al. (32), in ordered nickel-20 atomic percent molybdenum deformed by rolling. The bands are very numerous and are believed to be observed due to contrast effects caused by the formation of antiphase boundaries when dislocations passed through the domains (32). In Figure 102 can be seen numerous dislocation doublets (i.e., superdislocations).

Figure 103 shows an area of a subsurface slice in which recrystallization was observed. Thus, even though such areas were observed also in surface thin film samples, it would seem that recrystallization occurred on heat treating the test rings and was not induced by the wear of the surface.

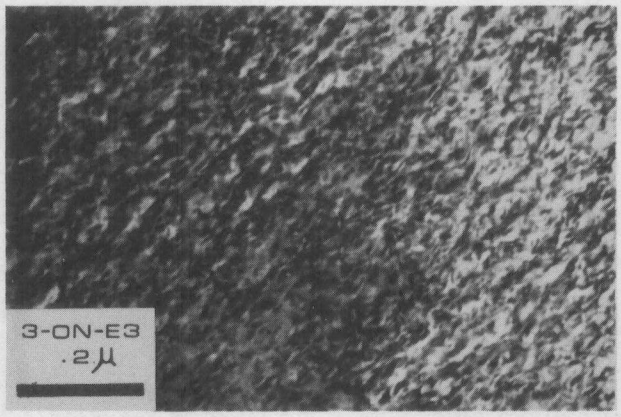

Figure 98. Microstructure of Undeformed Ordered Ni_4Mo.

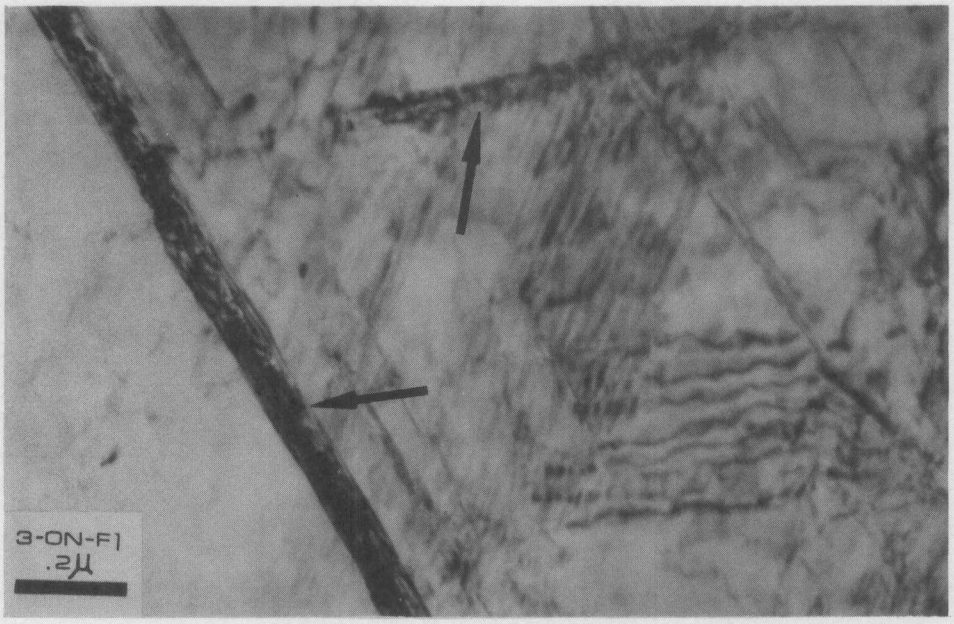

Figure 99. Deformed Material Near the West Track of an Ordered Test Ring.

The bands (arrows) are thought to be due to contrast effects caused by the passage of dislocations through the domains.

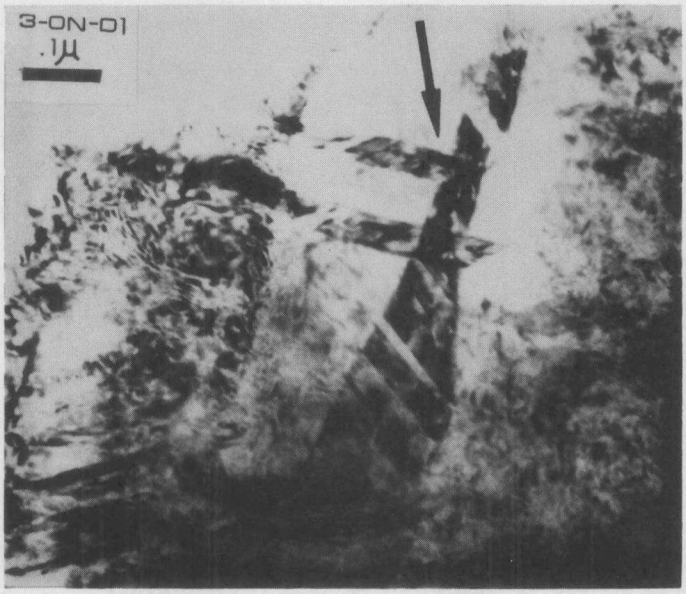

Figure 100. Microstructure of Deformed Material Near the Wear Track of Test Ring 3.

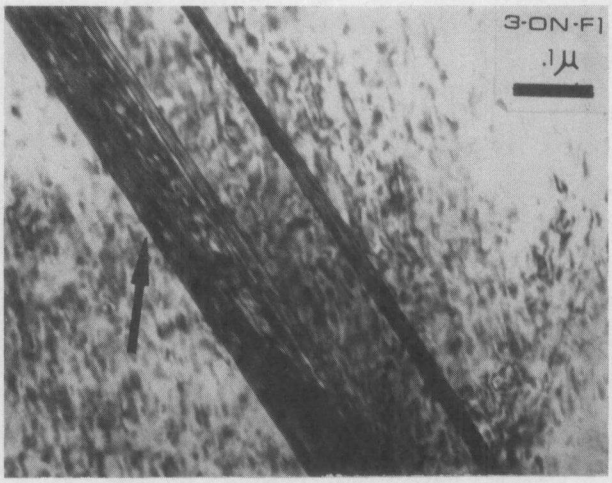

Figure 101. Another Area Showing Bands Similar in Appearance to Those Observed in Figures 99 and 100.

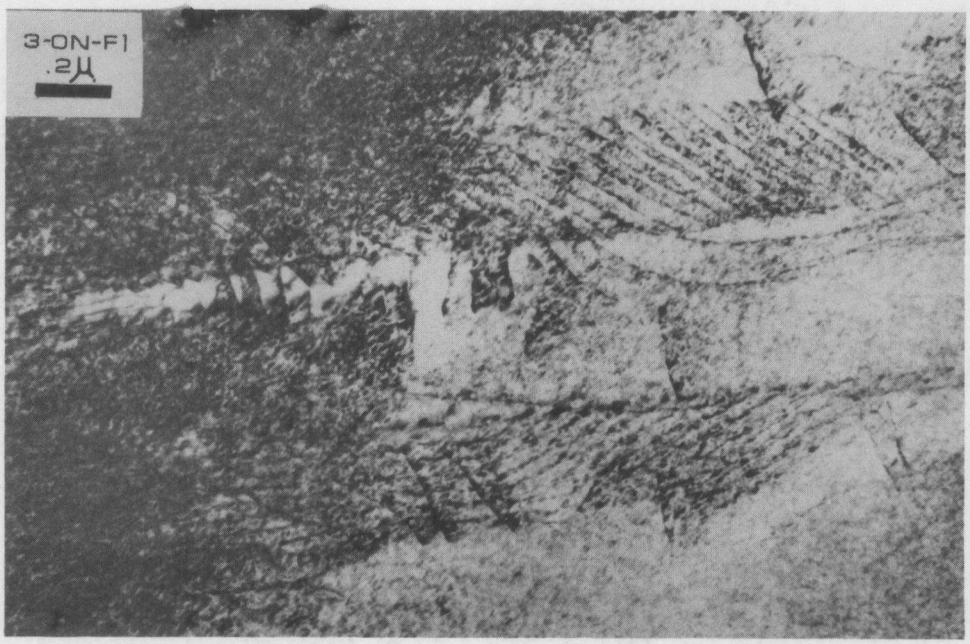

Figure 102. Superdislocations Observed Near the Wear Track on Ordered Test Ring 3.

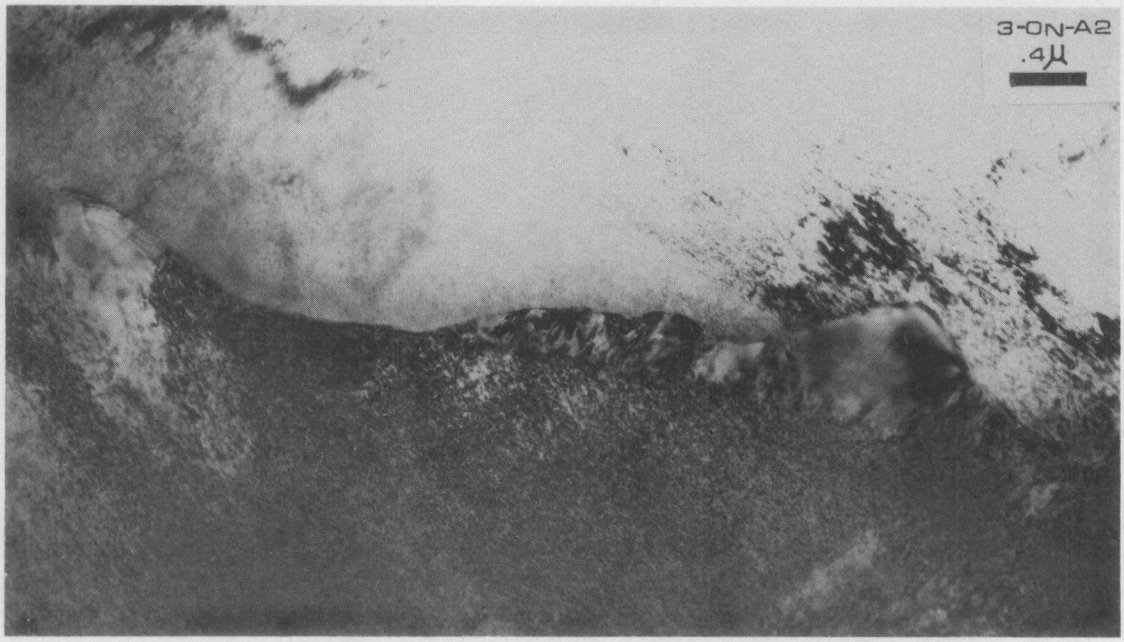

Figure 103. Subsurface Slice Showing Recrystallization in the Ordered Material.

CHAPTER IV

CONCLUSIONS AND RECOMMENDATIONS

The tremendously complex nature of surface interaction during dry sliding conditions should now be apparent. Both the mechanical properties of the materials and effects of the test conditions play a large part in determining what phenomena will be observed on wear surfaces. A number of points concerning the results of the tests run and the performance of the test apparatus can be made:

1. A profound difference in wear characteristics was observed between the three material conditions studied. The wear varied in severity from the massive surface destruction and plastic deformation observed on the nickel test rings to the less severe wear (characterized by relatively mild abrasion and scuffing) of the ordered nickel-molybdenum rings. Deformation of the surface of the disordered nickel-molybdenum rings was less severe than that of the nickel rings and more severe than ordered test rings (it was characterized by thermal softening and uniform surface flow). The relative hardness of the materials is thus seen to play a large part in the character of the wear observed. The disorder-order heat treatment of the nickel-molybdenum test rings, by increasing the hardness and the yield strength of the material, changed completely the dominant operating wear mechanisms.

2. Because test times were short and bulk interfacial temperatures were relatively low, the disorder-order transformation was not observed to occur as a result of frictional heating at the interface. It is

possible, however, that in localized instances (i.e., formation of particles, islands, etc.) long-range ordering occurred and it is probable that the degree of short-range order present at the surface increased due to heating.

3. Some evidence of melting of small amounts of material was found. Thus at localized hot spots temperatures must have been extremely high, much greater than would be indicated by the data and calculations of Chapter III.

4. Material transfer was observed to occur from nickel test rings to disordered nickel-molybdenum test rings, from disordered test rings to ordered nickel-molybdenum test rings, and from nickel test rings to ordered nickel-molybdenum test rings. Intuitively, this transfer of material from the softer to the harder is what one would expect (see the section on "Adhesive Wear," Chapter I). However, in one case material was transferred from an ordered test ring to a nickel ring, i.e., from the harder to the softer. Quite possibly, this transference could be attributed to the complicating effects of test conditions.

5. Transmission electron microscopy of ordered and disordered nickel-molybdenum wear samples yielded very complex microstructures indicating that the mechanisms involved in the wear of these materials are very complex. Further detailed analysis of the micrographs accumulated should be performed.

6. The boundary lubricated wear regime was not operating during the tests performed in this study due to vibration of the stator as indicated by torque and face loading data. This fact can be surmised

also by considering the gross surface deformation observed.

A number of recommendations can be made at this time in the interest of providing reliable quantitative test results and further information concerning the effect of the disorder-order transformation on surface interaction.

1. The test apparatus should be redesigned to provide for self alignment of the test rings and viscous damping of the stator.

2. Use should be made of accelerometers to detect the displacement caused by vibration and seal separation caused by wedge or island formation.

3. The use of irradiated material should be considered in order to detect transfer. This would be particularly useful when studying materials having the same elemental constituents but different heat treatment and mechanical properties.

4. Thin film transmission electron microscopy should be performed on as lapped surfaces to characterize mechanisms involved in plastic deformation of material during lapping. This would allow better comparison than is presently available. (In the present study, subsurface samples are being used for initial microstructural characterization.)

5. Tests run in a lubricant, although resulting in a more complex chemical environment, would reduce the severity of surface destruction allowing longer test times and better test control. In addition, a relatively incompressible lubricant used to apply face loading could provide enough viscous damping to aid in reduction of vibration.

6. Materials of a more wear resistant nature should be studied (perhaps commercial alloys). Hastelloy-B, the commercial equivalent of nickel-20 atomic percent molybdenum, should be tested, perhaps in the partially ordered state. Testing of disordered Hastelloy-B would most likely result again in severe surface destruction as observed in this research on disordered Ni_4Mo.

LIST OF REFERENCES

LIST OF REFERENCES

1. Matthes, D. K. "Wear Reactions Occurring at the Interfaces of Mechanical Face Seals in the Boundary Lubrication Condition." M. S. Thesis, The University of Tennessee (December, 1969).

2. Kragelskii, I. V. Friction and Wear. Washington: Butterworths, 1965.

3. Bowden, F. P., and D. Tabor. The Friction and Lubrication of Solids. Oxford: Clarendon Press, 1950.

4. Archard, J. F. "Contact and Rubbing and Flat Surfaces," J. Applied Physics, 24 (1953) 981.

5. Bowden, F. P., and D. Tabor. The Friction and Lubrication of Solids, Part II. Oxford: Clarendon Press, 1964.

6. Burwell and Strang. J. Applied Physics, 23 (1952) 18.

7. Rabinowicz, E., and A. Mutis. "Effect of Abrasive Particle Size on Wear," Wear, 8 (1965) 381.

8. Oberle, J. T. "Properties Influencing the Wear of Metals," J. Metals, 3 (1951) 451.

9. Finkin, E. F. "Abrasive Wear," Evaluation of Wear Testing, ASTM STP, 446 (1966) 55-90.

10. Krushov, M. M., and M. A. Babichev. "Resistance to Abrasive Wear of Structurally Inhomogeneous Materials," Friction and Wear in Machinery, Vol. 12, ASME, New York, 1958.

11. Miller, D. R. "Friction and Abrasion of Hard Solids at High Sliding Speeds," Proceedings of the Royal Society, A, Vol. 269 (1962) 368-384.

12. Lipson, C. Wear Considerations in Design. New Jersey: Prentice-Hall, 1967.

13. Quinn, T. F. J. "Some Microscopic Aspects of the Mild Wear of Steel," J. of Microscopy, 94, 2 (October 1971) 125-137.

14. Campbell, W. E. "Atmospheric Effects on Friction and Wear," Machine Design, August 27, 1964.

15. Braithwaite, E. R. Solid Lubricants and Surfaces. New York: The Macmillan Company, 1964.

16. Akhmatov, A. S. Molecular Physics of Boundary Friction. Trans. from Russian by N. Kaner. Jerusalem: Israel Program for Scientific Translations, 1966.

17. Spruiell, J. E., and Stansbury. Phys. Chem. Solids, 26 (1965) 811.

18. Harker, D. "The Crystal Structure of Ni_4Mo," J. Chem. Phys., 12 (1944) 315.

19. Lampe, B. T. "An Investigation of the Order-Disorder Transformation in the Nickel-29.1 Percent Molybdenum Alloy by Electrical Resistivity Measurements." M. S. Thesis, The University of Tennessee (December, 1963) 52.

20. Snyder, W. B., and C. R. Brooks. "Mechanical Properties and Domain Structure of Ordered Ni_4Mo," Ordered Alloys, Proceedings 3rd Bolton Landing Conference. Baton Rouge: Claitor's Publishing Division, 1970, 275-299.

21. Buckley, D. H. "The Influence of Various Physical Properties of Metals on Their Friction and Wear Behavior in Vacuum," Metals Engineering Quarterly ASM (May, 1967).

22. Headrick, M. R. "The Design and Construction of a Facility to Determine the Dynamics of a Face Seal." M. S. Thesis, The University of Tennessee (1968).

23. Dubose, C. K. H., and J. O. Stiegler. "Semiautomatic Preparation of Specimens for Transmission Electron Microscopy," Report ORNL-4066, Oak Ridge National Laboratory, Oak Ridge, Tennessee, U.S.A. (February, 1967).

24. Kreith, F. The Principles of Heat Transfer, 2nd Edition. Scranton: International Textbook Company (1965).

25. Archard, J. F. "The Temperature of Rubbing Surfaces," Wear, 2 (1958) 438-455.

26. Strom, T. N., L. P. Ludwig, and J. C. Hudelson. "Vibration of Shaft Face Seals and Stabilizing Effect of Viscous and Friction Damping," National Aeronautics and Space Administration Publication TN D-5161 (January, 1969).

27. Newman, G. T., O. D. Smith, D. K. Matthes, and C. R. Brooks. "Application of Electron Microscopy to the Study of Surface Topography and Subsurface Microstructure in Wear," Report ME70-T57-11, Department of Chemical and

Metallurgical Engineering, The University of Tennessee (September, 1970).

28. Frey, H., and H. G. Feller. "Investigations of Wear with the Scanning Electron Microscope," Practical Metallography, 9, 4 (April, 1972) 187-197.

29. Cocks, M. "The Formation of Wedges of Displaced Metal Between Sliding Metal Surfaces," Wear, 8 (1965) 85-92.

30. Macdonald, D. "The Development of Prow and Wedge Type Junctions in Shrink-Fitted Torsion Joints," Wear, 18 (1971) 41-50.

31. Feder, R., and P. Chaudhari. "Transmission Electron Microscopy of Wear Tracks," Wear, 19 (1972) 109-112.

32. Brooks, C. R., J. E. Spruiell, and C. K. H. DuBose. "Electron Microscopic Observations of Dislocations in Nickel and Ni-Mo Alloys," Mat. Res. Bull. 3 (1968) 381-388.

33. Lampe, B. T. "An Investigation of the Order-Disorder Transformation in the Nickel-29.1 Percent Molybdenum Alloy by Electrical Resistivity Measurements." M. S. Thesis, The University of Tennessee (December, 1963).

VITA

Edwin A. Merrick was born in Nashville, Tennessee, in 1948. He attended Vanderbilt University, receiving a Bachelor of Engineering degree in Mechanical Engineering in 1970. In August of 1973 he received his Master of Science in Metallurgical Engineering from The University of Tennessee. Since October of 1972 he has been employed as a Metallurgical Engineer with the Tennessee Valley Authority in Knoxville where he works on materials application, welding, and the implementation of codes and standards as applied to TVA's Nuclear Steam Supply Systems.

He has one son, Eddie, and is married to the former Marguerite Terhune of Nashville, Tennessee.